Master Thesis

Environmental conditions during deposition of oil shale in the Qingshankou Fm. (Songliao Basin, NE China)

Susanne Andrea Ingeborg Strobl, BSc

2011

Univ.-Prof. Mag.rer.nat. Dr.mont. Reinhard F. Sachsenhofer

Chair in Petroleum Geology

Department of Applied Geosciences and Geophysics

University of Leoben, Austria

Eidesstattliche Erklärung

Ich erkläre an Eides statt, dass ich diese Arbeit selbstständig verfasst, andere als die angegebenen Quellen und Hilfsmittel nicht benutzt und mich auch sonst keiner unerlaubten Hilfsmittel bedient habe.

Affidavit

I declare in lieu of oath, that I wrote this thesis and performed the associated research myself, using only literature cited in this volume.

Leoben, November 2011 ……

(Susanne Andrea Ingeborg Strobl, BSc)

Acknowledgements

I gratefully acknowledge Univ.-Prof. Mag. Dr. Reinhard F. Sachsenhofer (Chair in Petroleum Geology, University of Leoben, Austria) for his helpful advices and great support during the supervision of this master thesis.

I also express gratitude to Professor Zhaojun Liu (Oil Shale Laboratory Center, Jilin University, Changchun, China), who generously provided the core samples.

Special thanks to Ass.-Prof. Dipl.-Ing. Dr. Doris Reischenbacher, who gave me a broad understanding of the methodology. She always tried to help and to motivate me.

Furthermore I would like to thank Priv.Doz. Dipl.-Min. Dr. Achim Bechtel and Ass.-Prof. Dr. Reinhard Gratzer, who helped me on biomarker analysis.

I am very grateful to Dipl.-Ing. Jürgen Gusterhuber and to Dipl.-Ing. Stefan Neumeister, who explained technical details of sample preparation to me.

Many thanks are also due to Sabine Feuchter, who helped me to polish the sections for maceral analysis.

Special thanks appertain to my parents Senta and Franz Strobl and to my family, who always believed in me and who supported me at all time.

Last but not least I express my deepest gratitude to my husband Dipl.-Ing. Stefan Strobl. He always had a good advice for me and helped me a lot. Thank you so much!

Abstract

The Songliao Basin located in northeastern China is the country´s most oil-productive basin. It is interpreted as a Mesozoic-Cenozoic rift basin. Prolific source rocks occur in the Qingshankou and Nenjiang formations deposited during the Late Cretaceous post-rift phase. The most prolific source rock unit forms part of the first member of the Qingshankou Formation, where the rocks locally reach oil shale quality.

The main aim of the present study was to reconstruct the depositional environment of the organic-rich sediments of the Qingshankou Formation. In addition, the source rock potential and the maturity of the organic matter were evaluated.

A total of 70 well core samples from borehole NGN-dgk-02 were studied using Leco analysis (sulphur, inorganic and organic carbon content) and Rock Eval pyrolysis. A subset of the samples was selected for biomarker and isotope analysis, vitrinite reflectance measurements and maceral analysis. One additional sample representing an oil-stained sandstone from the Quantou Formation underlying the Qingshankou Formation was analysed to define the source of the oil.

The results of this study show that deposition of the first member of the Qingshankou Formation commenced in a lake with relative high salinity. The increase in salinity may reflect a marine inflow. Salinity stratification induced anoxic conditions, which reached upwards into the photic zone. Bioproductivity was high at the same time. Organic-rich sediments with TOC contents up to 24 % and containing type I kerogen were deposited in this environment. During the deposition of the overlying sediments, the salinity and bioproductivity decreased significantly. Nevertheless, sediments with TOC contents up to 4 % have been deposited. The organic matter is immature to marginal mature. The oil from the Quantou Formation was generated from sediments of the Qingshankou Formation with higher maturity implying migration from a deeper part of the basin.

Kurzfassung

Die Öl- und Gasvorkommen im Songliao Becken, einem mesozoisch-känozoischen Riftbecken im Nordosten Chinas, machen es zur bedeutendsten Kohlenwasserstoff-provinz des Landes. Die wichtigsten Muttergesteine wurden während der oberkretazischen Postrift-Phase abgelagert und treten in der Qingshankou-Formation sowie der Nenjiang-Formation auf. Die reichsten Muttergesteine befinden sich im ersten Member der Qingshankou-Formation, wo sie lokal Ölschieferqualität erreichen.

Wichtigstes Ziel der Arbeit ist es, die Ablagerungsbedingungen der organisch-reichen Sedimente der Qingshankou-Formation zu rekonstruieren. Daneben wurde das Muttergesteinspotential quantifiziert und die Reife des organischen Materials untersucht.

Insgesamt wurden 70 Kernproben der Bohrung NGN-dgk-02 mittels Leco Analyse (Schwefelgehalt, anorganischer und organischer Kohlenstoffgehalt) und Rock Eval Pyrolyse untersucht. Biomarker- und Isotopenuntersuchungen, sowie Vitrinitreflexions-messungen und Bestimmungen der Mazeralgehalte wurden an ausgewählten Proben durchgeführt. Zusätzlich wurde ein öl-imprägnierter Sandstein in der Quantou-Formation unterhalb der Qingshankou-Formation untersucht, um die Herkunft des Öles zu bestimmen.

Die Studie zeigt, dass der untere Teil der Sedimente des ersten Members der Qingshankou-Formation in einem See mit relativ hoher Salinität abgelagert wurde. Die Salinitätserhöhung spiegelt vermutlich marine Ingressionen wider. Salinitäts-stratifizierung führte zu anoxischen Bedingungen, die bis in die photische Zone reichten. Gleichzeitig war die Bioproduktivität hoch. In diesem Milieu gelangten organisch-reiche Sedimente mit TOC Gehalten bis 24 % TOC und einem Typ I Kerogen zur Ablagerung.

Während der Ablagerung der überlagernden Sedimente gingen die Salinität und die Bioproduktivität deutlich zurück. Trotzdem wurden Sedimente mit bis zu 4 % TOC abgelagert.

Das organische Material ist thermisch unreif bis marginal reif. Das Öl der unterlagernden Schichten (Quantou-Formation) wurde bei etwas höherer Reife in einem tieferen Beckenteil aus Sedimenten der Qingshankou-Formation generiert.

Contents

1 Introduction

The non-marine Songliao Basin is China's most oil-productive basin. More than 80 oil and/or gas fields were found to date (Ryder et al., 2003). The Upper Cretaceous Qingshankou and Nenjiang formations are considered the main source rocks, and are also known as major oil shale resources (Liu et al., 2009).

Nowadays oil shales are unconventional hydrocarbon reserves of great importance. Many well-explored oil shale deposits are located in Chinese basins.

The Songliao Basin is a Mesozoic-Cenozoic rift basin in northeast China (Figure 1). It is oval shaped and covers an area of approximately 260,000 km² (800 x 360 km).

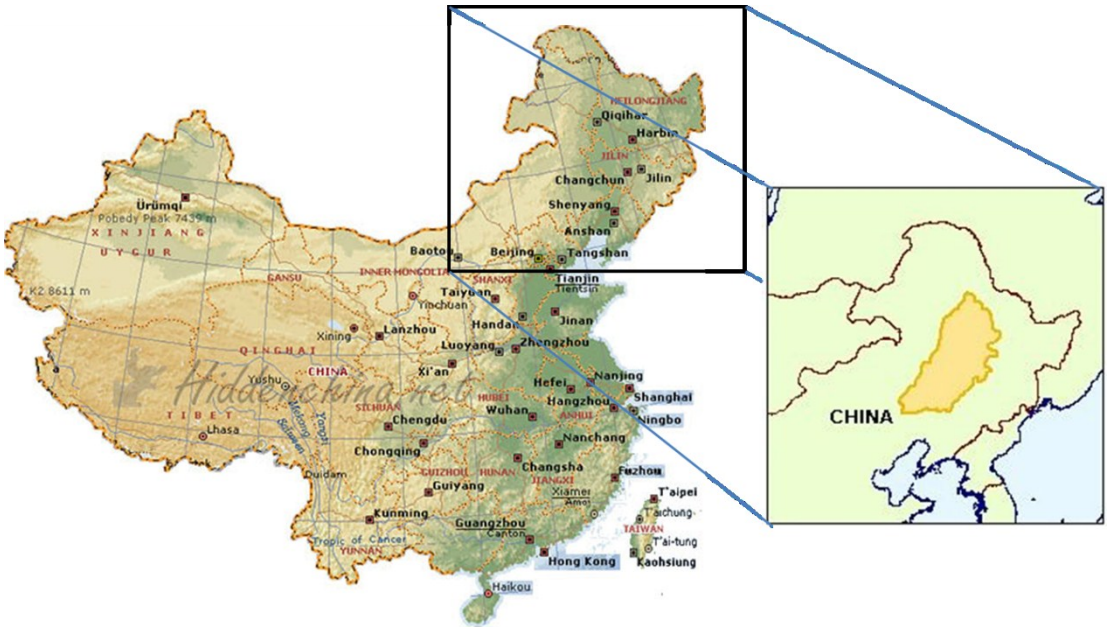

Figure 1: Location map of the Songliao Basin (modified after http://www.hiddenchina.net).

The oil shales of the studied Qingshankou Formation were deposited during the post-rift stage of basin evolution (Feng et al., 2010). Eutrophic and anoxic conditions predominated in a deep lake during this period, resulting in the deposition of organic-rich mudstones and oil shales. Hou et al. (2000) investigated biomarkers and dinoflagellate assemblages and concluded that deposition of the oil shales in the Songliao Basin occurred under conditions of enhanced salinity within a stratified water column.

Therefore, a marine transgression or a saline lacustrine environment has to be considered when studying the depositional environment of the Qingshankou Formation.

For the present study 70 well core samples were taken at the Oil Shale Lab of Jilin University (Changchun, China) from the first member of the Qingshankou Formation in borehole NGN-dgk-02. One additional sample represents an oil-stained sandstone within the Quantou Formation underlying the Qingshankou Formation.

The main aim of this study was to reconstruct the depositional environment of the oil-shale bearing succession in the Qingshankou Formation and its variability through time using a high-resolution approach. Additional aims included the evaluation of the petroleum source rock potential and the maturity of the Qingshankou Formation. To reach the goal, the samples have been studied using Leco elemental analysis and Rock Eval pyrolysis. A subset of the samples was selected for maceral analysis, vitrinite reflectance measurements, biomarker analysis, and carbon isotope analysis. In addition, the oil from the oil-stained sandstone in the Quantou Formation was correlated with extracts from the oil shales in the Qingshankou Formation.

2 Geological setting

2.1 Evolution of the Songliao Basin

The Songliao Basin is a Mesozoic to Cenozoic rift basin. Its evolution is controlled by the interactions between crust and mantle caused by the subduction of the Pacific Plate in the east and the subduction of the Mongol-Okhotsk Plate in the north beneath the Asian Plate (Ma et al., 1982; Li, 1995; Yin and Nie, 1996).

The stratigraphic column of the Songliao Basin (Figure 2) outlines the different formations and their lithologies. The specific sedimentary environments and the tectonic stages of the basin evolution are also shown.

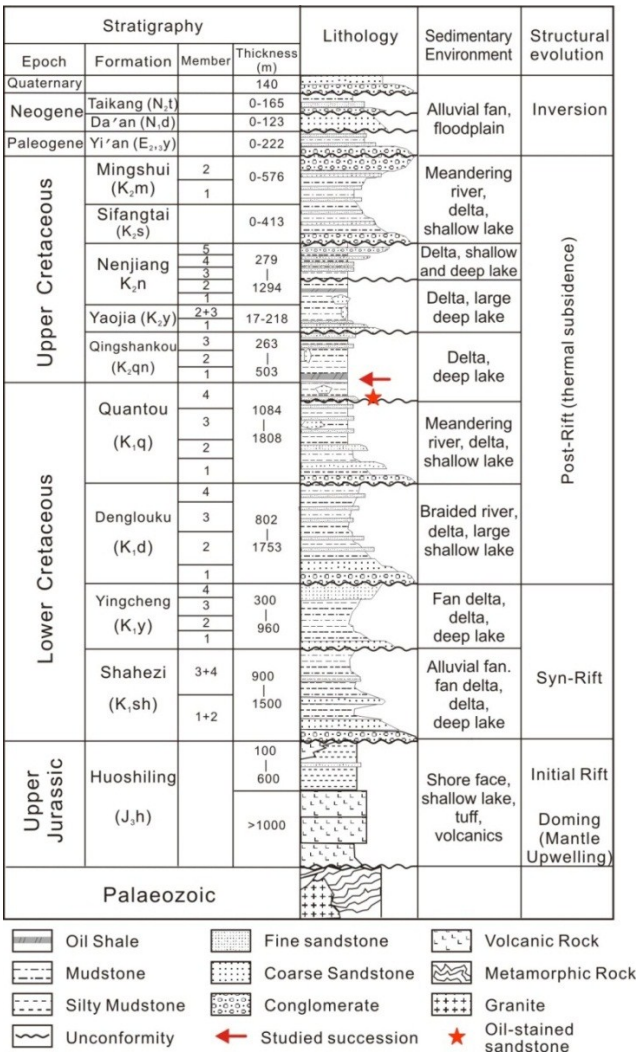

Figure 2: Stratigraphic column of the Songliao Basin (modified after Feng et al., 2010). An arrow and a star indicate formations from which samples were taken.

Feng et al. (2010) subdivided the basin evolution into four tectonic stages (Figure 2):

Pre-rift to initial-rift stage:
The Middle to Late Jurassic pre-rift stage is characterised by mantle upwelling resulting in doming, extension and volcanism. The Upper Jurassic Huoshiling Formation representing the initial-rift stage occurs in most of the fault blocks and consists of andesitic volcanic flows and volcaniclastic rocks which are intercalated by floodplain and swamp deposits.

Syn-rift stage:
Upper Jurassic to Lower Cretaceous syn-rift sediments were deposited within isolated fault blocks (Figure 3). The strata of the Lower Cretaceous Shahezi Formation is characterised by grey to black lacustrine mudstones and siltstones interbedded with grey sandstone and conglomerate. The Yingcheng Formation mainly consists of sandstones and mudstones.

Post-rift stage:
Sediments of the Early to Late Cretaceous thermal subsidence post-rift stage cover the whole Songliao Basin and overlie the syn-rift sediments. This stage comprises seven formations (Denglouku, Quantou, Qingshankou, Yaojia, Nenjiang, Sifangtai, Mingshui). The lowermost Denglouku and Quantou formations mainly consist of fluvial, deltaic and shallow lacustrine deposits which are characterised by conglomerates and sandstones interbedded with mudstones. The deltaic and deep lacustrine Qingshankou, Yaojia and the two lowermost members of the Nenjiang formations comprise oil shales, mudstones, siltstones and fine grained sandstones. The three uppermost members of the Nenjiang, Sifangtai and Mingshui formations are characterised by shallow lacustrine, deltaic and fluvial conglomerate, sandstone and mudstone deposits.

Basin inversion stage:
Cenozoic structural basin inversion including folding and uplift mainly occurred in the eastern part of the basin. It is characterised by alluvial fan and floodplain deposits. Quaternary and Neogene sediments were locally deposited in the western part.

Figure 3 shows the structural elements and strata in a west-east-trending cross section through the Songliao Basin. Figure 4 informs on the subdivision of the Songliao Basin

into six structural domains according to Gao et al. (1994): Western Slope, Northern Plunge, Central Depression, Northeastern Uplift, Southeastern Uplift and Southwestern Uplift. Although both figures are taken from the same paper (Feng et al., 2010), the used terminology is different (and the scale of Figure 3 is probably incorrect).

The thickest accumulation of sediments (ca. 6500 m) is preserved in the Qija-Gulong Sag, which is a post-rift structural element of the Western Rift Belt (Figure 3) and Western Slope (Figure 4).

The studied well NGN-dgk-02 is located in the Southeastern Uplift (Figure 4).

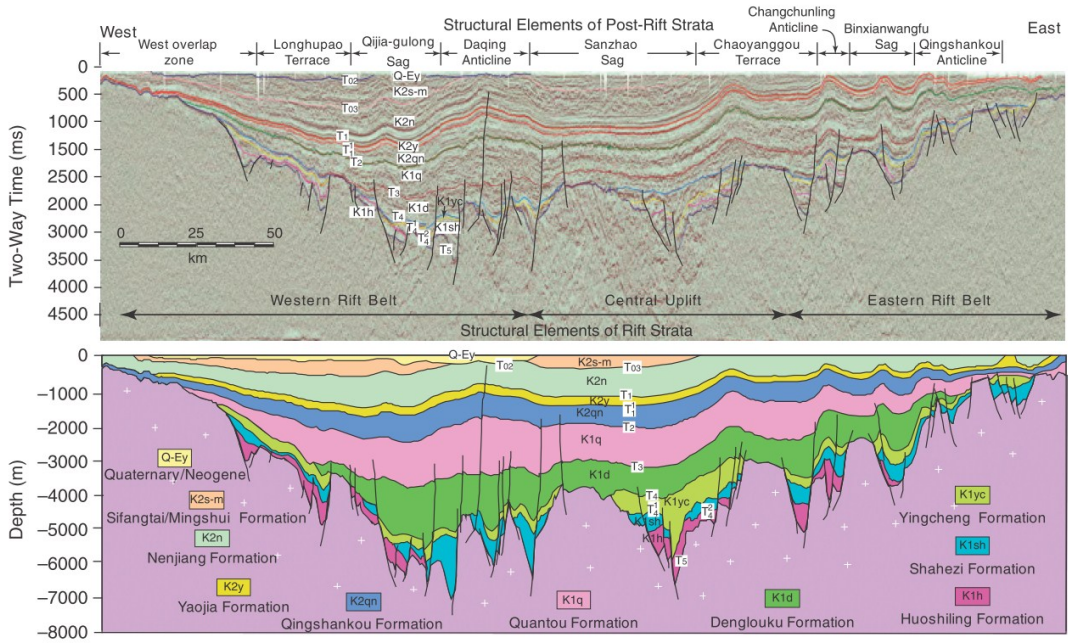

Figure 3: Seismic and structural cross section through the Songliao Basin (Feng et al., 2010). The location of the cross section is indicated in Figure 4.

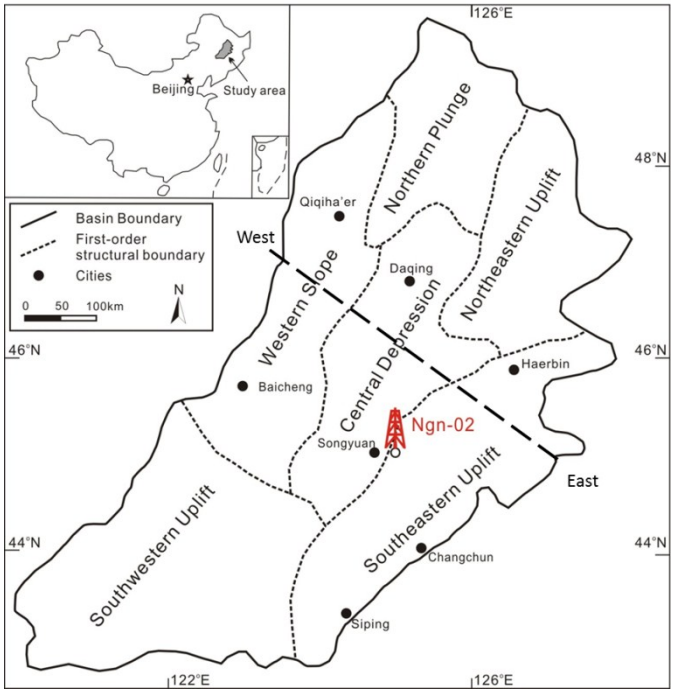

Figure 4: Map of the six structural domains with location of the W-E-trending profile in Figure 3 and the well NGN-dgk-02 (modified after Feng et al., 2010).

2.2 Quantou and Qingshankou formations

In this section, special focus is taken on the Quantou and Qingshankou formations because the studied successions are part of these two formations.

The Quantou Formation is subdivided into four members containing important reservoir horizons, especially in the eastern part of the basin (Yang, 1984). The lowermost three members were deposited under arid or semi-arid conditions, resulting in red-brown, purple and purple-brown sandstones and conglomerate of fluvial and floodplain origin. The central area of the Songliao Basin during deposition of the third member was characterised by shallow lacustrine and deltaic deposits (Figure 5 a). The fourth member of the Quantou Formation contains greyish green or black mudstones, siltstones and sandstones originating from fluvial or lacustrine environments (Figure 5 b; Feng et al., 2010).

The Upper Cretaceous Qingshankou Formation is subdivided into three members. Oil shale occurs in the lower part of the first member, while grey, dark grey and black mudstones are predominant in the overlying succession. During the deposition of the first member of the Qingshankou Formation, the lake had reached its maximum depth and extent of about 87,000 km² (Figure 5 b). Deep lacustrine black mudstone was deposited across the entire central down warp during this period. This sequence is 60 to 100 m thick (Feng et al., 2010).

The uppermost part of the second member and third member of the Qingshankou Formation are characterised by large prograding deltaic systems prograding from the north and west. The area of the lake decreased to about 41,000 km² during these periods (Figure 5 c). The deep lacustrine shales of both members reach a thickness of 300 m (Feng et al., 2010).

According to Wu et al. (2009), the time and duration of the deposition of the oil shale sequence of the Qingshankou Formation (onset: ca. 94.21-94.18 Ma; duration: ca. 210-310 Ka) can be compared with those of the oceanic anoxic event 2 (onset: 94.21 Ma; duration: 320-900 Ka; Hart and Leary, 1989).

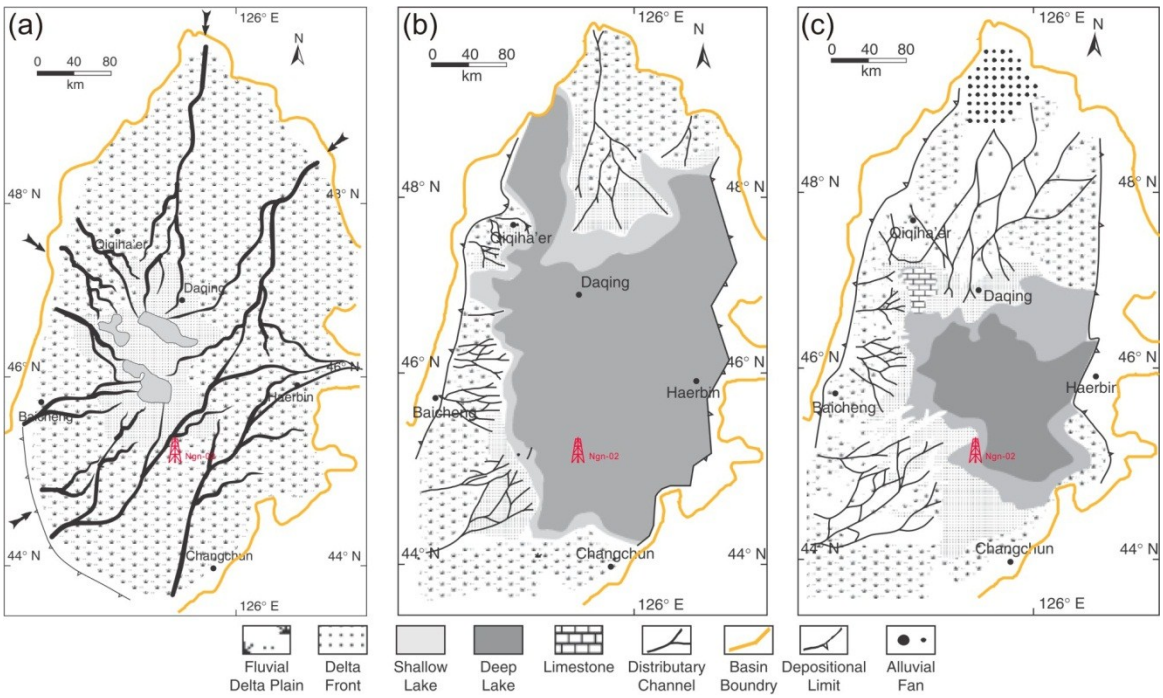

Figure 5: Depositional facies maps of the third member of the Quantou Formation (a), of the fourth member of the Quantou Formation and of the first member of the Qingshankou Formation (b) and of the second and third members of the Qingshankou Formation (b) (modified after Feng et al., 2010). The location of well NGN-dgk-02 is indicated by a red drill rig symbol.

2.3 Geology of borehole NGN-dgk-02

The borehole NGN-dgk-02 was drilled by Shell plc. in the course of an oil shale exploration program. It reaches a total depth of 331.75 m and drilled a succession comprising Quaternary deposits, Qingshankou Formation (member 2 and 1) and Quantou Formation (member 4; Table 1). With the exception of the Quaternary succession, the entire borehole was cored and logged.

Table 1: Formations drilled in borehole NGN-dgk-02.

Top [m]	Bottom [m]	Formation
0.00	30.00	Quaternary
30.00	150.40	Member 2, Qingshankou Fm.
150.40	252.80	Member 1, Qingshankou Fm.
252.80	331.75	Member 4, Quantou Fm.

Figure 6 shows gamma ray (GR), spontaneous potential (SP), acoustic (AC), formation resistivity (Rt) and density (DEN) log curves. The lithology profile is coloured corresponding to the colour of the rocks.

In general, there is a remarkable poor fit between lithology and log response. For example coarser grained sediments in the first member of the Qingshankou Formation between 150 and 190 m are not reflected in the GR response. Nevertheless, oil shale horizons are generally characterised by low density and high GR readings (e.g. between 230 and 240 m).

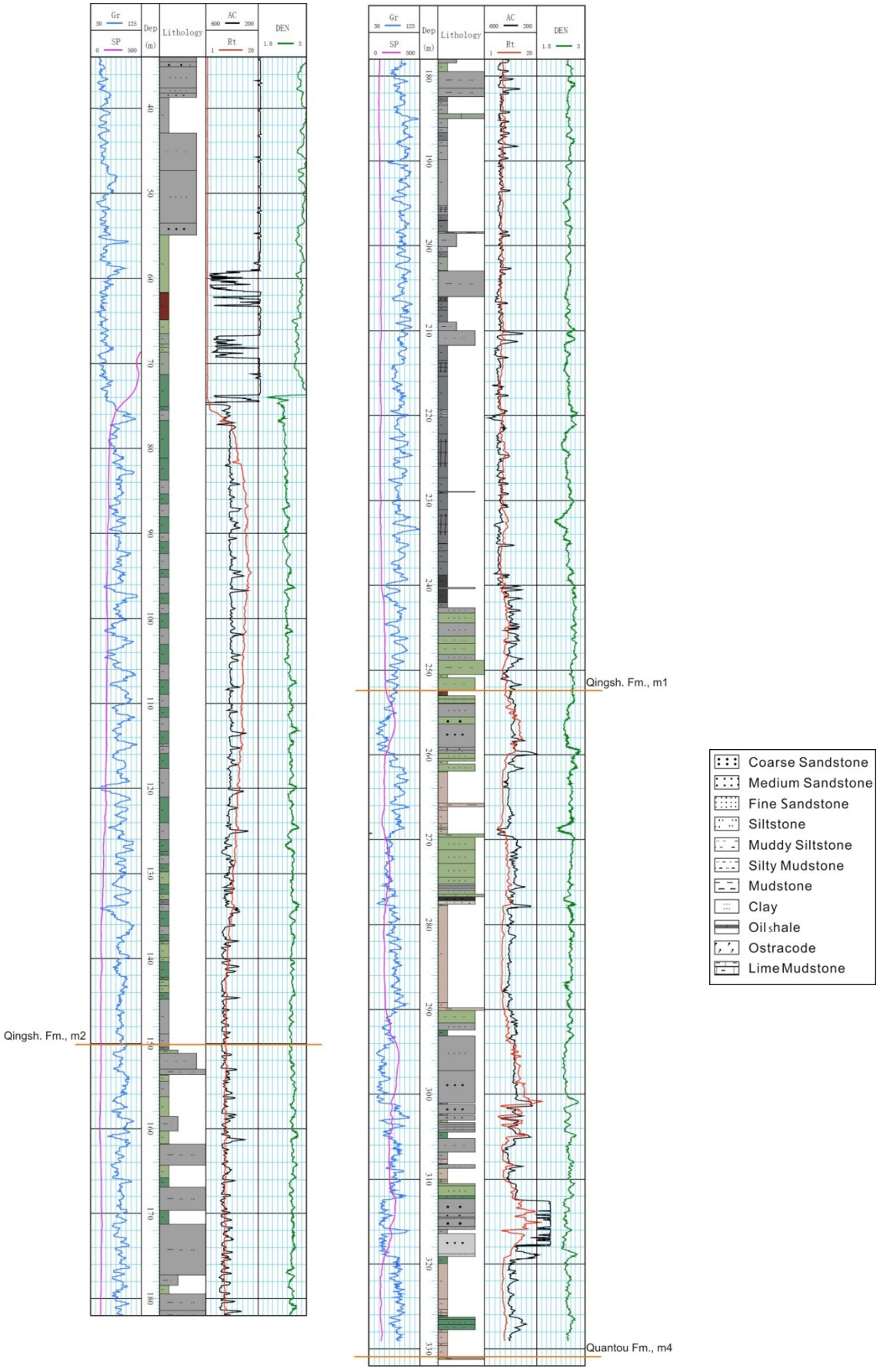

Figure 6: Lithology and log curves of well NGN-dgk-02 (provided by J. Jia; Jilin University).

The fourth member of the Quantou Formation in borehole NGN-dgk-02 mainly consists of greenish, reddish and grey mudstones, siltstones and sandstones. An oil-stained sandstone occurs at a depth of ca. 277 m (Figure 7). The sample "Oil 1" was taken from this layer.

Figure 7: Oil-stained sandstone in the Quantou Formation of borehole NGN-dgk-02.

Core photographs of the first member of the Qingshankou Formation between 155.30 and 245.00 m depth are shown in Appendix 1. This member mainly contains greenish and middle to dark grey mudstone, siltstone, fine to coarse grained sandstone and oil shale. Five oil shale layers occur within the first member at depths of ca. 196, 206, 214, 222 and 233 m (Appendix 1, e.g. box 231.33-233.35 m). The two lowermost layers reach maximum thicknesses of about 3 to 4 m. The middle and dark grey mudstones and siltstones are intercalated with fine to coarse grained light brownish sandstones (Appendix 1, e.g. box 223.20-225.20 m). Sub horizontal calcite veins (Appendix 1, e.g. box 231.33-233.35 m), bioturbation structures (Appendix 1, e.g. box 233.35-235.65 m), thin carbonate layers and nodules (Appendix 1, e.g. box 233.35-235.65 m) occur in some mudstone layers.

The second member of the Qingshankou Formation is characterised by light grey and greenish mudstones.

2.4 Petroleum geological aspect

The first discovery of oil in the Songliao Basin was in the year 1959 in the Fuyu Oil Field at the giant Daqing complex. China's largest oil field – the Daqing Oil Field – is located in the Central Depression zone. A total amount of about 80 detected oil and/or gas fields is distributed in the whole basin, most of them in the Central Depression zone, the Western Slope and the Southeastern Uplift. Oil fields are predominant in comparison to gas fields. Until 1996, approximately 17.6 billion BBOE (barrels oil equivalent) of recoverable oil and 0.3 billion BBOE of recoverable associated gas had been discovered (Ryder et al., 2003).

Ryder et al. (2003) identified two petroleum systems (PS):

Qingshankou-Putaohua/Shaertu PS:
The primary source rock of the Upper Cretaceous Qingshankou-Putaohua/Shaertu petroleum system is the Qingshankou Formation. The first member of the Nenjiang Formation is obtained as secondary source rock. The most productive reservoirs are the Putaohua (member 1 of the Yaojia Formation) and the Shaertu (members 2 and 3 of the Yaojia Formation and member 1 of the Nenjiang Formation) sandstone reservoirs. Most of the petroleum, which mainly migrated vertically, is trapped in large faulted anticlines, fault blocks and faulted anticlinal noses in combination with facies-change and/or diagenetic stratigraphic traps. Numerous local mudstone and siltstone units serve as seal rocks, but in this PS most of the source rocks also act as seals. About 99 % of know petroleum in the Songliao Basin is derived from the Qingshankou-Putaohua/Shaertu system.

Jurassic coal-Denglouku/Nongan PS:
The Jurassic coal-Denglouku/Nongan petroleum system is relatively underexplored. It involves the generation of natural gas from Upper Jurassic coal-bearing source rocks. Major reservoir rocks are sandstones and conglomeratic sandstones of the Lower Cretaceous Denglouku Formation (member 1 and 3) and Quantou Formation (member 1, Nongan reservoir). Most of the vertically migrated gas is trapped in fault blocks and anticlines. The major seal rock is the widespread lacustrine black shale and mudstone of the Qingshankou Formation. Less than 1 % of known petroleum in the Songliao Basin is derived from this PS.

According to Feng et al. (2010), the lacustrine mudstone deposit of the first member of the Qingshankou Formation is a petroleum source rock of high quality. It is 60 to 135 m thick and covers an area of about 87,000 km² (Figure 8). Typical TOC (total organic carbon content) values of the deep lake mudstones vary between 3 and 4 %, decreasing towards the basin margins. The organic matter within this formation originates from sapropelic kerogen (kerogen type I).

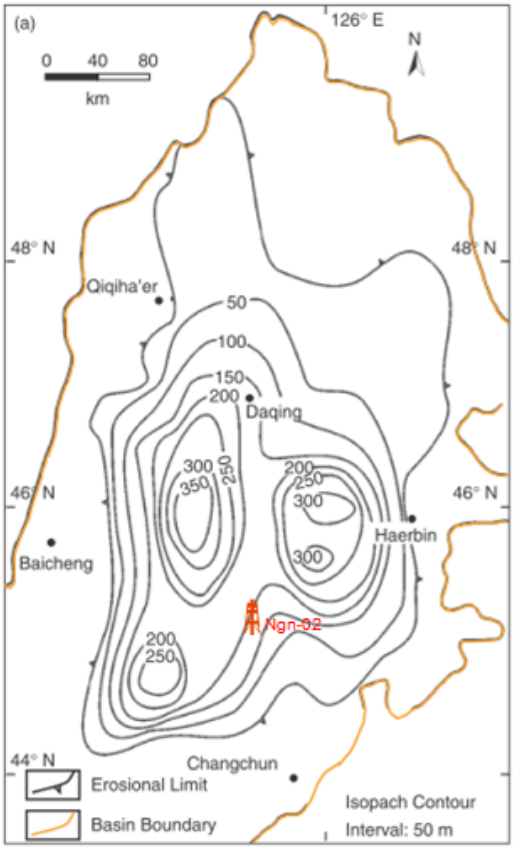

Figure 8: Isopach map of lacustrine mudstone within the first member of the Qingshankou Formation (Feng et al., 2010). The location of well NGN-dgk-02 is indicated by a red drill rig symbol.

According to Liu et al. (2009), Upper Cretaceous source rocks in the Songliao Basin (first member of the Qingshankou Formation; first and second members of the Nenjiang Formation) reach oil shale quality ("Nong'an" oil shales). The oil shale bearing area mainly covers the Southeastern Uplift structural zone and is located about 100 km north of Changchun. The oil shales of the Qingshankou Formation contain kerogen type I and II. According to Liu et al. (2009), the oil shale in the Nong'an area is immature. A thickness map is provided in Figure 9. The first member of the Qingshankou Formation contains five recoverable oil shale layers. The thickness of the oil shale sequence

increases towards the basin centre. Oil shales were formed during maximum flooding periods in an anaerobic semi-deep to deep lacustrine environment. An amount of 155,5748 x 10^4 t of oil shale resources is estimated by Liu et al. (2009).

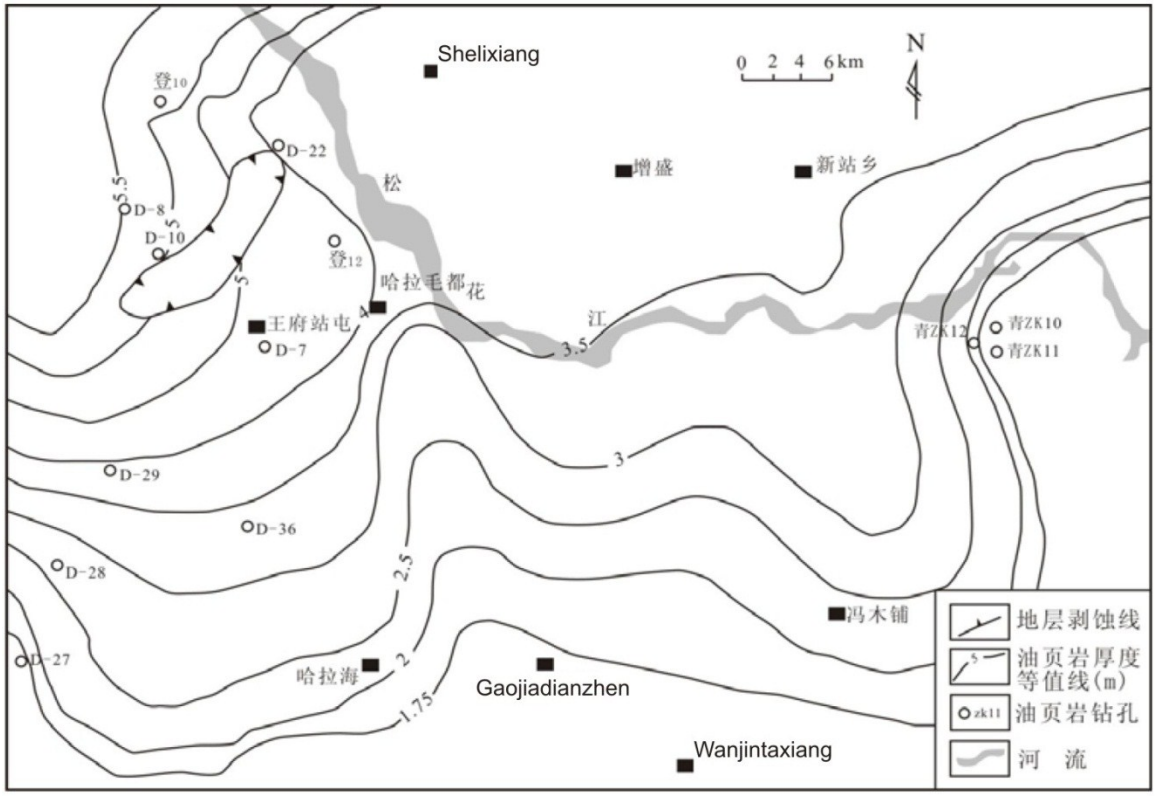

Figure 9: Thickness map of oil shale in the Nong'an area 100 km north of Changchun (modified after Liu et al. (2009)). (Well NGN-dgk-02 is located outside the map area).

3 Samples and methods

A total of 70 samples were collected from drill cores from the well NGN-dgk-02 representing the depth interval from 242.6 m to 156.2 m. The mainly grey-black and dark-grey mudstones including oil shales represent the first member of the Qingshankou Formation. An oil-stained sandstone sample of the Quantou Formation (276.9 m) was also analysed for oil to source rock correlation. Core photographs are shown in Appendix 1. The applied methods are described in the following sections.

3.1 Leco elemental analysis

Leco elemental analysis was used to determine the amount of organic matter in a rock, hence its quality as source rock or oil shale. The total organic carbon content (TOC) was measured in weight% of a powdered dry sample. Good source rocks have TOC contents >2.0 weight% and oil shales have TOC contents >20.0 weight%. However, the latter value strongly depends on the economic situation (i.e. oil price).

All 70 samples, which were powdered, were used for Leco elemental analysis. 20 mg to 50 mg of each sample were prepared with alcohol to determine the total carbon (TC) and sulphur (S) content. The total organic carbon content (TOC) was measured on 20 mg to 50 mg of each sample, which were pre-treated with concentrated hydrochloric acid (HCl) and alcohol. The total inorganic carbon content (TIC) is calculated by the difference between total carbon and TOC and defines the abundance of carbonate minerals. The TIC is used to calculate calcite equivalent percentages (TIC x 8.333) of the samples.

After drying, some tungsten and iron chips were added to the samples. These chips acted as an accelerator for the measurement. The samples were burned at 1500 °C in an oxygenated atmosphere with a Leco 300 CS elemental analyser. Carbon reacted to carbon dioxide (CO_2) and sulphur to sulphur dioxide (SO_2), which was measured by an infrared detector. After every tenth measurement the analyser was calibrated with carbon (501-937) and sulphur (502-449) standards. Every sample was measured four times, i.e. two times for total carbon and sulphur content and another two times for TOC content.

3.2 Rock Eval pyrolysis

The hydrocarbon generation potential, the type of organic matter (kerogen type) and the stage of maturity were defined by Rock Eval pyrolysis, which is a temperature controlled pyrolysis.

A Rock Eval 2 plus analyser from Vinci Technologies was used for this study. 20 mg to 80 mg of each pulverised sample were heated gradually in an inert atmosphere. The amount of pyrolysate (mg HC/g rock) released from kerogen was measured. At first, the sample was heated up to 300 °C. At constant temperature for three minutes, free hydrocarbons were released and were recorded as S_1-peak. Afterwards the sample was heated up to 550 °C with a rate of 25 °C per minute. During this heating period hydrocarbons were generated by thermal cracking of non-volatile organic matter. These hydrocarbons defined the S_2-peak. During the heating process CO_2 was released and measured by an infrared detector as the S_3-peak, but this value had not been recorded in this study. The temperature of maximum hydrocarbon generation (T_{max}) was measured at the maximum value of the S_2-peak. Figure 10 shows the analysis cycle and an example of record of Rock Eval pyrolysis.

Every sample had been recorded twice. A standard and a blank (= empty pot) were measured after every tenth sample for calibration.

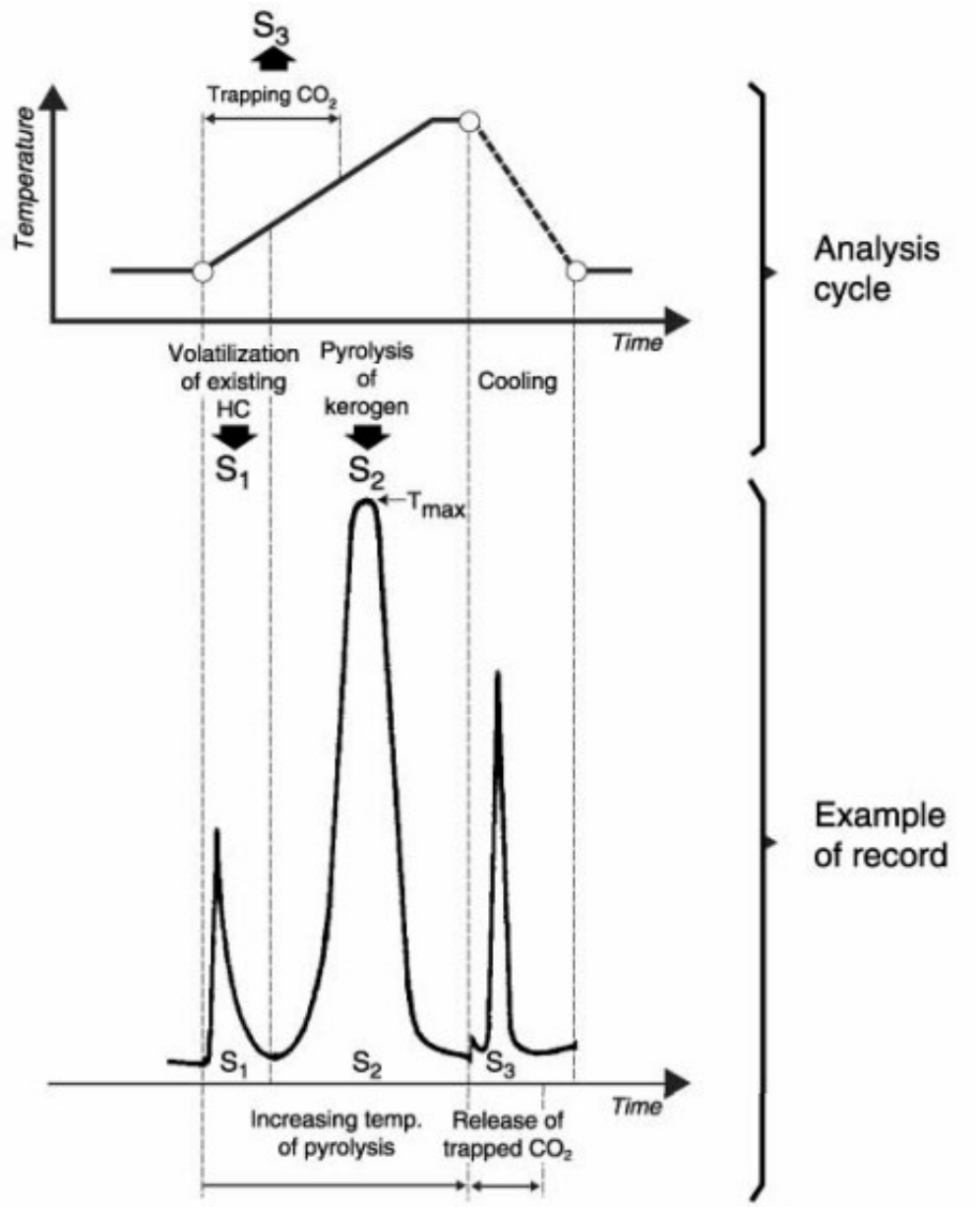

Figure 10: Analysis cycle and an example of record of Rock Eval pyrolysis (Tissot and Welte, 1984).

The hydrocarbon generation potential of a sample can be identified by the sum of S_1 and S_2.

The production index (PI) is the ratio between free hydrocarbons and hydrocarbons which were generated during the heating process:

$$PI = \frac{S_1}{S_1+S_2}$$

This ratio increases with increasing maturity, i.e. the S_1 value increases and the S_2 value decreases. The T_{max} value also gives information about the stage of maturity. These two indices together with the vitrinite reflectance R_o describe the level of thermal maturation (Table 2). The T_{max} value is directly proportional to maturity and reveals that more thermal energy is needed to form hydrocarbons from the kerogen at higher stages of maturity (Killops and Killops, 1997).

Table 2: Geochemical parameters describing level of thermal maturation (Peters, 1986).

	PI [1]	**T_{max} [°C]**	**R_o [%]**
Top of oil window	~0.1	~435-445	~0.6
Bottom of oil window	~0.4	~470	~1.4

The Rock Eval pyrolysis gives general information about the type of organic matter in the sample, if the S_2 value is interpreted together with the TOC content. The hydrogen index (HI) is calculated by the following equation:

$$\mathrm{HI} = \frac{S_2}{\mathrm{TOC}} \times 100 \quad [\mathrm{mg\ HC/g\ TOC}]$$

Oil is generated if the hydrogen index exceeds 300 mg HC/g TOC and if the level of thermal maturity is equivalent to a vitrinite reflectance value of 0.60 % R_o (Peters, 1986).

The composition of kerogen depends on environmental conditions during deposition, i.e. the type of kerogen depends on its original organic matter. Peters, Walters, and Moldowan (2005) distinguish between four types of kerogen:

Kerogen type I:

Type I mainly contains liptinite macerals. Vitrinites and inertinites occur seldom. Kerogens of type I are dominated by algae and remains of bacteria originated in a lacustrine environment. The H/C ratio is high and the sulphur content is relative low. This kerogen type is high oil-prone. The HI exceeds 600 mg HC/g TOC (Peters and Cassa, 1994). Oil shales (e.g. chinese oil shales) mainly contain type I kerogen (Hutton et al., 1980).

Kerogen type II:

Type II is dominated by liptinite, but it can also contain little amounts of vitrinite and inertinite. Type II originates from phytoplankton, zooplankton and bacteria, once living in a marine environment. The H/C ratio is lower and sulphur occurs in a relative high

abundance compared to kerogen type I. This kerogen type is oil-prone. The HI ranges between 300 mg HC/g TOC and 600 mg HC/g TOC (Peters and Cassa, 1994).

Kerogen type III:
Type III kerogen originates from terrigenous plants and mainly contains vitrinite macerals. This kerogen type is gas-prone and yields less hydrocarbons dyring pyrolysis or burial maturation than kerogen types I and II.

Kerogen type IV:
Type IV kerogen is mainly composed of inertinite macerals. This kerogen type is called "dead" carbon because it does not yield significant amounts of hydrocarbons.

3.3 Microscopy

Ten samples were selected for organic petrological investigation. These samples were cut perpendicular to the bedding plane and then embedded in epoxy resin. The grinding and polishing of the polished blocks was done in six different steps using silicon carbide powder (graining: 220, 600 and 1200) and diamond suspension (3 µm, 1 µm and 0.05 µm). Ethylene glycol was used instead of water during the grinding and polishing procedure because of the relative high amount of clay minerals in the samples. This was done to avoid destruction of the sections.

Maceral analysis was performed with a Leica MPV microscope using reflected white and fluorescent light. An oil immersion objective (50x magnification) was used. 500 points per polished section were counted using the single scan-method (Taylor et al., 1998).

Macerals are classified into three groups (vitrinite, liptinite, inertinite). Vitrinite originates from terrestrial organic matter (higher plants), liptinite from lipid-rich plant material (e.g. algae, pollen, spores, resin, cork, cuticules), and inertinite from oxidised material (e.g. char coal). Reflectivity, fluorescence and hydrocarbon potential of the maceral groups is shown in Table 3.

Table 3: Reflectivity, fluorescence and HC potential of different maceral groups.

Maceral group	Reflectivity	Fluorescence	HC potential
Vitrinite	middle	no or weak	gas
Liptinite	dark	strong	oil & gas
Inertinite	bright	no	no

3.4 Vitrinite reflectance

The degree of maturity is determined by the reflectance of vitrinite macerals (Tissot and Welte, 1984; Mukhopadhyay and Dow, 1994). The reflectance increases progressively with thermal maturation. Vitrinite reflectance can only be measured for kerogen types II and III, because of absence of vitrinite in kerogen type I (Killops and Killops, 1997). The oil window is represented by vitrinite reflectance values between 0.65 % R_o and 1.30 % R_o, but oil generation can already start at 0.50 % R_o. R_o values exceeding 1.30 % R_o refer to the gas generating zone.

Two samples which contained the highest amount of vitrinite macerals were selected to measure vitrinite reflectance.

Mean random vitrinite reflectance (R_o) was measured with an incident light Leica MPV microscope using an oil immersion objective (100x magnification). The intensity of reflected monochromatic light with a wavelength of 546 nm was measured with a photomultiplier. An yttrium-aluminium-garnet standard (R=0,899 %) was used for calibration.

3.5 Biomarker analysis

Biomarkers are molecular fossils derived from once living organisms. Biomarkers are complex organic compounds, which consist of carbon, hydrogen, and other elements. Biomarkers can be used to assess the source of organic matter (terrestrial, lacustrine, marine), the depositional environment (salinity, oxidation and reduction conditions), the

maturity, the age of the source rock, and to correlate crude oils with specific source rocks (Peters, Walters and Moldowan, 2005).

23 samples were selected for organic geochemical analysis. The powder of these samples was extracted with dichloromethane at 75 °C and 50 bar in a Dionex ASE 200 accelerated solvent extractor for approximately one hour. After evaporation to 0.5 ml in a Zymark TurboVap 500 closed cell concentrator, asphaltenes were precipitated from a hexane-dichloromethane solution (80:1) and centrifugation was used to separate them. The hexane-soluble fractions were split into saturated hydrocarbons, aromatic hydrocarbons, and NSO (nitrogen, sulphur and oxygen) compounds with Liquid Chromatography (MPLC) of a Köhnen-Willsch instrument (Radke et al., 1980).

The saturated and aromatic hydrocarbons were analysed with a gas chromatograph (Figure 11) equipped with a 30 m DB-5MS fused silica column (inner diameter of 0.25 mm and a film thickness of 0.25 µm) and coupled to a Finnigan MAT GCQ ion trap mass spectrometer (GC-MS system). The temperature of the oven increased from 70 °C up to 300 °C with a rate of 4 °C per minute. At 300 °C temperature was held constant for 15 minutes. Helium was used as carrier gas. The sample was injected split less at a temperature of 275 °C. The electron ionisation mode operated over a scanning range from mass/charge (m/z) 50 to 650 (0.7 seconds per scan). A Finnigan data system processed the data. Compounds were identified on the basis of retention time in the total ion current (TIC) chromatogram and by comparison of the mass spectra with published data.

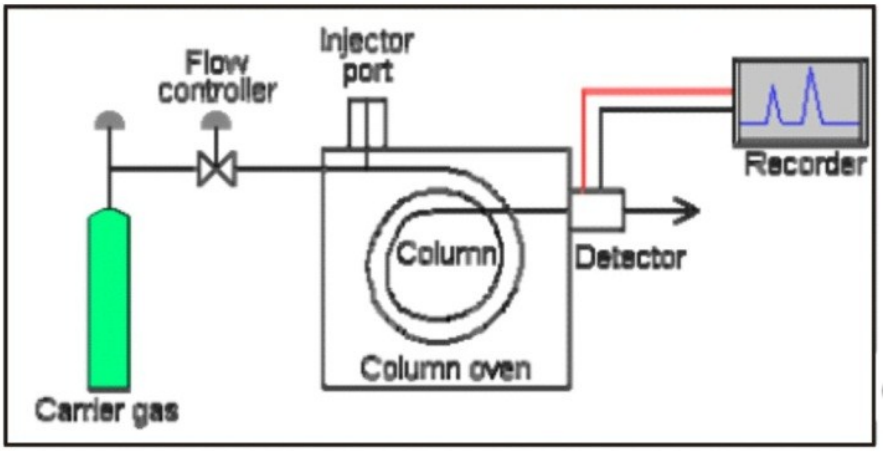

Figure 11: Principle of a gas chromatograph.

Proportions and absolute concentrations of different compound groups were calculated using peak areas in the TIC chromatograms versus internal standards (deuteriated n-tetracosane and 1,1'-binaphthyl) or by integration of peak areas in appropriate mass chromatograms using response factors to correct for the intensities of the fragment ion used for quantification of the total ion abundance. Concentrations were normalised to the TOC content.

3.6 Carbon isotopy

Stable carbon isotopes together with biomarkers are used to determine genetic relationships among oils and bitumens (Peters, Walters and Moldowan, 2005).

The carbon isotopic composition of individual compounds was analysed using 11 samples. For this purpose n-alkanes were separated from branched and cyclic compounds by a 5Å molecular sieving method according to Grice et al. (2008). Carbon isotope determination of n-alkanes, branched and cyclic hydrocarbons was performed by a Trace GC ultra instrument attached to the isotope ratio MS instrument. CO_2 was injected at the beginning and end of each analysis, for calibration. The gas chromatograph column and the temperature programme were the same as for GC-MS. Isotopic compositions were presented as $\delta^{13}C$ (in parts per thousand, ‰) relative to the Peedee Belemnite (PDB) standard. A negative $\delta^{13}C$ value means that the sample is depleted in the heavy isotope relative to the standard (Peters, Walters and Moldowan, 2005).

4 Results and discussion

The main results discussed in this chapter are also presented in a paper submitted to *Organic Geochemistry* (Bechtel et al., 2011).

Most of the results are plotted together with a lithology profile of the Qingshankou Formation.

4.1 Leco elemental analysis

Leco data (total carbon content (TC), total organic carbon content (TOC), sulphur content (S), total inorganic carbon content (TIC), TOC/S ratio and calcite equivalent (Calc.equiv.)) are listed in Appendix 2.

Total organic carbon contents range from 0.74 wt.% to 23.82 wt.%. The measured TOC data fit well with the depth trend which is defined by average TOC content of 1 m core (grey line) provided generously by Shell plc. Sulphur contents vary between 0.35 wt.% and 5.29 wt.%. The distribution of these indicators is shown in Figure 12.

Three cycles with upward increasing TOC (243-232 m, 231-222 m and 221-212 m) can be identified in the lower part of the first member of the Qingshankou Formation. In the upper part of the studied interval TOC values show an upward decreasing trend. The highest TOC values are situated in the lowermost part of the Formation. The maximum TOC content of 23.82 wt.% occurs in sample 29 (Appendix 1; box 231.33-233.35 m). Sulphur contents show an increasing downward trend.

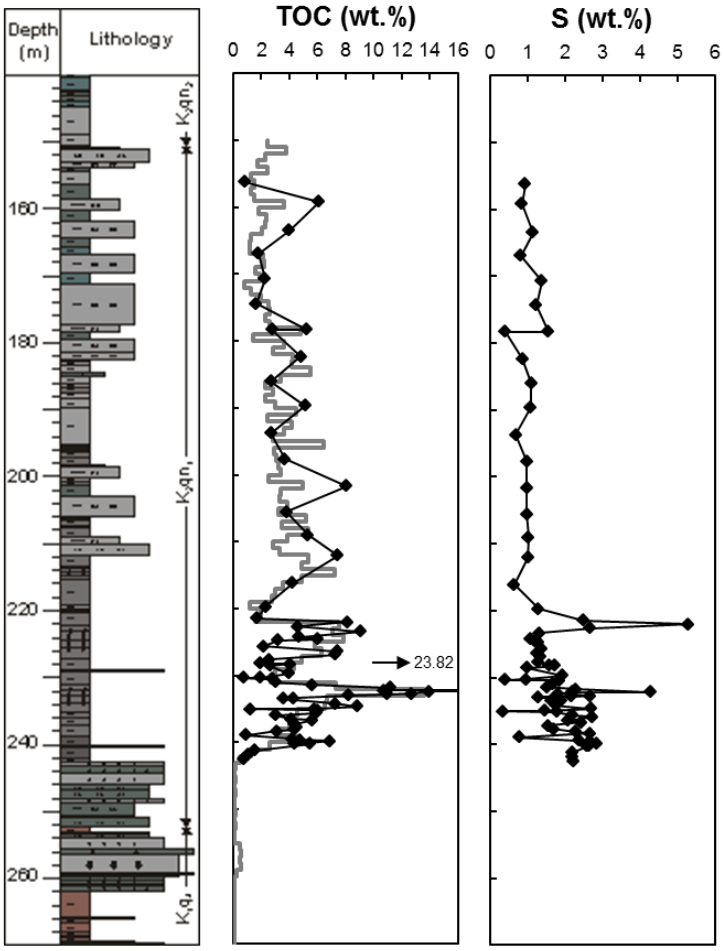

Figure 12: Profiles of TOC and S together with lithology.

In Figure 13 the total inorganic carbon contents, the calcite equivalent percentages (TIC x 8.333) and the TOC/S ratios are plotted.

Carbonate contents are generally low (< 2 wt.% TIC, < 20 wt.% Calc.equiv.). Exceptionally high values were measured in thin carbonate layers or nodules (e.g. sample 19; Appendix 1, box 233.35-235.65 m).

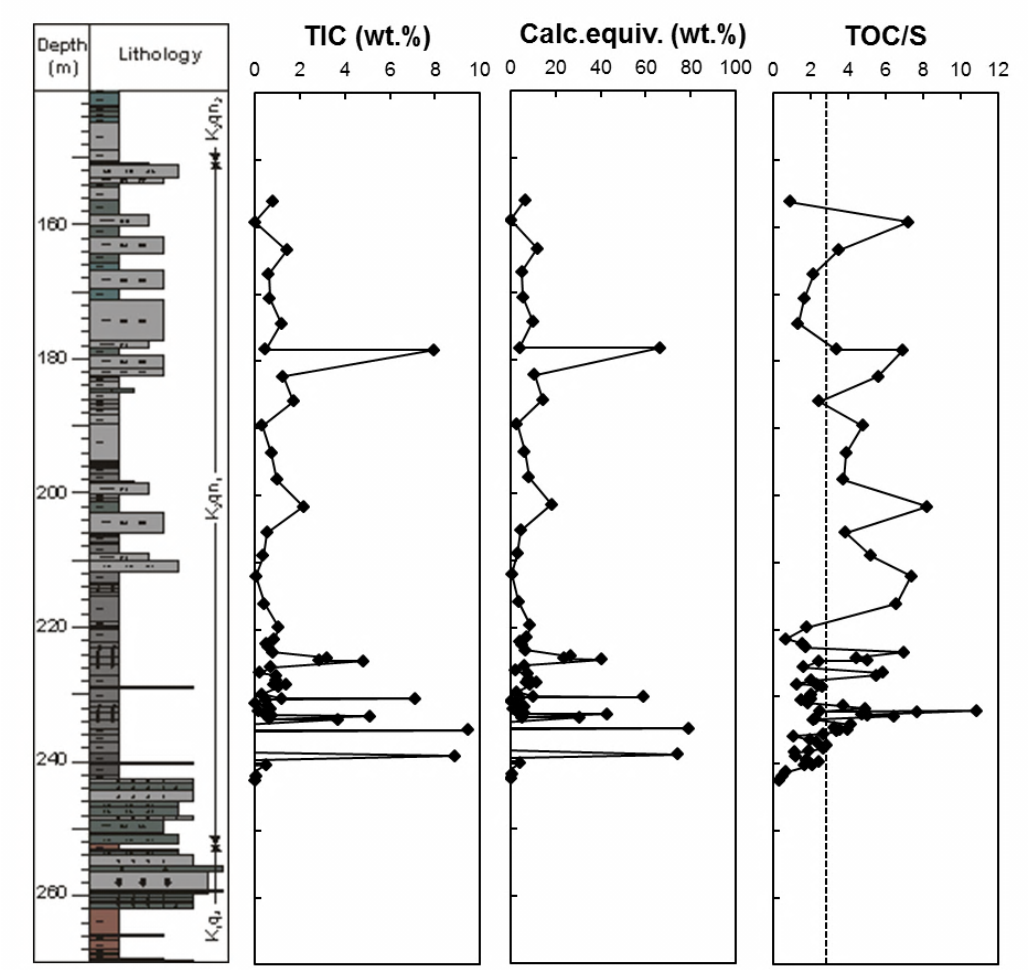

Figure 13: Profiles of TIC, calcite equivalent and TOC/S together with lithology.

TOC/S ratios of 2.8 indicate normal-marine environments. Higher ratios (> 2.8) are observed in freshwater environments, whereas lower ratios (< 2.8) are encountered in oxygen-depleted environments (Berner, 1984).

Within the oil shale sequence of the Qingshankou Formation (below 220 m) TOC/S ratios are typically < 2.8 and show higher TOC/S ratios only in samples with high TOC values. In this interval high values are interpreted to reflect sulphate-limited pyrite formation during periods of high bioproductivity and organic-matter deposition. In the upper part of the first member of the Qingshankou Formation TOC/S ratios are typically > 2.8 and show lower TOC/S ratios at approximately 170 m which can indicate a marine inflow.

4.2 Rock Eval pyrolysis

Data of the Rock Eval pyrolysis (S_1, S_2, temperature of maximum hydrocarbon generation (T_{max}), hydrocarbon generation potential (S_1+S_2), production index (PI) and hydrogen index (HI)) are listed in Appendix 3.

The calculated indices (S_1+S_2, PI and HI) and the lithology profile are shown in Figure 14.

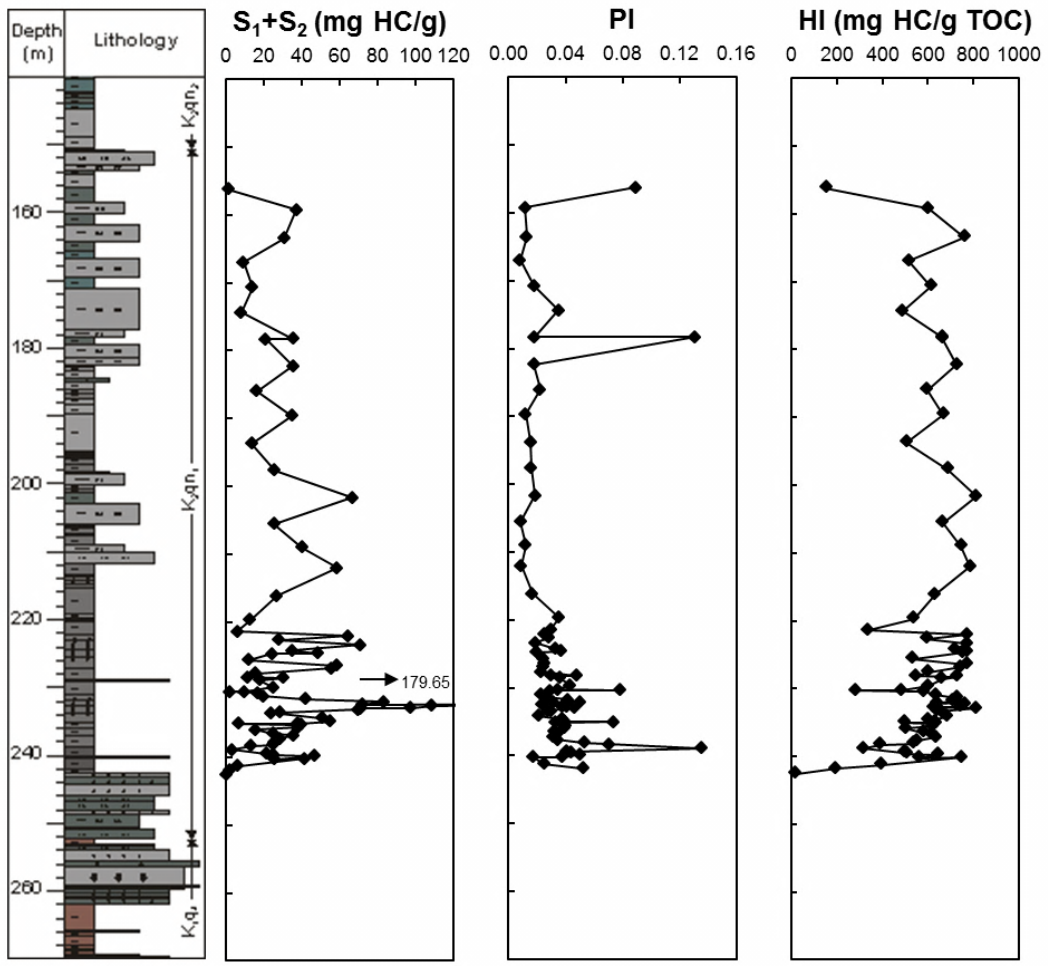

Figure 14: Profiles of S1+S2, PI and HI together with lithology (corresponding legend see Figure 6).

The highest values for the hydrocarbon generation potential are situated within the range of oil shale distribution (220-240 m). Similar to the TOC profile (Figure 12), this index also shows three increasing upward cycles (243-232 m, 231-222 m and 221-212 m) in the lower part of the Qingshankou Formation. Within the oil shale sequence, the hydrocarbon

generation potential has an average value of 37.74 mg HC/g. The highest value amounts to 179.65 mg HC/g and the lowest one to 0.26 mg HC/g.

The low PI values (< 0.1) and the observed T_{max} values (430-443 °C) indicate marginal maturity (Peters, 1986).

The majority of HI values are within a range of 600 mg HC/g TOC to 800 mg HC/g TOC, i.e. most of the samples contain a type I kerogen (Figure 15).

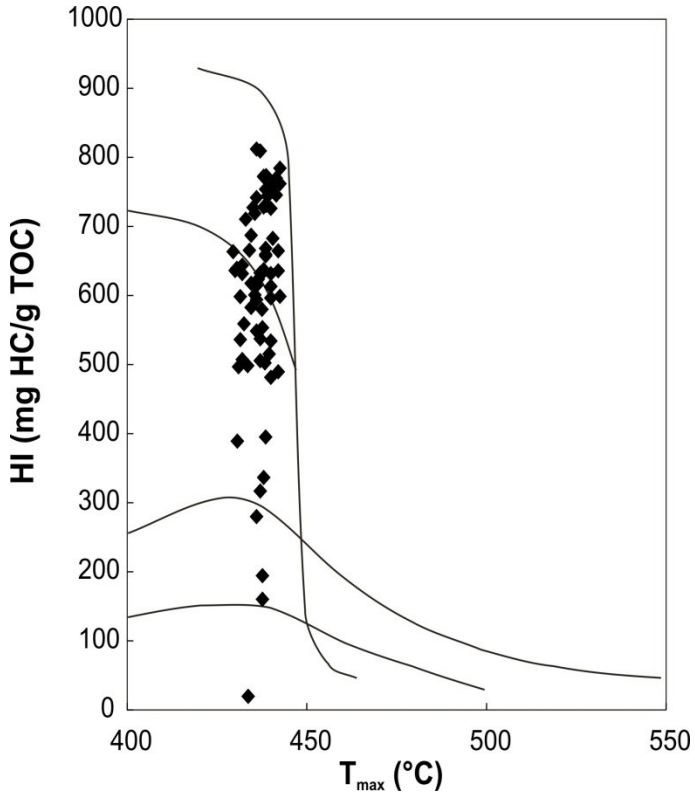

Figure 15: Samples of the Qingshankou Formation (black dots) plotted in the HI versus T_{max} diagram (according to Espitalié et al., 1984).

A plot of S_2 versus TOC (Langford and Blanc-Valleron, 1990) is shown in Figure 16. Both parameters show a very good correlation (R^2=0.98) indicating little (or no) variation in the kerogen type. The "true" average HI is indicated by the slope of the regression line (x 100). Therefore, according to Figure 16, the "true" HI of samples from the Qingshankou Formation is 760. This indicates that relatively low HI values in Figure 15 are due to the mineral matrix effect (Langford and Blanc-Valleron, 1990).

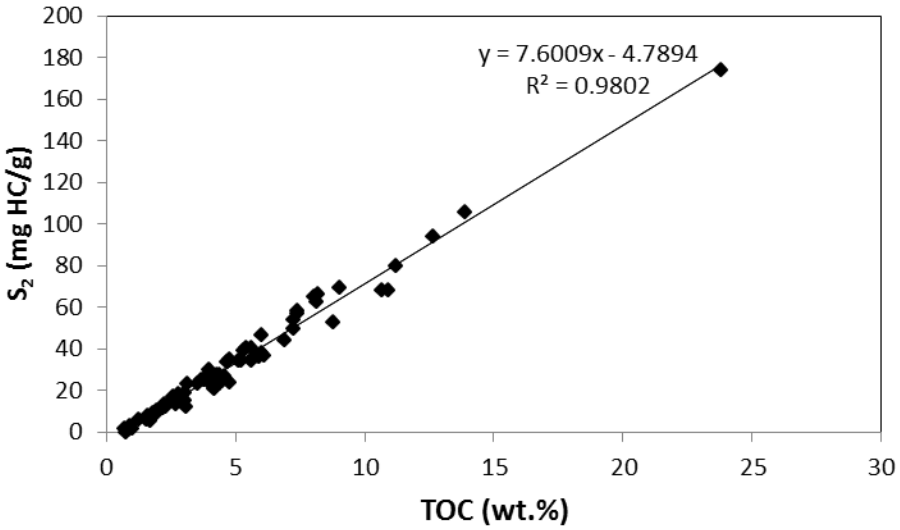

Figure 16: Samples of the Qingshankou Formation (black dots) plotted in the S_2 versus TOC diagram (according to Langford and Blanc-Valleron, 1990).

4.3 Microscopy

10 samples from the oil shale sequence were selected for maceral analysis.

The following macerals have been distinguished (typical microphotographs of these macerals are shown in Appendix 6):

- Vitrinite (e.g. microphotograph of sample 17)
- Inertinite (e.g. microphotograph of sample 30)
- Lamalginite (e.g. microphotograph of sample 29)
- Telalginite (e.g. microphotograph of sample 25)
- Sporinite (no microphotograph)
- Exsudadinite (e.g. microphotograph of sample 45)

The most abundant macerals are lamalginite and telalginite.

Inertinite and vitrinite occur very rarely and form tiny fragments. Inertinite particles are distinguishable from vitrinite mainly on the basis of their higher reflectance. Both macerals show no fluorescence.

Lamalginite originates from thin-walled colonial or unicellular algae and bacteria which occur as distinct laminae but show little to no recognisable biological structure. Telalginite consists of large colonial or thick-walled unicellular organisms which show some internal structure. Telalginite originates from algae like Botryococcus, Tasmanites and Gloeocapsomorpha (Hutton, 1987). The macerals of the liptinite group show a strong fluorescence.

Sporinite occurs only in sample 27 and looks like a flattened spheroid with a strong fluorescence.

Exsudadinite is located in the cracks of fishbones. This maceral is known as migrated bitumen which exhibits a strong fluorescence.

The relative amounts of different macerals and mineral matrix for each sample are listed in Appendix 4. The percentage of macerals on a mineral matrix free basis (mmf) is listed in Appendix 5. The sum of terrestrial organic matter (sum of sporinite, vitrinite and inertinite), lamalginite and telalginite (mmf) is shown in Table 4 and plotted versus depth in Figure 17.

Table 4: Proportions of terrestrial organic matter (vitrinite, inertinite and sporinite), lamalginite and telalginite calculated on a mineral matter free basis.

Sample	Depth [m]	Terrestrial OM [%]	Lamalginite [%]	Telalginite [%]
45	224.75	0.57	99.43	0.00
36	230.31	0.00	53.74	46.26
35	230.35	0.00	100.00	0.00
30	232.19	0.58	87.86	11.56
29	232.15	0.96	95.18	3.86
27	232.74	2.71	88.24	9.05
25	232.94	1.01	63.09	35.91
17	235.60	0.00	83.33	16.67
12	237.69	0.78	70.31	28.91
4	240.20	1.94	98.06	0.00

The input of terrestrial organic matter during the deposition of oil shales in the Qingshankou Formation is relative low (< 5 vol.%). Lamalginite dominates in all samples. Telalginite is also present in a relatively high amount in samples 12, 17, 25, 27, 29, 30 and 36. Within this depth interval proportions are very variable. Thus, a depth trend is not definable.

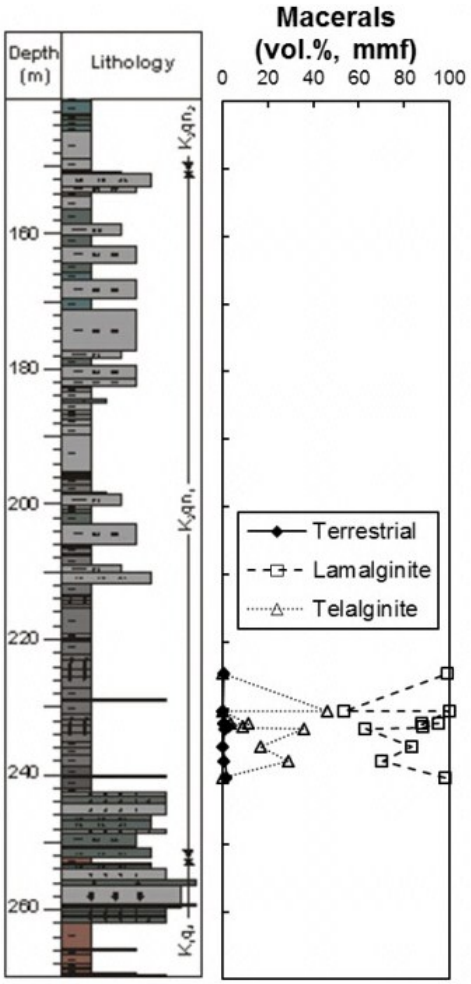

Figure 17: Proportions of terrestrial organic matter (sum of vitrinite, inertinite and sporinite), lamalginite and telalginite (mineral matter free basis).

4.4 Vitrinite reflectance

Two samples (No. 4 and 27) were selected for vitrinite reflectance measurement. The selection was based on the content of vitrinite. As discussed in a previous section, vitrinite is very rare in type I kerogen. Thus, a very small amount of vitrinite is present within the samples of the oil shale sequence of the Qingshankou Formation. Sample 4 and 27 contain some – but still a low amount of - vitrinite particles. Consequently, the number of measuring points is low and the calculated mean values are not very reliable.

The results of the vitrinite reflectance measurement are listed in Table 5. R_o values around 0.7 indicate that the organic matter is marginal mature (top of oil window according to Table 2; chapter 3.2).

Table 5: Results of the vitrinite reflectance measurement (R_o= mean random reflectance, n= number of measuring points, s=standard deviation).

	Sample 4	**Sample 27**
R_o[%]	0.68	0.72
n	25	13
s	0.028	0.046

4.5 Biomarker analysis

Concentrations and concentration ratios of compounds and compound groups in the hydrocarbon fractions of 23 samples of the Qingshankou Formation and of the extracted oil of the oil-stained sandstone of the Quantou Formation are listed in Appendix 7.

The amount of extractable organic matter (EOM) and its composition in terms of saturated hydrocarbons (Sat.HC), aromatic hydrocarbons (Aro.HC), heterocompounds (NSO) and asphaltenes (Asphalt.)) are listed in Appendix 8.

The extractable organic matter (EOM) ranges from 15.5 to 69.5 mg/g TOC. The highest values are obtained from samples of the oil shale sequence. The relative amount of saturated hydrocarbons (average of 34 % of EOM) is higher than that of aromatic hydrocarbons (average of 9 % of EOM) in all samples. The amount of heterocompounds (NSO) varies between 42 and 68 % of the extractable organic matter. The percentages of the asphaltenes are low (average of 5 % of EOM).

Figure 18 shows total ion chromatograms of the alkane fractions of representative samples of the oil shale sequence of the Qingshankou Formation and of the oil-stained sandstone of the Quantou Formation (oil 1).

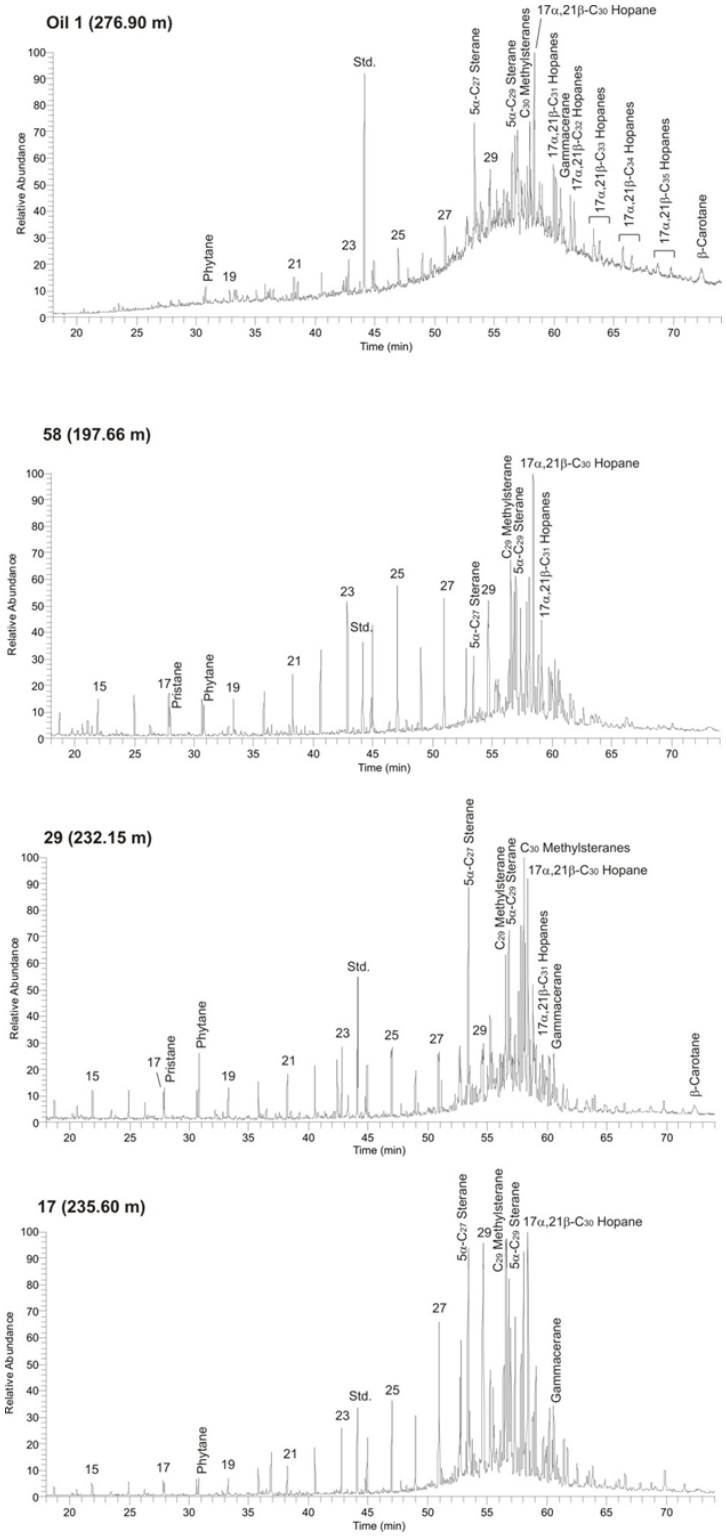

Figure 18: Total ion chromatograms of saturated hydrocarbon fractions of samples of the oil shale sequence of the Qingshankou Formation and of extracted oil from oil-stained sandstone from the Quantou Formation (oil 1). n-alkanes are labelled according to their carbon number. (Std.=standard; deuteriated n-tetracosane).

Gas chromatograms of aromatic hydrocarbon fractions of four samples of the Qingshankou Formation and one of the extracted oil from oil-stained sandstone of the Quantou Formation (oil 1) are plotted in Figure 19.

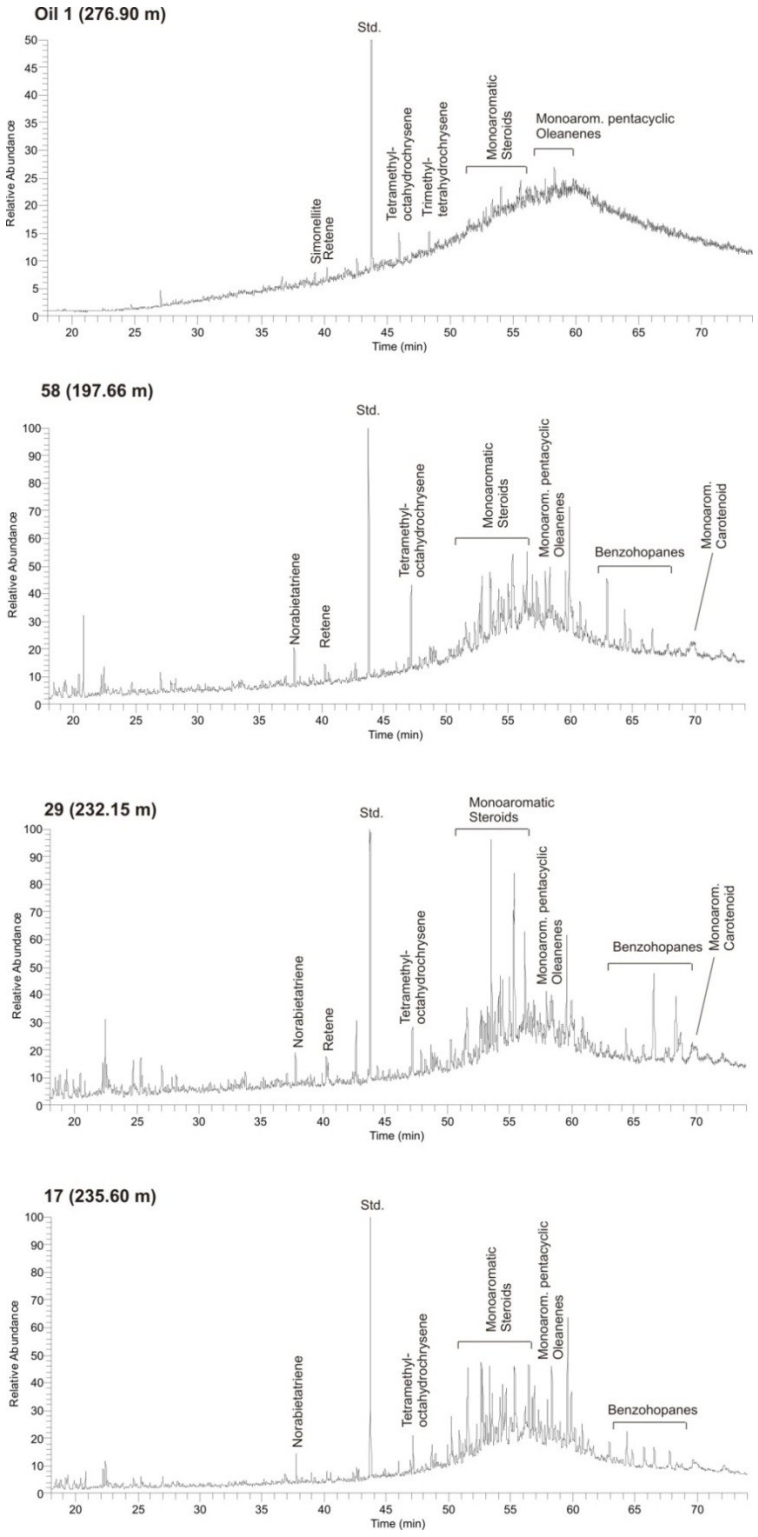

Figure 19: Gas chromatograms of aromatic hydrocarbon fractions of samples of the oil shale sequence of the Qingshankou Formation and of extracted oil from oil-stained sandstone from the Quantou Formation (oil 1). (Std.=standard; 1,1'binaphthyl).

4.5.1 Straight chain alkanes

Alkanes of the Qingshankou Formation are characterised by high abundances of n-alkanes of intermediate chain length (C_{21}-C_{25}) and of long chain length ($\geq C_{27}$). Odd numbered n-alkanes are dominating over the even numbered n-alkanes. This predominance is reflected in the carbon preference index (CPI) which is calculated using the formula of Bray and Evans (1961):

$$\mathrm{CPI} = \frac{1}{2}\left(\frac{C_{25}+C_{27}+C_{29}+C_{31}+C_{33}}{C_{24}+C_{26}+C_{28}+C_{30}+C_{32}} + \frac{C_{25}+C_{27}+C_{29}+C_{31}+C_{33}}{C_{26}+C_{28}+C_{30}+C_{32}+C_{34}}\right)$$

All samples are characterised by CPI values between 1.0 and 1.8 (Figure 28).

Differences in n-alkane distributions can be seen from four representative mass chromatograms of samples from the Qingshankou Formation (Figure 20).

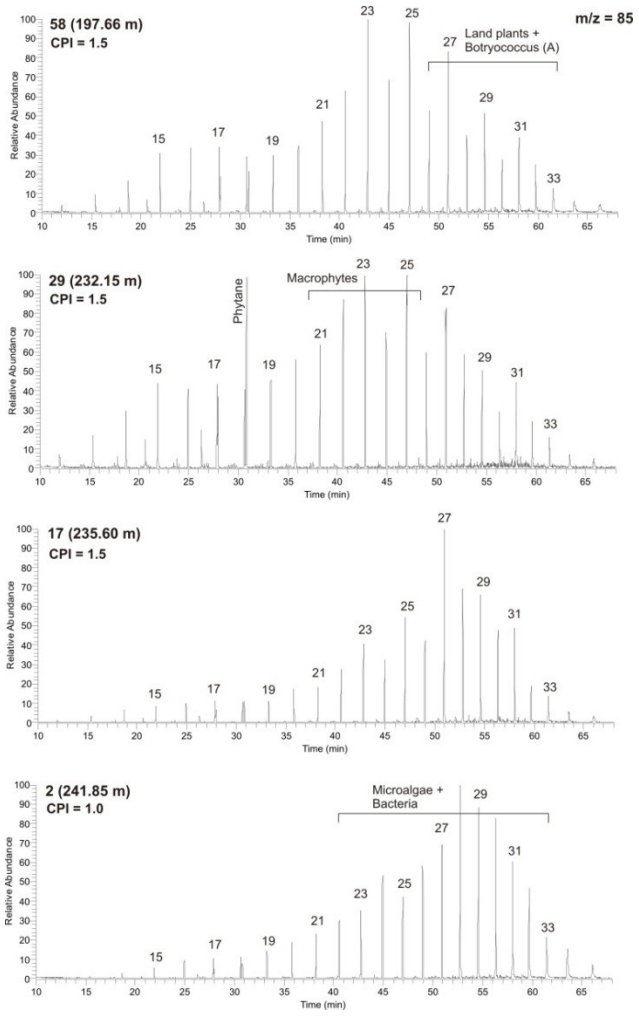

Figure 20: Mass chromatograms (m/z 85) of four representative samples of the Qingshankou Formation, showing differences in n-alkane distributions. n-alkanes are labelled according to their carbon number and possible origins are indicated.

Samples from the lower parts of the Qingshankou Formation (sample 1 to 25) show high proportions of long chain n-alkanes ($\geq C_{27}$) without a significant odd/even predominance (OEP). These distributions are usually obtained from mature sediments with high abundances of terrestrial organic matter (e.g. vascular plants; Tissot and Welte, (1984)). Due to the higher content of n-alkanes in land plants than in aquatic organic matter, terrestrial organic matter is usually overestimated on the basis of alkanes (Peters, Walters and Moldowan, 2005). Moreover, the low vitrinite content and the relative low CPI values are inconsistent with a high land plant contribution. According to Volkman et al. (1998), long chain n-alkanes may also originate from microalgae or bacteria and according to Derenne et al. (1988) and Metzger et al. (1991), certain non-marine algae (e.g. botryococcus braunii) may contribute to n-alkanes $\geq C_{27}$.

Samples from the upper parts of the Qingshankou Formation (sample 27 to 29) show higher abundance of n-alkanes with intermediate chain length (C_{21}-C_{25}). This may be a result of increased organic matter originating from submerged or floating freshwater aquatic macrophytes (Ficken et al., 2000).

4.5.2 Isoprenoids

Pristane and phytane belong to the compound group of isoprenoids. Both of them are present in all samples of the Qingshankou Formation (Figure 26). The Pristane to Phytane ratio values (Pri/Phy) are relative low (0.27-0.29). Pri/Phy values lower than 1.0 indicate an anaerobic environment during early diagenesis (Didyk et al., 1978). The observed low Pri/Phy values are consistent with anoxic bottom water conditions with free H_2S in the water column (Kohnen et al., 1991).

4.5.3 Steroids

Mass chromatograms (m/z 217+231) for steranes and methylsteranes of a representative sample (sample 29) of the Qingshankou Formation and of the oil-stained sandstone (oil 1) of the Quantou Formation are shown in Figure 21.

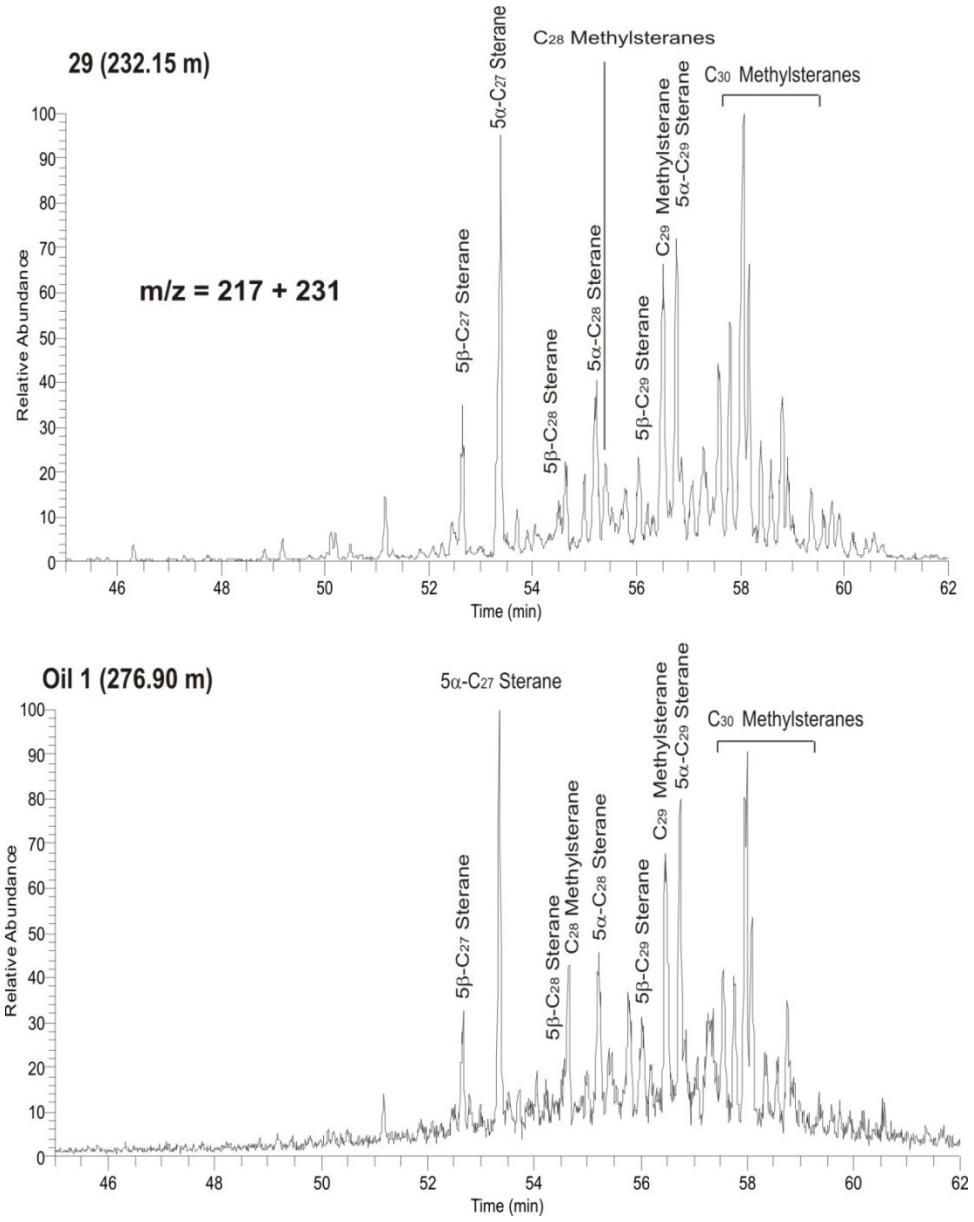

Figure 21: Mass chromatograms (m/z 217+231) for steranes and methylsteranes of a representative sample (sample 29) of the Qingshankou Formation and of the oil-stained sandstone (oil 1) of the Quantou Formation.

A high amount of steranes is present in all samples of the Qingshankou Formation. The highest values for the absolute concentration of steranes (> 500 µg/g TOC) occur within the oil shale sequence of the Qingshankou Formation (Figure 28).

C_{28} to C_{30} methylsteranes are present in high abundance (Figure 28). Monoaromatic steroids occur in all samples within a range of 5 and 167 µg/g TOC.

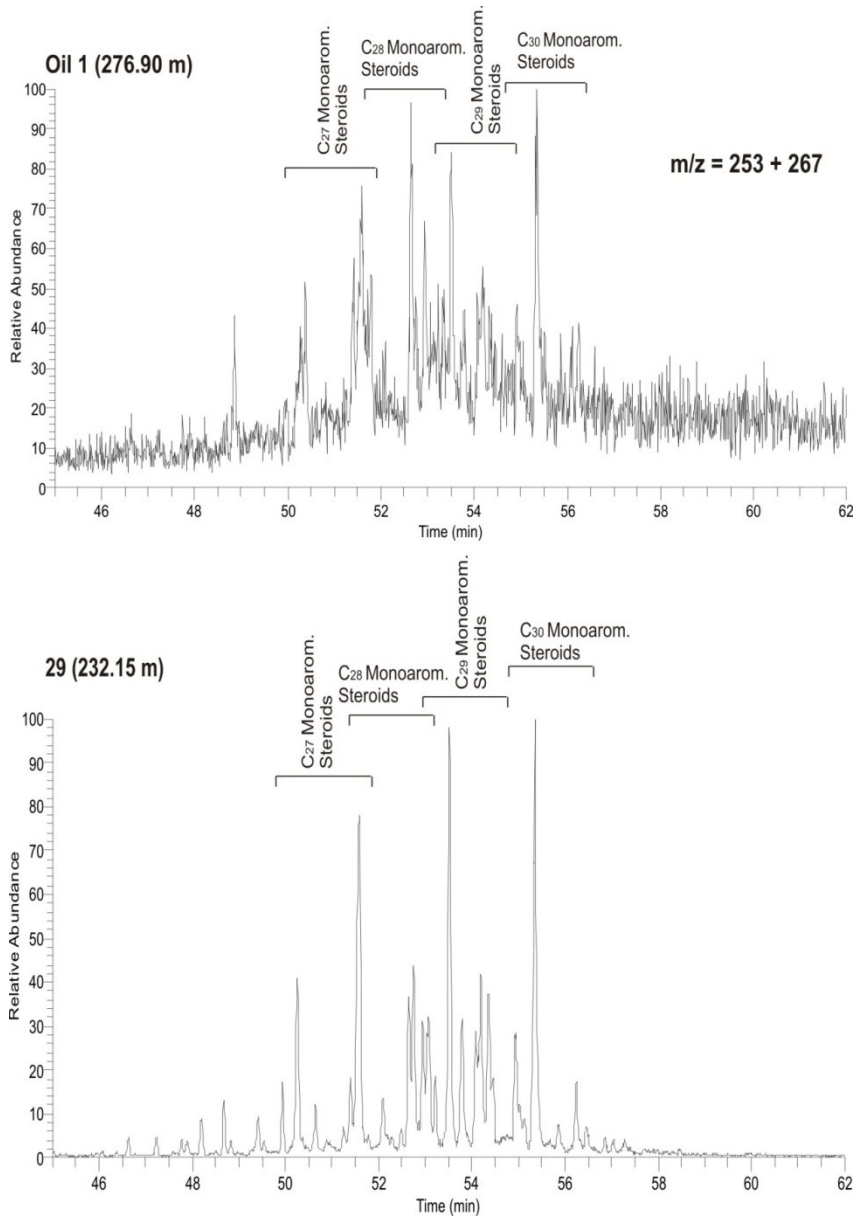

Figure 22: Mass chromatograms (m/z 253+267) for monoaromatic steroids of the sample of the oil-stained sandstone of the Quantou Formation (oil 1) and of a representative sample of the oil shale sequence of the Quingshankou Formation (sample 29).

C_{27} sterols are primarily produced by algae, C_{29} sterols by land plants (Volkman, 1986). Methylsteroids with a C_{30} dinosterol structure originate from dinoflagellates (Robinson et al., 1984), while C_{30} 4-methylsteroids are related to marine and lacustrine bacteria and dinoflagellates (Peters, Walters and Moldowan, 2005).

All this information may indicate that the organic matter originates from lacustrine phytoplankton living in the photic zone with a minor input of terrestrial organic matter (e.g. land plants). The relative high amount of 4-methylsteranes may originate from

dinoflagellates. According to Hou et al. (2000), dinoflagellates occurring in brackish water were actually found in significant amounts in the first member of the Qingshankou Formation.

4.5.4 Hopanoids

Hopanoids are non-aromatic cyclic triterpenoids. Mass chromatograms (m/z 191) for triterpenoids of the sample of the oil-stained sandstone of the Quantou Formation (oil 1) and of one representative sample from the oil shale sequence in the Qingshankou Formation (sample 29) are plotted in Figure 23.

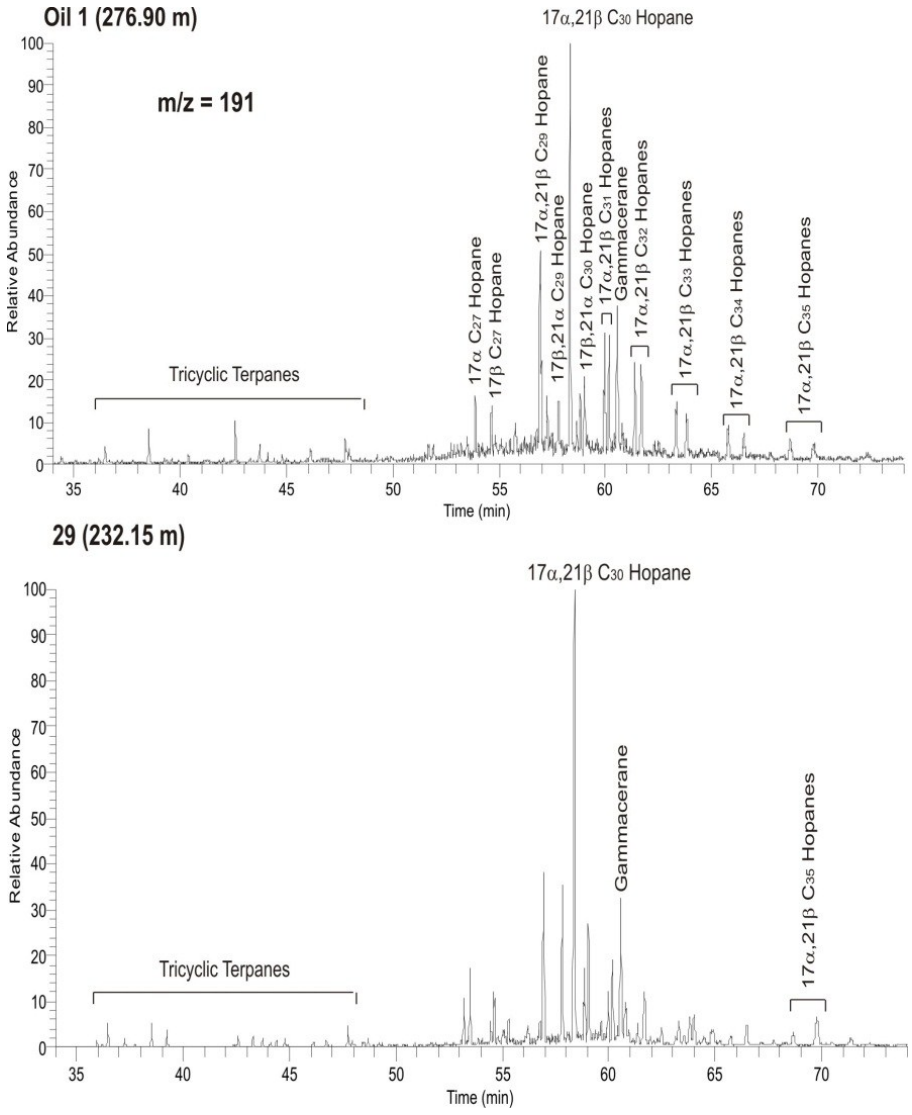

Figure 23: Mass chromatograms (m/z 191) for triterpenoids of the sample of the oil-stained sandstone of the Quantou Formation (oil 1) and of one representative sample of the oil shale sequence of the Qingshankou Formation (sample 29).

The 17α,21β C_{30} hopane is predominating in the hopanoid patterns. The average of the (22S/(22S+22R))-isomer ratios of the 17α,21β C31 hopane shows a value of 0.41. This average value agrees with a vitrinite reflectance value of ca. 0.5 % R_r (Mackenzie and Maxwell, 1981). This value is slightly lower than the values obtained from the vitrinite reflectance measurements. The highest concentrations of hopane (> 500 µg/g TOC) are obtained within the oil shale sequence of the Qingshankou Formation (Figure 28). The C_{31} methylhopane occurs in all samples and shows highest abundances within the oil shale sequence.

The hopane compounds may derive from bacteriohopanepolyols (Ourisson et al., 1979; Rohmer et al., 1992), which have been identified in bacteria and in some cryptogams (e.g. moss, ferns).

The values for the steroid to hopanoid ratio are relative high (> 1.0) and show the highest values within the oil shale sequence of the Qingshankou Formation (Figure 28). A high value is typically observed from algal-dominated organic facies (Mackenzie, 1984). The high values of the steroid/hopanoid ratios during the deposition of the Qingshankou Formation may indicate eutrophic conditions and high bioproductivity within the photic zone of the water column (Peters, Walters and Moldowan, 2005).

4.5.5 Gammacerane

Gammacerane occurs in all samples of the Qingshankou Formation (Figure 27). The gammacerane index can be calculated according to the equation of Sinnighe Damsté et al. (1995):

$$\text{Gammacerane Index} = \frac{\text{Gammacerane}}{\text{Gammacerane} + \alpha\beta C_{30}\ \text{hopane}}$$

The values of the gammacerane indices are negatively related to the values of the Pri/Phy ratios and vary between 0.07 and 0.43.

The presence of gammacerane indicates salinity stratification of the water column during deposition of the sediments. Gammacerane occurs in lacustrine and marine sediments (Sinnighe Damsté et al., 1995; Grice et al., 1998). According to Peters, Walters and

Moldowan (2005), high values of the gammacerane index occur together with low values of Pri/Phy ratios and carotenoid derived components.

4.5.6 Chromans

MTTCs (methylated 2-methyl-2-(trimethyltridecyl)chromans) are present in all samples (Figure 27). The amount varies between 2 and 23 µg/g TOC.

MTTCs have been used for the reconstruction of paleosaline environments (Sinnighe Damsté et al., 1993; Barakat and Rullkötter, 1997).

The MTTC ratio is defined as the concentration ratio of trimethyl MTTC relative to the sum of methylated MTTCs (Sinnighe Damsté et al., 1987). Similar to the gammacerane index, the MTTC ratio reflects salinity stratification. The values of the MTTC ratio show a negative relationship to the values of the gammacerane index (Figure 24).

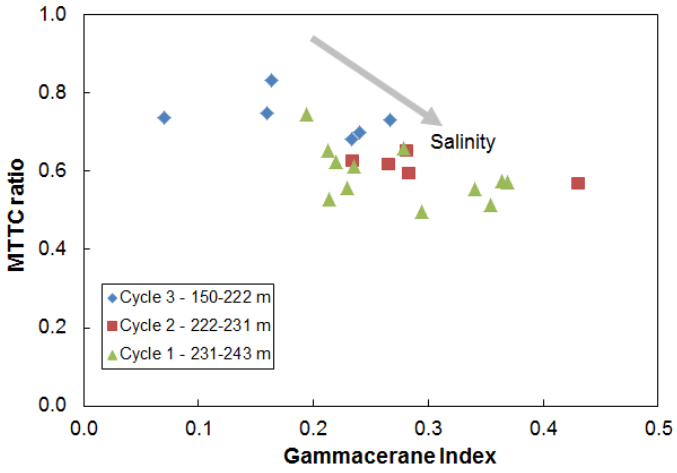

Figure 24: Cross correlation of MTTC ratio versus gammacerane index, outlining salinity stratification. The samples are separated into three cycles. Cycle 3 defines the upper part of the Qingshankou Formation, Cycle 2 and 1 define the oil shale sequence of the Qingshankou Formation.

Figure 25 shows a cross plot of MTTC ratio and Pri/Phy ratio. Areas of environments with different salinities are displayed according to ten Haven et al. (1988). The position of the samples in the plot indicates that the upper part of the Qingshankou Formation was deposited during normal saline conditions and the oil shales were deposited during mesosaline conditions.

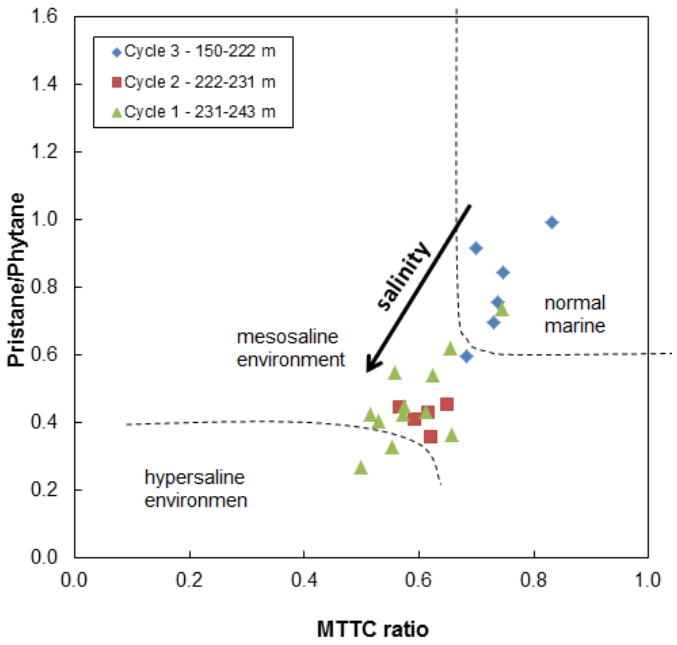

Figure 25: Cross correlation of Pri/Phy ratio versus MTTC ratio, outlining salinity stratification. The samples are separated into three cycles. Cycle 3 defines the upper part of the Qingshankou Formation, Cycle 2 and 1 define the oil shale sequence of the Qingshankou Formation.

4.5.7 Carotenoid derived components

A relative high concentration of β-carotane is present within the oil shale sequence of the Qingshankou Formation (Figure 26). β-carotane is an indicator for highly reducing conditions involving salinity stratification. It occurs in lacustrine and highly restricted marine depositional settings (Peters, Walters and Moldowan, 2005). The values of β-carotane show a negative relationship to the values of MTTC ratio.

The C_{14} arylisoprenoid is present in all samples of the Qingshankou Formation and shows a relative high abundance within the oil shale sequence (Figure 26).

Arylisoprenoids originate from the photosynthetic green sulphur bacteria (Summons and Powell, 1987). According to Summons (1993), these bacteria need light and H_2S for growth. Thermal and salinity stratification are usually involved, and euxinic conditions in the water column are required (Pfennig, 1977).

4.5.8 Diterpenoids and non-hopanoid triterpenoids

Aromatic diterpenoids occur in low abundances in all samples of the Qingshankou Formation and show a slightly enhanced occurrence within the oil shale sequence (> 10 µg/g TOC).

Non-hopanoid triterpenoids are present within the whole Qingshankou Formation (Figure 28). Non-hopanoid triterpenoids are possible biomarkers for angiosperms, which originate from wood, roots and bark (Karrer et al., 1977).

4.5.9 Vertical variation of facies-dependant biomarker

Down core variations of facies-dependant biomarker ratios are plotted versus depth in Figure 26, Figure 27 and Figure 28.

Redox proxies:

Well established redox proxies are the pristane/phytane (Pri/Phy) ratio, the concentrations of β-carotane and C_{14} arylisoprenoids (Peters, Walters and Moldowan, 2005; Figure 26).

Pri/Phy values are lower than 1.0. The lowest values are obtained in the oil shale sequence. In the upper cycle of the Qingshankou Formation the values are increasing upwards, but show a decrease between 170 and 180 m.

Relative high abundances of β-carotane occur within the oil shales of the Qingshankou Formation. The concentration of β-carotane decreases at the top of the first cycle within the oil shale sequence and then increases again in the second cycle. The values are relatively low in the third cycle.

C_{14} arylisoprenoids show a relative high abundance in the oil shale sequence. They show an increasing upward trend in the first cycle, but are decreasing at the top. These values stay constant in the second cycle, but increase at the top. The concentrations decrease upwards above the oil shales.

These redox proxies indicate an anoxic environment involving a stratified water column with free H_2S during the deposition of the oil shales (cycle 1 and 2) and freshwater

conditions in the third cycle. Hence, the anoxic-oxic boundary shows the highest position during the deposition of the first cycle. It is located lower in the second cycle compared to the first cycle, but shows the lowest position during the deposition of the third cycle.

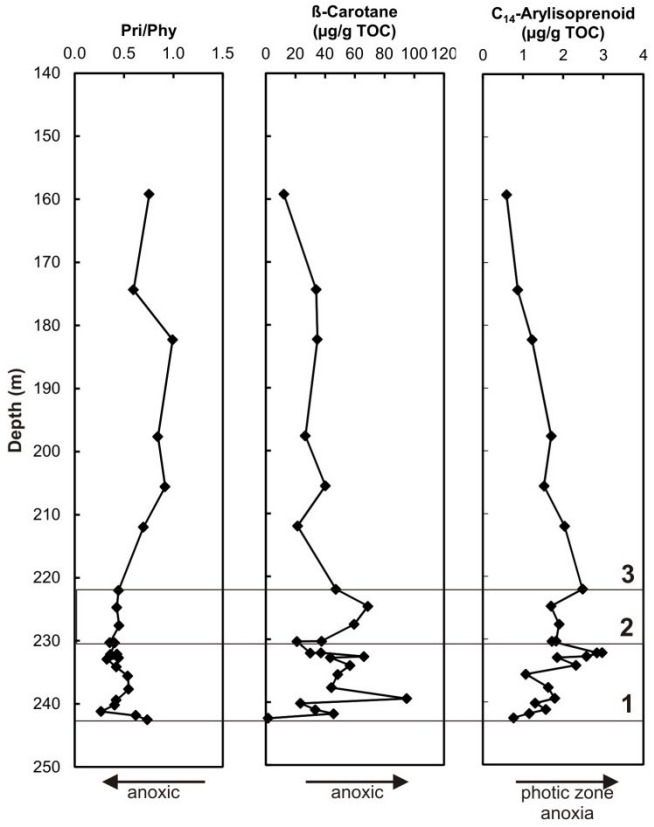

Figure 26: Vertical variability of redox proxies. The numbers 1, 2 and 3 indicate the base of the three cycles of the first member of the Qingshankou Formation.

Salinity parameters:

Typical salinity parameters are the gammacerane index and the MTTC ratio (Figure 27).

The highest values of the gammacerane index occur in the oil shales of the Qingshankou Formation. The values a decreasing upwards in the third cycle, but show an increase between 170 and 180 m.

The values of the MTTC ratio are negatively related to the values of the gammacerane index.

These two salinity parameters reflect a salinity stratification of the water column during deposition of the oil shales (cycle 1 and 2). They may indicate a short marine inflow

between 170 and 180 m during the freshwater conditions of the third cycle. Both parameters show a very good correlation to the TOC/S profile (Figure 13).

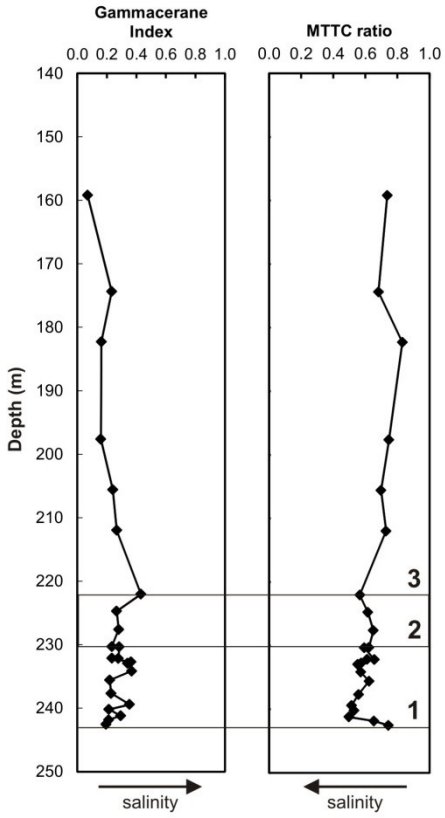

Figure 27: Vertical variability of salinity parameters. The numbers 1, 2 and 3 indicate the base of the three cycles of the first member of the Qingshankou Formation.

Bioproductivity:

Parameters reflecting bioproductivity are the CPI values, the concentrations of steranes, methylsteranes, hopanes, triterpenoids and the steroids/hopanoids ratio (Figure 28).

The highest CPI values occur in the first cycle of the first member of the Qingshankou Formation. These values are decreasing at the top of cycle 1 and show an increasing upward trend in the second cycle. In the third cycle, values stay constant up to 205 m, afterwards they are increasing, but show a short decrease between 170 and 180 m.

The highest concentration values for steranes and methylsteranes are obtained in the oil shale sequence, with a maximum in the first cycle. The lowest values occur in the third cycle, with exceptional high values between 170 and 180 m.

The highest concentrations of hopanes occur in the oil shale sequence, with a maximum in the first cycle. In both cycles of the oil shale sequence the amount of hopanes is increasing upwards. The lowest values are obtained in the third cycle, with exceptional high values between 170 and 180 m.

The highest steroids/hopanoids ratios are obtained during the deposition of the oil shales (cycle 1 and 2). These ratios are decreasing upwards in the third cycle, but they show a short increase between 170 and 180 m.

The highest concentrations of triterpenoids occur in the oil shale sequence, with a maximum in the first cycle. Both cycles (cycle 1 and 2) show an increasing upward trend. The concentrations of triterpenoids are low in the third cycle, with exceptional high values between 170 and 180 m.

All these parameters reflect a high bioproductivity during the deposition of the oil shale sequence of the Qingshankou Formation, with a maximum in the first cycle. Bioproductivity was reduced during the deposition of the third cycle, with an exception between 170 and 180 m.

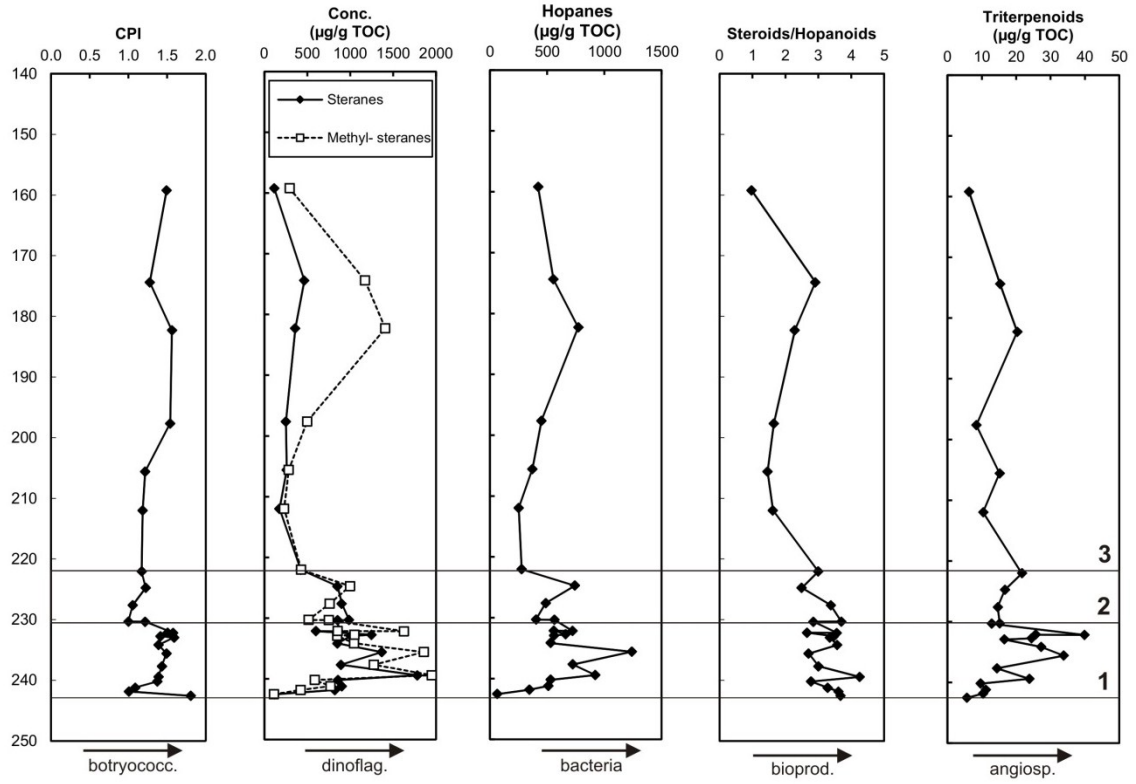

Figure 28: Vertical variability bioproductivity-related biomarkers. The numbers 1, 2 and 3 indicate the base of the three cycles of the first member of the Qingshankou Formation.

Figure 29 shows the variation of paleoenvironmental conditions during the deposition of the first member of the Qingshankou Formation.

Cycle 1:

This lowermost cycle of the oil shale sequence in the Qingshankou Formation shows very high TOC values (up to 24 %) resulting from high bioproductivity (e.g. botrycoccus and dinoflagellates) and a strictly anoxic water column. The latter was caused by salinity stratification and photic zone anoxia was present.

Cycle 2:

The upper unit of the oil shale sequence is characterised by TOC values up to 10 %. During the deposition of the second cycle bioproductivity was not as high and significant as in the first cycle. Salinity stratification and photic zone anoxia continued, but were not as strong as during cycle 1.

Due to the high salinity, a marine inflow may be postulated during the deposition of the oil shale sequence in the Qingshankou Formation (cycle 1 and 2).

Cycle 3:

Low TOC values (~ 4 %) are obtained in the organic-rich mudstones in the upper part of the Qingshankou Formation. Moderate bioproductivity and low salinity had occurred during the deposition of this cycle. A short marine inflow during deposition of sediments between 170 and 180 m is indicated by several biomarker ratios and by the TOC/S ratio.

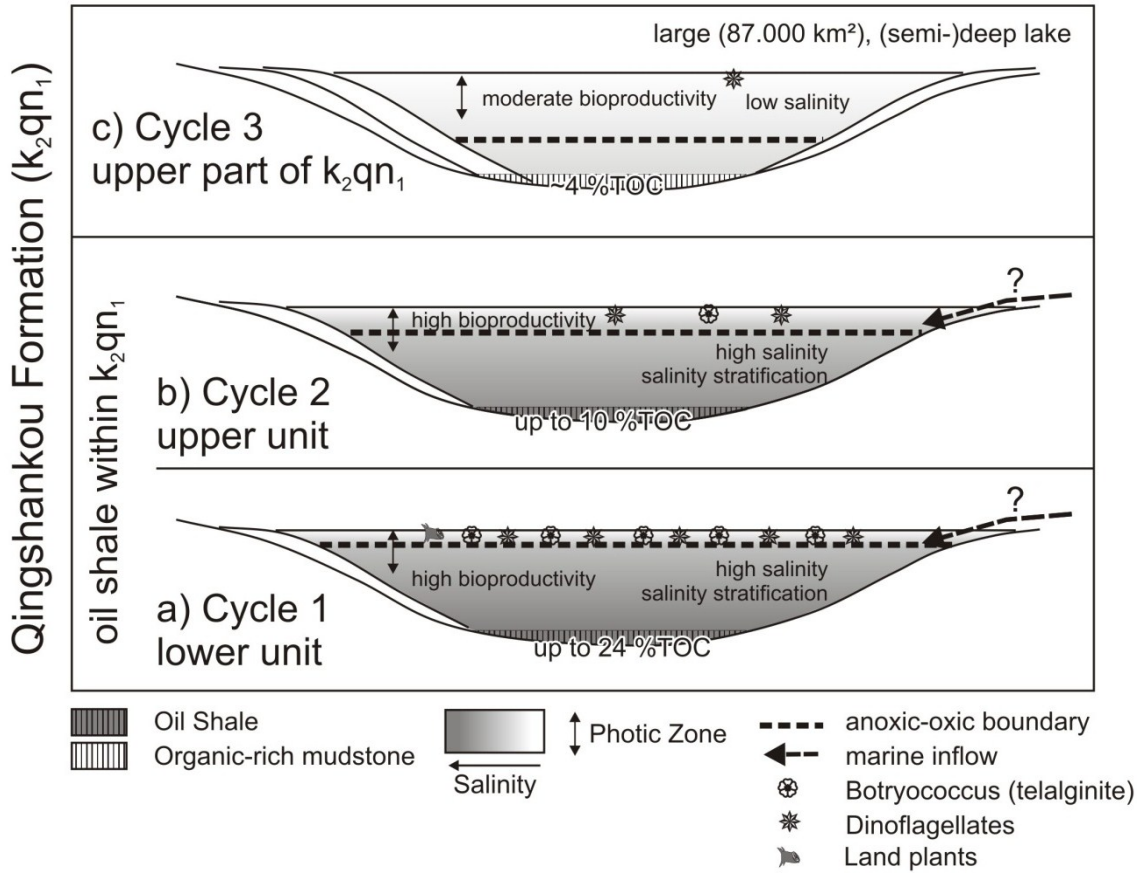

Figure 29: Cartoon illustrating three major cycles of the first member of the Qingshankou Formation. The extent and depth of the lake accord to Feng et al. (2010). K_2qn_1 = first member of Qingshankou Formation.

4.5.10 Characterisation of oil and oil to source rock correlation

The n-alkanes ($\geq C_{19}$) of the extracted oil of the oil-stained sandstone of the Quantou Formation show a relative lower abundance and a hump in the higher boiling range compared to the samples of the Qingshankou Formation. Moreover, the oil 1 sample shows a reduction in short chain n-alkanes (Figure 18), a high phytane to n-C_{18} ratio (3.07), and an absence of pristane. All these parameters indicate biodegradation.

Good oil to source rock correlation is obtained between the oil of the oil-stained sandstone and the samples within the oil shale sequence of the Qingshankou Formation. This match can be seen from biomarkers in the m/z 217+231 chromatograms for steranes and methylsteranes (Figure 21) and in the m/z 253+267 chromatograms for monoaromatic steroids (Figure 22). The biomarkers in the mass chromatogram (m/z 191)

for triterpenoids of the oil extract match with those of the sample of the oil shale sequence (Figure 23). However, the (22S/(22S+22R))-isomer ratio of the 17α,21β C31 hopane shows a higher value for the oil sample (0.54) than for the oil shale samples of the Qingshankou Formation. Therefore, the maturity of the source rock is assumed to be higher.

This indicates that the oil in the Quantou Formation originates from the oil shale sequence of the Qingshankou Formation in a deeper part in the Songliao Basin, where the oil shale has attained slightly higher maturity.

4.6 Carbon isotopy

The carbon isotopic composition of selected compounds in saturated hydrocarbon fractions of 11 samples from the Qingshankou Formation is plotted in Figure 30. The measured data is listed in Appendix 9.

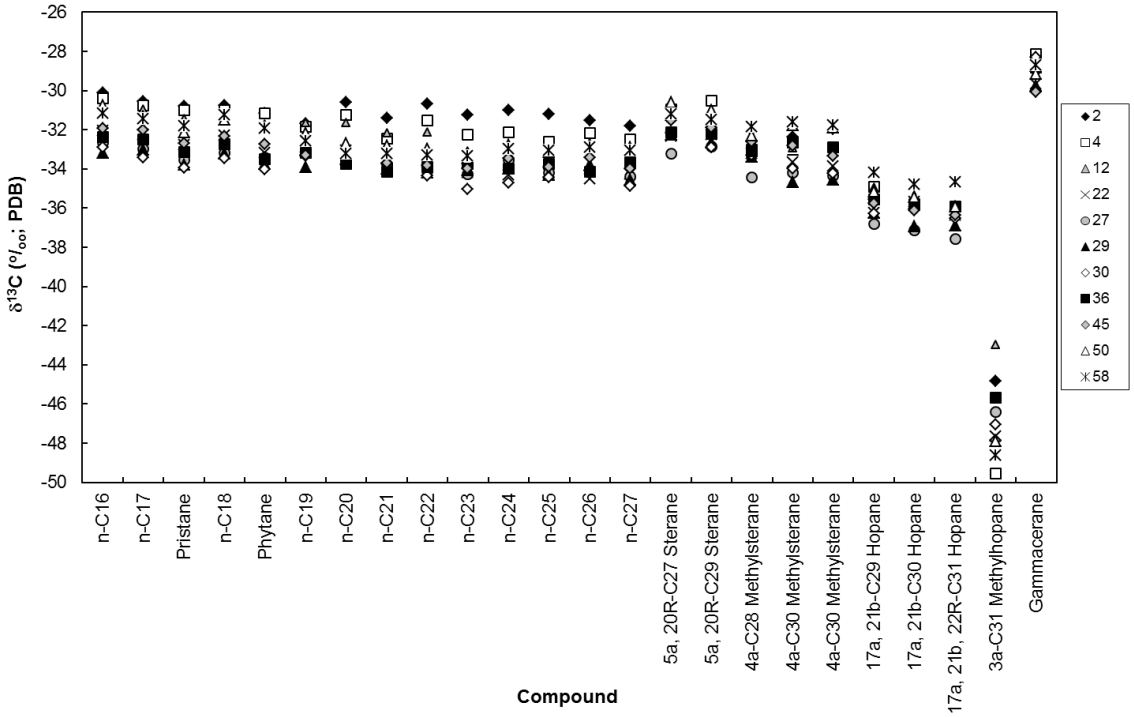

Figure 30: Carbon isotopic composition of selected compounds in saturated hydrocarbon fractions.

The n-C_{16} to n-C_{27} alkanes show a decrease in $\delta^{13}C$ of ca. 2 ‰ with increasing chain length. Such a distribution is known from leaf lipids of land plants and from terrestrial organic matter (Collister et al., 1994; Murray et al., 1994). Odd n-alkanes are more depleted in ^{13}C as the neighbouring even n-alkanes. These differences are less pronounced in the samples of the oil shale sequence (sample 22 to 30). Schouten et al. (1998) obtained the same systematics of $\delta^{13}C$ for long chain n-alkanes for organic matter from mixed sources, which indicates an enhanced contribution of algae and bacteria to even n-alkanes. These results show a mixture of n-alkanes from aquatic and terrestrial sources. $\delta^{13}C$ values are lower in the samples from the oil shale sequence than in the samples from the mudstone sections. These data suggest that during periods of high bioproductivity there had been an increased use of ^{13}C-depleted CO_2. The CO_2 has derived from decomposition of organic matter and bacterial activity in the lower parts of the water column, through primary producers (Imbus et al., 1992).

The $\delta^{13}C$ values for the acyclic isoprenoids pristane and phytane are lower than those of the aquatic n-alkanes (n-C_{17} and n-C_{18}). According to Hayes (1993), this is a result of isotopic differences between straight chain carbon skeletons and isoprenoids. Pristane and phytane show nearly equal $\delta^{13}C$ values. This similarity argues for the same source (i.e. chlorophyll).

The $\delta^{13}C$ values of the 5α-C_{27} and 5α-C_{29} steranes vary between -30.5 and -33.2 ‰. These values are more or less the same as for the short chain n-alkanes, but they are higher than the ones obtained for pristane and phytane. The methylsteranes are more depleted in ^{13}C in comparison to the isotopic composition of the steranes.

The $\delta^{13}C$ values of the $C_{29}\alpha\beta$ hopane to the $C_{31}\alpha\beta$ hopane are within a range from -34.2 to -37.6 ‰. These isotopic compositions are lower than those for biomarkers, which originates from organic matter living in the photic zone (e.g. short chain n-alkanes, phytane, steranes). The C_{31} methylhopane is strongly depleted in ^{13}C. It shows $\delta^{13}C$ values between -43.0 and -49.5 ‰. ^{13}C-depleted C_{31} methylhopane originates from methanotrophic bacteria (Collister et al., 1992; Summons et al., 1994).

The carbon isotopic composition of the gammacerane shows higher $\delta^{13}C$ values than the other biomarkers discussed before. The $\delta^{13}C$ values are between -28.2 and -30.1 ‰. According to Sinnighe Damsté et al. (1995), gammacerane originates from bacterivorous ciliates which were partially feeding on green sulphur bacteria.

5 Conclusions

70 well core samples of the well NGN-dgk-02 were taken within member 1 of the Upper Cretaceous Qingshankou Formation to evaluate the environment of deposition, the quality of organic matter, the petroleum source rock potential, and the maturity of the mudstones and oil shales. One additional oil-stained sandstone was taken from the Quantou Formation to correlate the oil with the potential source rocks in the Qingshankou Formation.

The most important results of the study include:

- The highest TOC contents (up to 23.82 %) occur within cycle 1 of the oil shale sequence.
- TOC/S ratios are low (below 2.8) within the oil shales, indicating free H_2S in the bottom water resulting from a stratified water column.
- T_{max} values and vitrinite reflectance measurements indicate a marginal maturity.
- Organic matter containing type I kerogen was mainly deposited. This information results from high HI values and maceral analysis. The organic matter is dominated by liptinite (lamalginite and telalginite).

Based on TOC, HI and the considerable thickness, the oil shale of the Qingshankou Formation is an excellent source rock for oil.

The results of the biomarker and carbon isotopy analysis indicate the following paleoenvironmental conditions:

- Freshwater conditions in the upper unit of the Qingshankou Formation with a possible marine inflow between 170 and 180 m.
- Presence of a stratified water column with free H_2S and saline, anoxic conditions in the bottom water during oil shale deposition (cycles 1 and 2).
- Organic matter originates mainly from algae (with a minor contribution of land plants).
- Highly reducing conditions involving salinity stratification are obtained within the oil shale sequence. Such conditions are usually obtained for lacustrine and highly restricted marine depositional settings.

The extracted oil from the oil-stained sandstone of the Quantou Formation shows moderate biodegradation. Good oil to source rock correlation is obtained between the oil and the oil shale samples of the Qingshankou Formation. The oil in the Quantou Formation may be migrated from the oil shale sequence of the Qingshankou Formation from a deeper part in the Songliao Basin, because the maturity of the source rock is assumed to be higher than that of the reservoir rock.

6 References

Barakat, A.O., and Rullkötter, J., 1997, A comparative study of molecular paleosalinity indicators: chromans, tocopherols and C_{20} isoprenoid tiophenes in Miocene lake sediments (Nördlinger Ries, Southern Germany): Aquatic Geochemistry, v. 3, p. 169-190.

Bechtel, A., Jia, J., Strobl, S.A.I., Sachsenhofer, R.F., Liu, Z., Gratzer, R., and Püttmann, W., 2011, Paleoenvironmental conditions during deposition of the Upper Cretaceous oil shale sequences in the Songliao Basin (NE China): implications from geochemical analysis: submitted to Organic Geochemistry,.

Berner, R.A., 1984, Sedimentary pyrite formation: An update: Geochimica et Cosmochimica Acta, v. 48, p. 605-615.

Bray, E.E., and Evans, E.D., 1961, Distribution of n-paraffins as a clue to recognition of source beds: Geochimica et Cosmochimica Acta, v. 22, p. 2-15.

Collister, J.W., Rieley, G., Stern, B., Eglinton, G., and Fry, B., 1994, Compound-specific ^{13}C analysis of leaf lipids from plants with differing carbon dioxide metabolism: Organic Geochemistry, v. 21, p. 619-627.

Collister, J.W., Summons, R.E., Lichtfouse, E., and Hayes, J.M., 1992, An isotopic biogeochemical study of the Green River OIls Shale: Organic Geochemistry, v. 19, p. 265-276.

Derenne, S., Largeau, C., Casadevall, E., and Connan, J., 1988, Comparison of torbanites of various origins and evolutionary stages. Bacterial contribution to their formation. Cause of lack of botryococcane in bitumens: Organic Geochemistry, v. 12, p. 43-59.

Didyk, B.M., Simoneit, B.R.T., Brassell, S.C., and Eglinton, G., 1978, Organic geochemical indicators of paleoenvironmental conditions of sedimentation: Nature, v. 272, p. 216-222.

Espitalié, J., Marquis, F., and Barsony, I., 1984, Geochemical logging, *in* Voorhess, K.J. ed., Analytical Pyrolysis, Butterworths, Boston, p. 53-79.

Feng, Z.Q., Jia, C.Z., Xie, X.N., Zhang, S., Feng, Z.H., and Cross, T., 2010, Tectonostratigraphic units and stratigraphic sequences of the nonmarine Songliao basin, northeast China: Basin Research, v. 22, p. 79-95.

Ficken, K.J., Li, B., Swain, D.L., and Eglinton, G., 2000, An n-alkane proxy for the sedimentary input of submerged/floating freshwater aquatic macrophytes: Organic Geochemistry, v. 31, p. 745-749.

Gao, R., Zhang, Y., and Cui, T., 1994, Cretaceous petroleum bearing strata in the Songliao Basin: Petroleum Industry Press, Beijing.

Grice, K., de Mesmay, R., Glucina, A., and Wang, S., 2008, An improved and rapid 5Å molecular sieve method for gas chromatography isotope ratio mass spectrometry of n-alkanes (C_8-C_{30}+): Organic Geochemistry, v. 39, p. 284-288.

Grice, K., Schouten, S., Peters, K.E., and Sinnighe Damsté, J.S., 1998, Molecular isotopic characterisation of hydrocarbon biomarkers in Paleocene-Eocene evaporitic, lacustrine source rocks from the Jianghan Basin, China: Organic Geochemistry, v. 29, p. 1745-1764.

Hart, M.B., and Leary, P.N., 1989, The stratigraphic and paleoceanographic setting of the late Cenomanian "anoxic" event: Journal of the Geological Society, London, v. 146, p. 305-310.

ten Haven, H.L., de Leeuw, J.W., Sinnighe Damsté, J.S., Schenk, P.A., Palmer, S.E., and Zumberge, J.E., 1988, Application of biological markers in the recognition of paleohypersaline environments, *in* Kelts, K., Fleet, A.J., and Talbot, M. eds., Lacustrine Petroleum Source Rocks, Geological Society Special Publication No. 26, Blackwell, Oxford, p. 123-140.

Hayes, J.M., 1993, Factors controlling 13C contents of sedimentary organic compounds: Principles and evidence: Marine Geology, v. 133, p. 111-126.

Hou, D., Li, M., and Huang, Q., 2000, Marine transgressional events in the gigantic freshwater lake Songliao: paleontological and geochemical evidence: Organic Geochemistry, v. 31, p. 763-768.

Hutton, A.C., 1987, Petrographic classification of oil shales: International Journal of Coal Geology, v. 8, p. 203-31.

Hutton, A.C., Kantsler, A.J., Cook, A.C., and Mckirdy, D.M., 1980, Organic matter in oil shales: Journal of the Australian Petroleum Exploration Association, v. 20, p. 44-67.

Imbus, S.W., Macko, S.A., Elmore, R.D., and Engel, M.H., 1992, Stable isotopes (C, S, N) and molecular studies on the Precambrian Nonesuch Shale (Wisconsin, Michigan, USA): evidence for differential preservation rates, depositional environment and hydrothermal influence: Chemical Geology, v. 101, p. 255-281.

Karrer, W., Cherbuliez, E., and Eugster, C.H., 1977, Konstitution und Vorkommen der organischen Pflanzenstoffe. Ergänzungsband I: Birkhäuser, Basel, Stuttgart.

Killops, S.D., and Killops, V.J., 1997, Einführung in die organische Geochemie: Ferdinand Enke Verlag, Stuttgart.

Kohnen, M.E.L., Sinnighe Damsté, J.S., and de Leeuw, J.W., 1991, Biases from natural sulphurization in paleoenvironmental reconstruction based on hydrocarbon biomarker distribution: Nature, v. 349, p. 775-778.

Langford, F.F., and Blanc-Valleron, M.-M., 1990, Interpreting Rock-Eval pyrolysis data using graphs of pyrolyzable hydrocarbons vs. total organic carbon: AAPG Bulletin, v. 74, p. 799-804.

Li, D., 1995, Hydrocarbon habitat in the Songliao rift basin, China, *in* Lambiase, J.J. ed., Hydrocarbon habitat in rift basins, Geological Society Special Publication 80, p. 317-329.

Liu, Z.J., Dong, Q.S., Zhu, J.W., Guo, W., Ye, S.Q., Liu, R., Meng, Q.T., Zhang, H.L., and Gan, S.C., 2009, Oil Shale in China: Petroleum Industry Press, Beijing.

Ma, L., Ge, T., Zhao, X., Zie, T., Ge, R., and Dang, Z., 1982, Oil basins and subtle traps in the eastern part of China, *in* Halbouty, M.T. ed., The deliberate search for the subtle trap, American Association of Petroleum Geologists Memoir 32, p. 287-315.

Mackenzie, A.S., 1984, Application of biological markers in petroleum geochemistry, *in* Brooks, J. and Welte, D.H. eds., Advances in Petroleum Geochemistry, Academic Press, London, p. 115-214.

Mackenzie, A.S., and Maxwell, J.R., 1981, Assessment of thermal maturation in sedimentary rocks by molecular measurements, *in* Brooks, J. ed., Organic maturation studies and fossil fuel exploration, Academic Press, London, p. 239-254.

Metzger, P., Largeau, C., and Casadevall, E., 1991, Lipids and macromolecular lipids of the hydrocarbon-rich microalga Botryococcus braunii. Chemical structure and biosynthesis. Geochemical and biotechnological importance, *in* Herz, W. ed., Progress in the Chemistry of Organic Natural Products, Springer, Berlin, p. 1-70.

Mukhopadhyay, P.K., and Dow, W.G., 1994, Vitrinite reflectance as a maturity parameter - applications and limitations: ACS Symposium Series, v. 570, p. 1-24.

Murray, A.P., Summons, R.E., Boreham, C.J., and Dowling, L.M., 1994, Biomarker and n-alkane isotope profiles for Tertiary oils: Relationship to source rock depositional setting: Organic Geochemistry, v. 22, p. 521-542.

Ourisson, G., Albrecht, P., and Rohmer, M., 1979, The hopanoids: palaeo-chemistry and biochemistry of a group of natural products: Pure Appl. Chem., v. 51, p. 709-729.

Peters, K.E., 1986, Guidelines for evaluating petroleum source rocks using programmed pyrolysis: AAPG Bulletin, v. 70, p. 318-329.

Peters, K.E., and Cassa, M.R., 1994, Applied source rock geochemistry, *in* Magoon, L.B. and Dow, W.G. eds., The Petroleum System - From Source to Trap, AAPG, Tulsa, p. 93-117.

Peters, K.E., Walters, C.C., and Moldowan, J.M., 2005a, The Biomarker Guide - Biomarkers and Isotopes in Petroleum Exploration and Earth History: Cambridge University Press, New York.

Peters, K.E., Walters, C.C., and Moldowan, J.M., 2005b, The Biomarker Guide - Biomarkers and Isotopes in the Environment and Human History: Cambridge University Press, Cambridge.

Pfennig, N., 1977, Phototrophic green and purple bacteria: a comparative, systematic survey: Annual Review of Microbiology, v. 31, p. 275-290.

Radke, M., Willsch, H., and Welte, D.H., 1980, Preparative hydrocarbon group type determination by automated medium pressure liquid chromatography: Analytical Chemistry, v. 52, p. 406-411.

Robinson, N., Eglinton, G., Brassell, S.C., and Cranwell, P.A., 1984, Dinoflagellate origin for sedimentary 4α-methylsteroids and 5β(H)-stanols: Nature, v. 308, p. 439-442.

Rohmer, M., Bisseret, P., and Neunlist, S., 1992, The hopanoids, prokaryotic triterpenoids and precursors of ubiquitous molecular fossils, *in* Moldowan, J.M., Albrecht, P., and Philp, R.P. eds., Biological Markers in Sediments and Petroleum, Prentice Hall, Englewood Cliffs, p. 1-17.

Ryder, R.B., Qiang, J., McCabe, P.J., Nuccio, V.F., and Persits, F., 2003, Qingshankou-Putaohua / Shaertu and Jurassic Coal – Denglouku / Nongan Total Petroleum Systems in the Songliao Basin , China: U.S. Geological Survey Bulletin, v. 2203-A, p. 1-26.

Schouten, S., Schoell, M., Sinnighe Damsté, J.S., Summons, R.E., and de Leeuw, J.W., 1998, Molecular biogeochemistry of Monterey sediments (Naples Beach, U.S.A.). II: Carbon isotopic composition of free and sulphur-bound carbon skeletons, *in* Isaacs, C.M. and Rullkötter, J. eds., The Monterey Formation: From Rock to Molecules, Columbia University Press, New York, p. 175-188.

Sinnighe Damsté, J.S., Keely, B.J., Betts, S.E., Baas, M., Maxwell, J.R., and de Leeuw, J.W., 1993, Variations in abundances and distributions of isoprenoid chromans and long-chain alkylbenzenes in sediments of the Mulhouse Basin: a molecular sedimentary record of paleosalinity: Organic Geochemistry, v. 20, p. 1201-1215.

Sinnighe Damsté, J.S., Kenig, F., Koopmans, M.P., Köster, J., Schouten, S., Hayes, J.M., and de Leeuw, J.W., 1995, Evidence for gammacerane as an indicator of water column stratification: Geochimica et Cosmochimica Acta, v. 59, p. 1895-1900.

Sinnighe Damsté, J.S., Kock-Van Dalen, A.C., de Leeuw, J.W., Schenk, P.A., Guoying, S., and Brassell, S.C., 1987, The identification of mono-, di-, and trimethyl 2-methyl-2-(4,8,12-trimethyltridecyl)chromans and their occurence in geosphere: Geochimica et Cosmochimica Acta, v. 51, p. 2393-2400.

Summons, R.E., 1993, Biogeochemical cycles: A review of fundamental aspects organic matter formation, preservation, and composition, *in* Engel, M.H. and Macko, S.A. eds., Organic Geochemistry - Principles and Applications, Plenum Press, New York, p. 3-21.

Summons, R.E., and Powell, T.G., 1987, Identification of aryl isoprenoids in source rocks and crude oils: biological markers for the green sulphur bacteria: Geochimica et Cosmochimica Acta, v. 51, p. 557-566.

Summons, R.E., Jahnke, L.L., and Rokasandic, Z., 1994, Carbon isotopic fractionation in lipids from methanotrophic bacteria: Relevance for interpretation of the geochemical record of biomarkers: Geochimica et Cosmochimica Acta, v. 58, p. 2853-2863.

Taylor, H., Teichmüller, M., Davis, A., Diessel, C.F.K., Littke, R., and Robert, P., 1998, Organic Petrology: Borntraeger, Berlin-Stuttgart.

Tissot, B.T., and Welte, D.H., 1984, Petroleum Formation and Occurrence: Springer, Berlin.

Volkman, J.K., 1986, A review of sterol markers for marine and terrigenous organic matter: Organic Geochemistry, v. 9, p. 83-99.

Volkman, J.K., Barrett, S.M., Blackburn, S.I., Mansour, M.P., Sikes, E.L., and Gelin, F., 1998, Microalgae biomarkers: A review of recent research developments: Organic Geochemistry, v. 29, p. 1163-1179.

Wu, H., Zhang, S., Jiang, G., and Huang, Q., 2009, The floating astronomical time scale for the terrestrial Late Cretaceous Qingshankou Formation from the Songliao Basin of Northeast China and its stratigraphic and paleoclimate implications: Earth and Planetary Science Letters, v. 278, p. 308-323.

Yang, W., 1984, Oil and gas distribution and prediction of exploration prospects in the Songliao Basin, *in* Yang, W. ed., Songliao Basin - History of Daqing oil field, Chinese Petroleum Geology, Petroleum Industry Press, Beijing, p. 1-14.

Yin, A., and Nie, S., 1996, A Phanerozoic palinspastic reconstruction of China and its neighbouring regions, *in* Yin, A. and Harrison, M.T. eds., The tectonic evolution of Asia, Cambridge University Press, p. 442-485.

7 Appendices

7.1 Core photographs

Appendix 1: Core photographs of well NGN-dgk-02. Samples investigated in the present study are labelled.

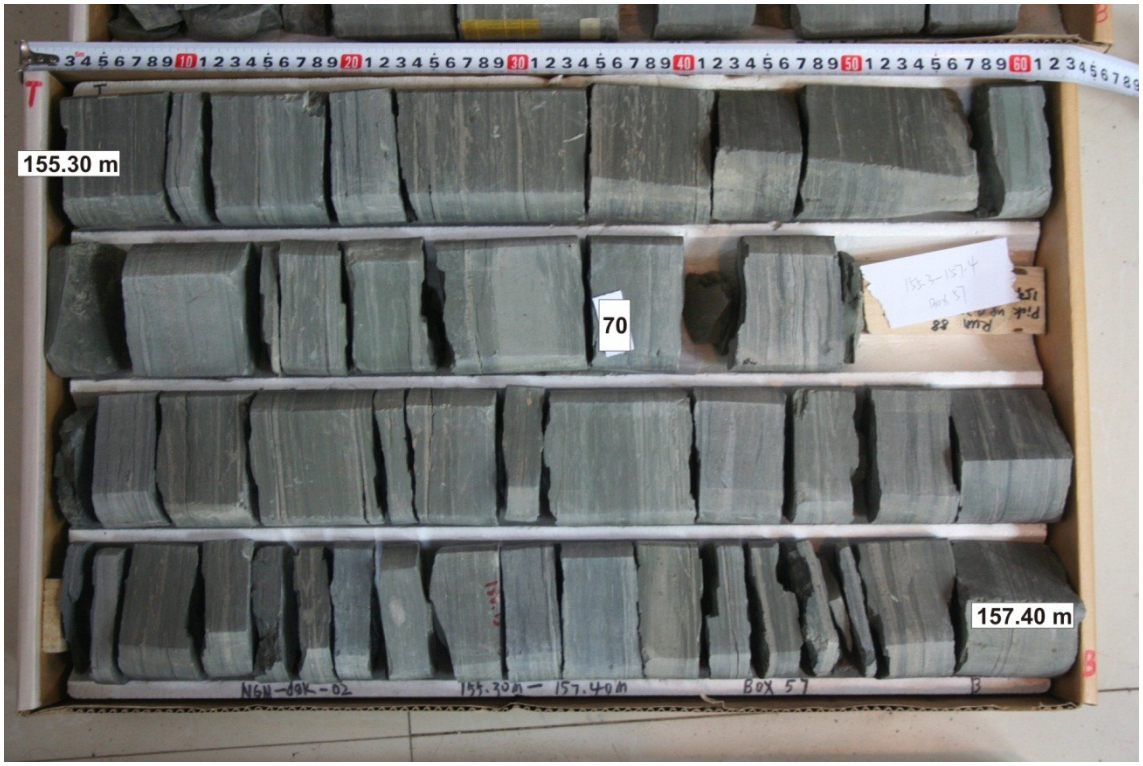


159.40 m
69
161.55 m


161.55 m
68
163.70 m

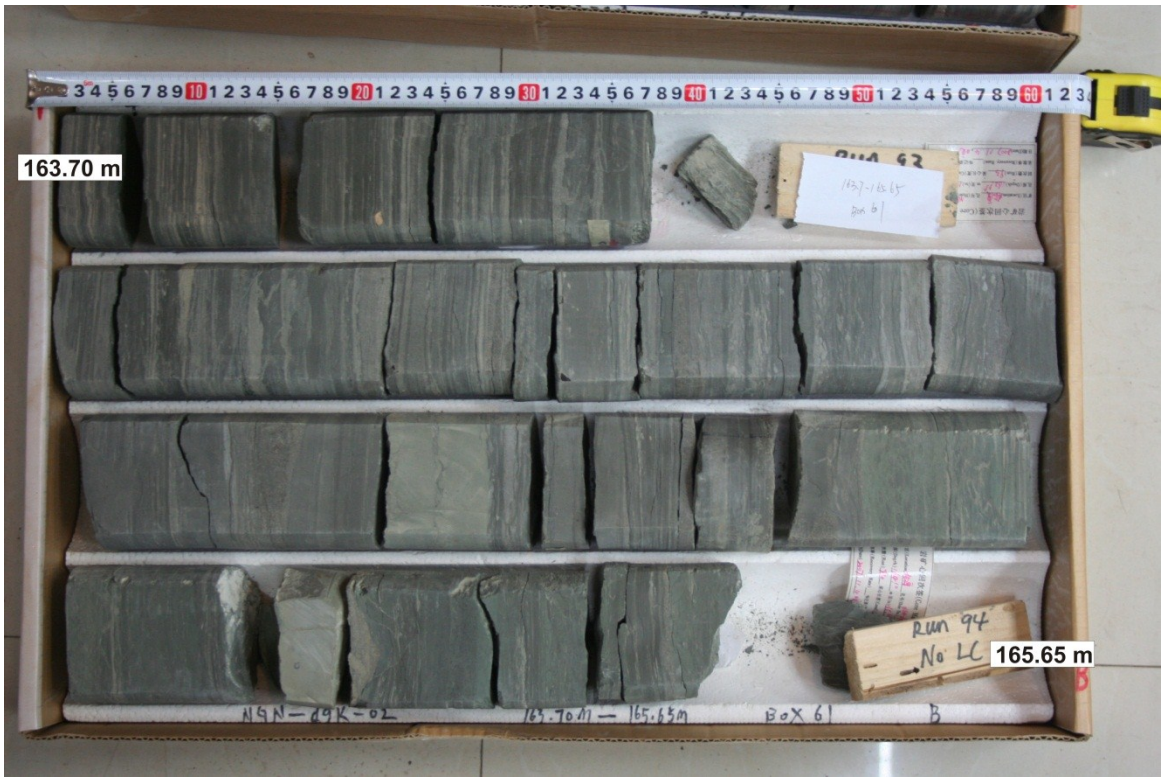
163.70 m
Run 94
No LC
165.65 m
NGN-09K-02
163.70m — 165.65m
Box 61
B


165.65 m
67
167.70 m
NGN-02
Box 62
164.65 — 167.70 m
B


167.70 m
169.65 m


169.65 m
66
171.80 m

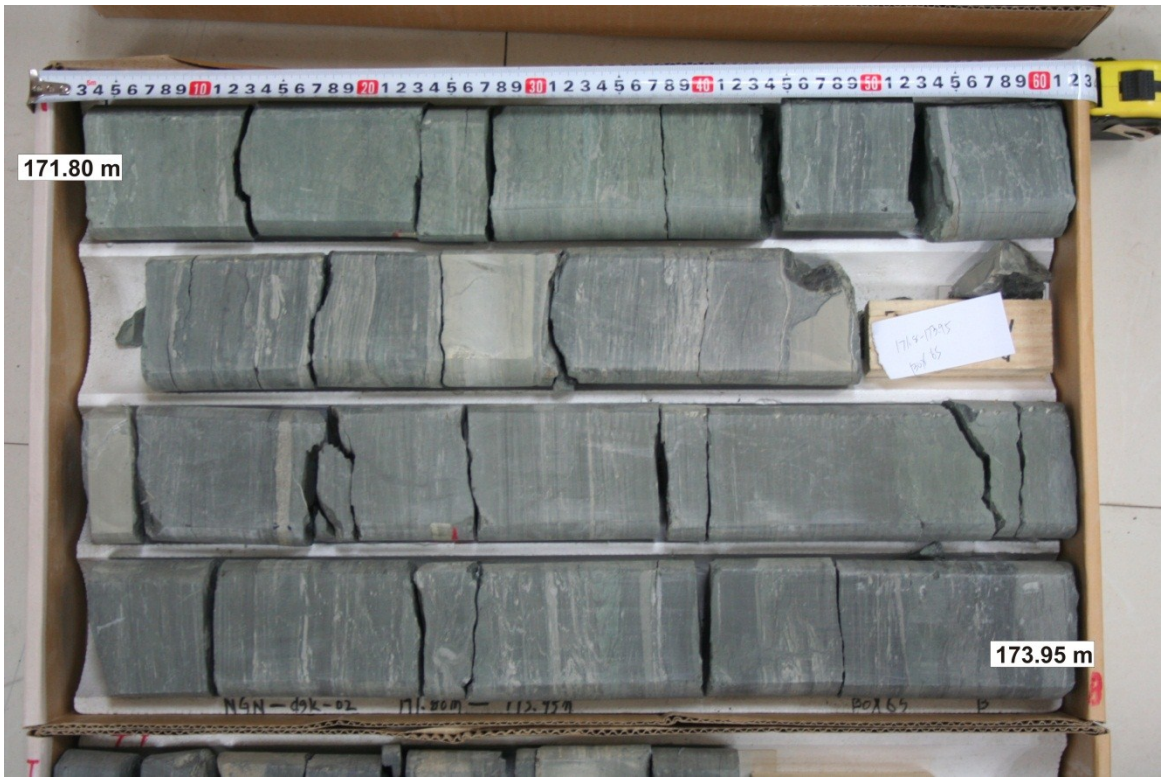
171.80 m
173.95 m

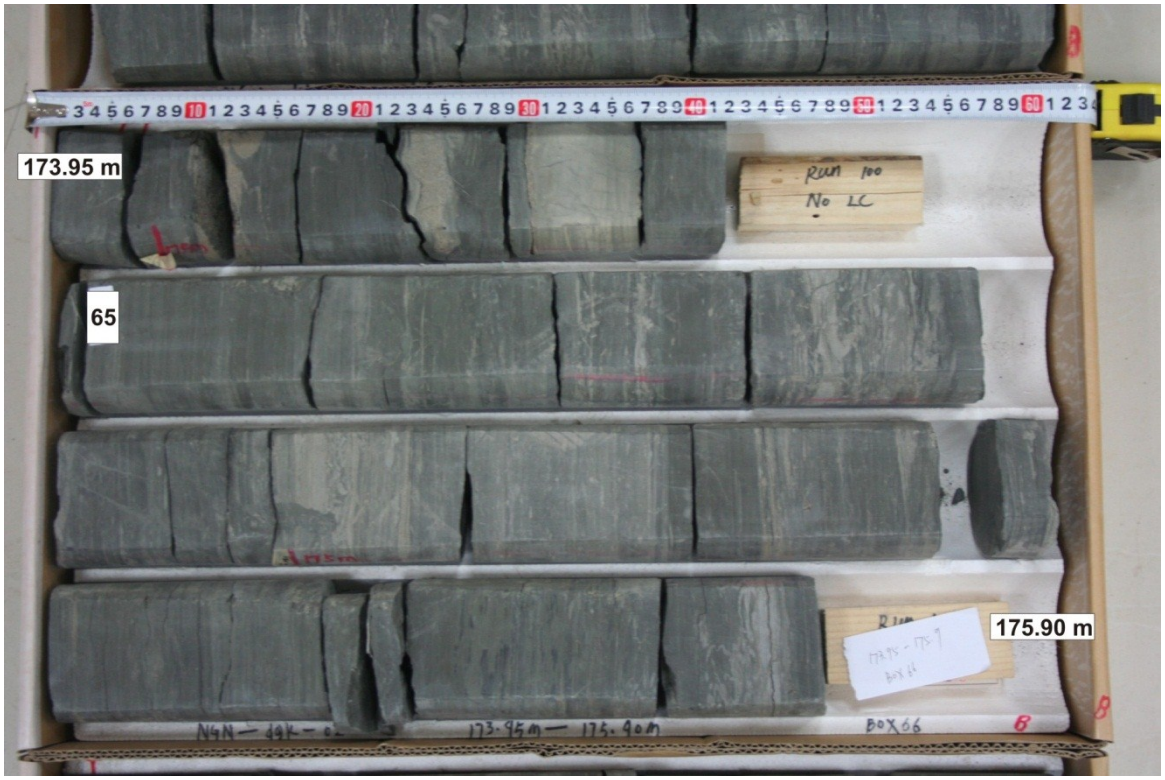
173.95 m
65
175.90 m


175.90 m
178.10 m

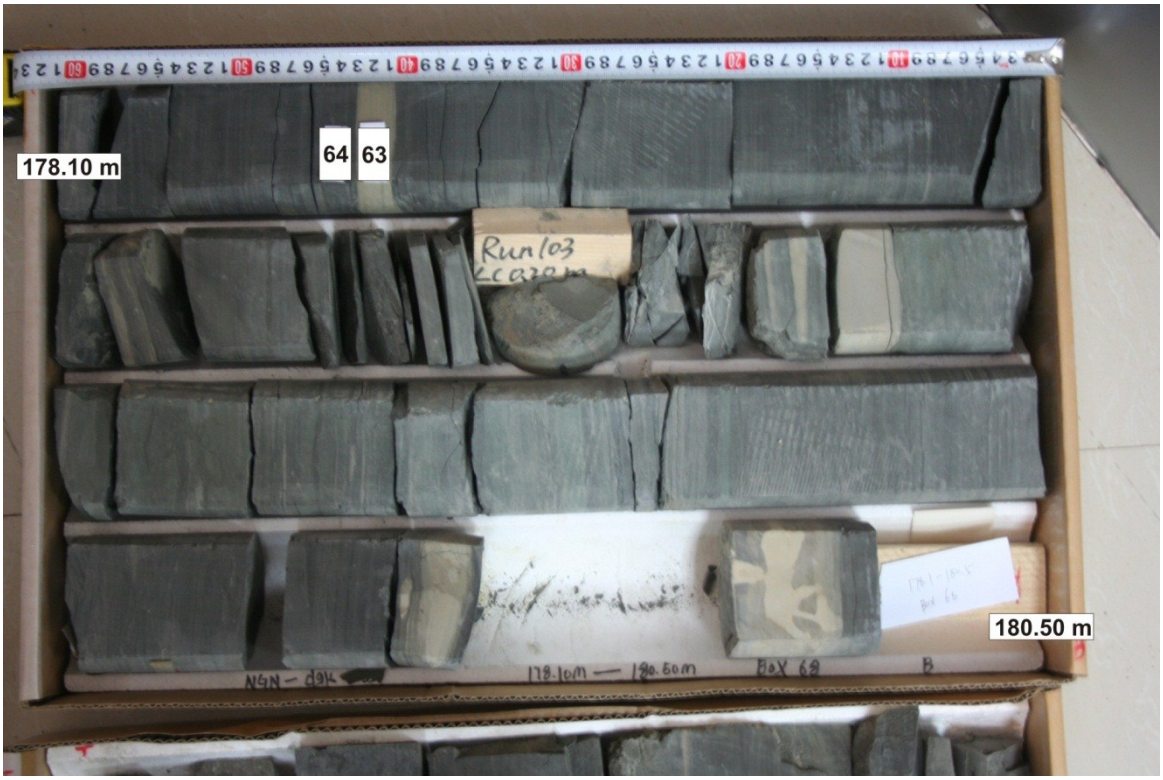
178.10 m
64
63
Run 103
180.50 m


180.50 m
182.46 m
62

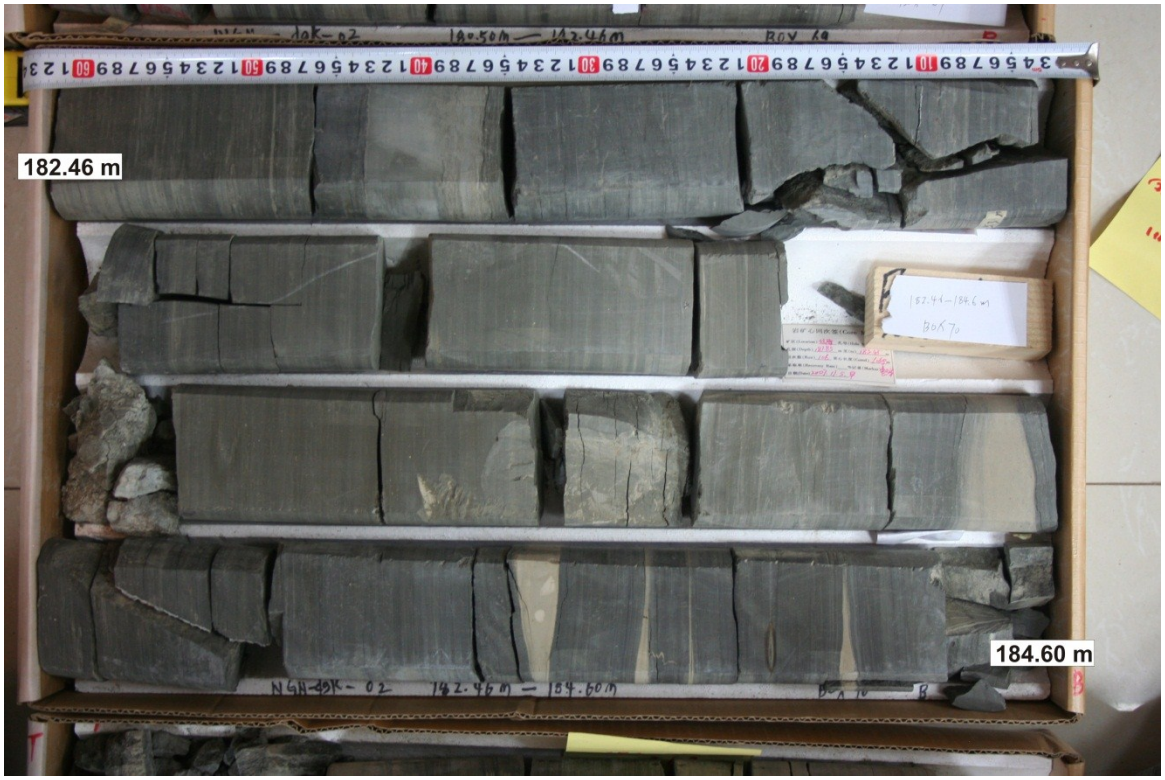
182.46 m
184.60 m

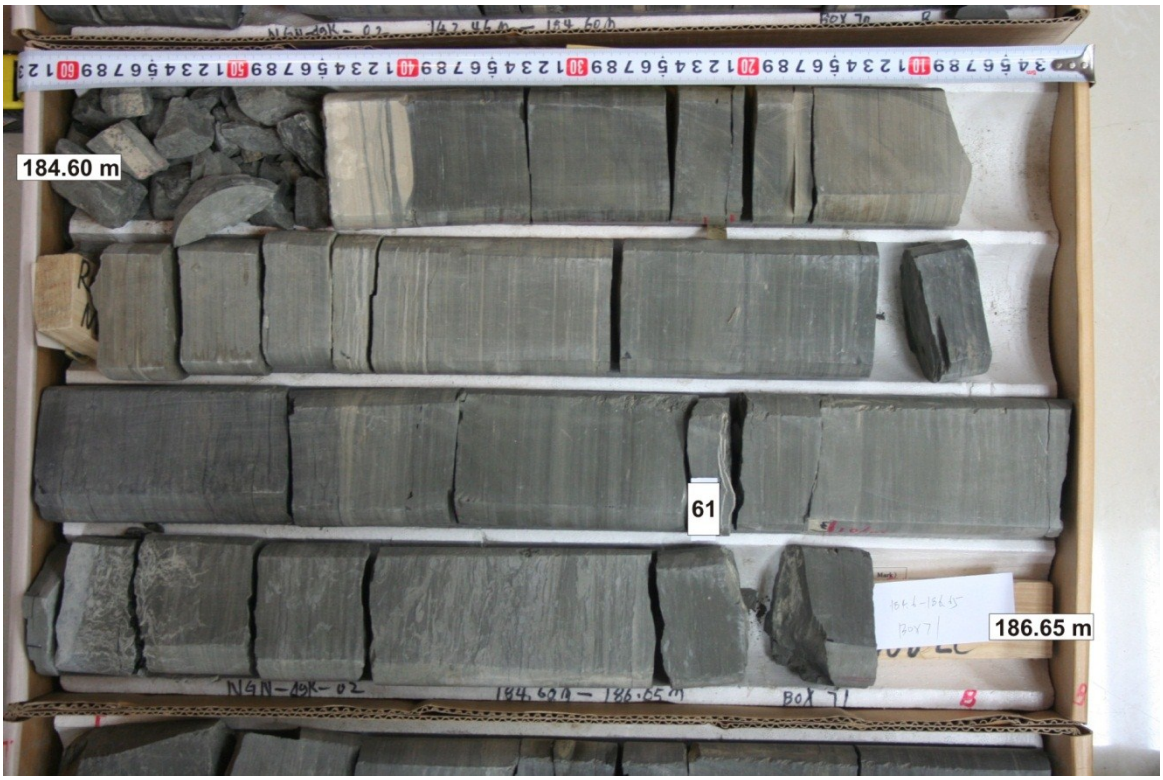
184.60 m
61
186.65 m
NGN-09K-02
184.60m — 186.65m
Box 71

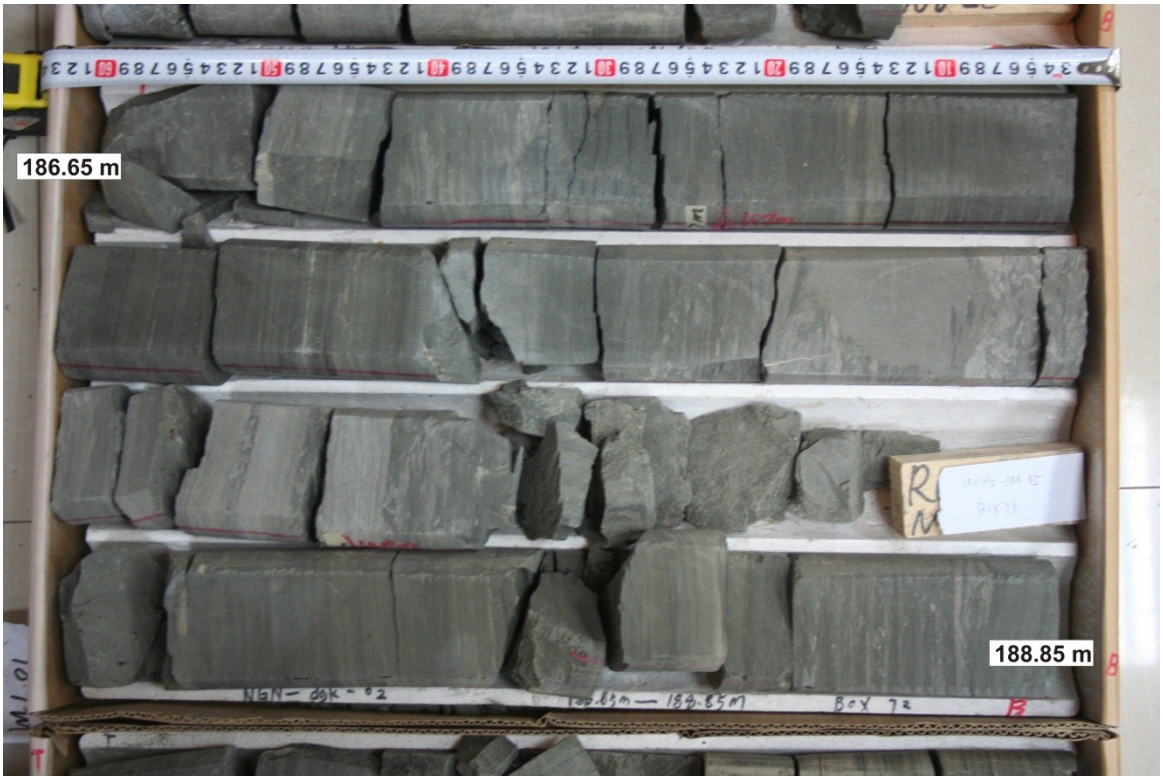
186.65 m
188.85 m
NGN-09K-02
186.65m — 188.85m
Box 72


188.85 m
60
190.85 m


190.95 m
Run 111
No LC
193.33 m

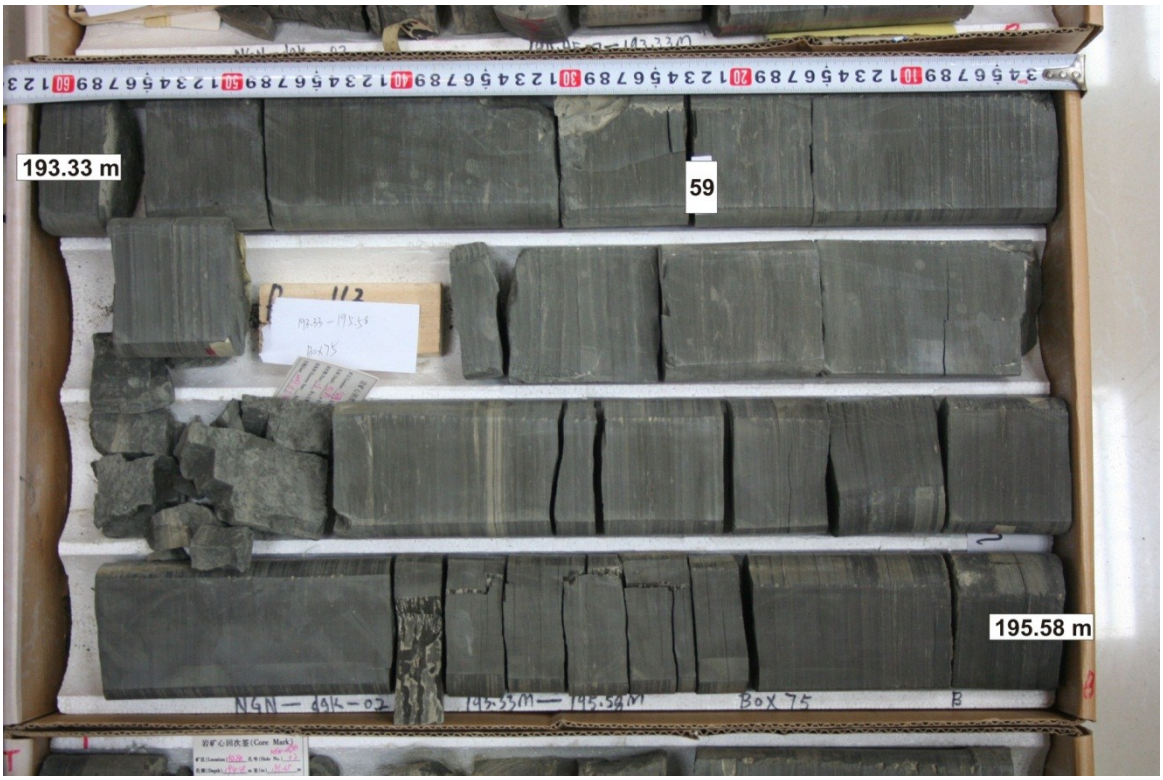
193.33 m
59
195.58 m
NGN-09K-02
Box 75
B


195.58 m
Run 114
No Lc & pieces
58
198.60 m
NGN-09K-02
Box 76
B


198.60 m
Run 116
200.20 m


200.20 m
57
202.50 m

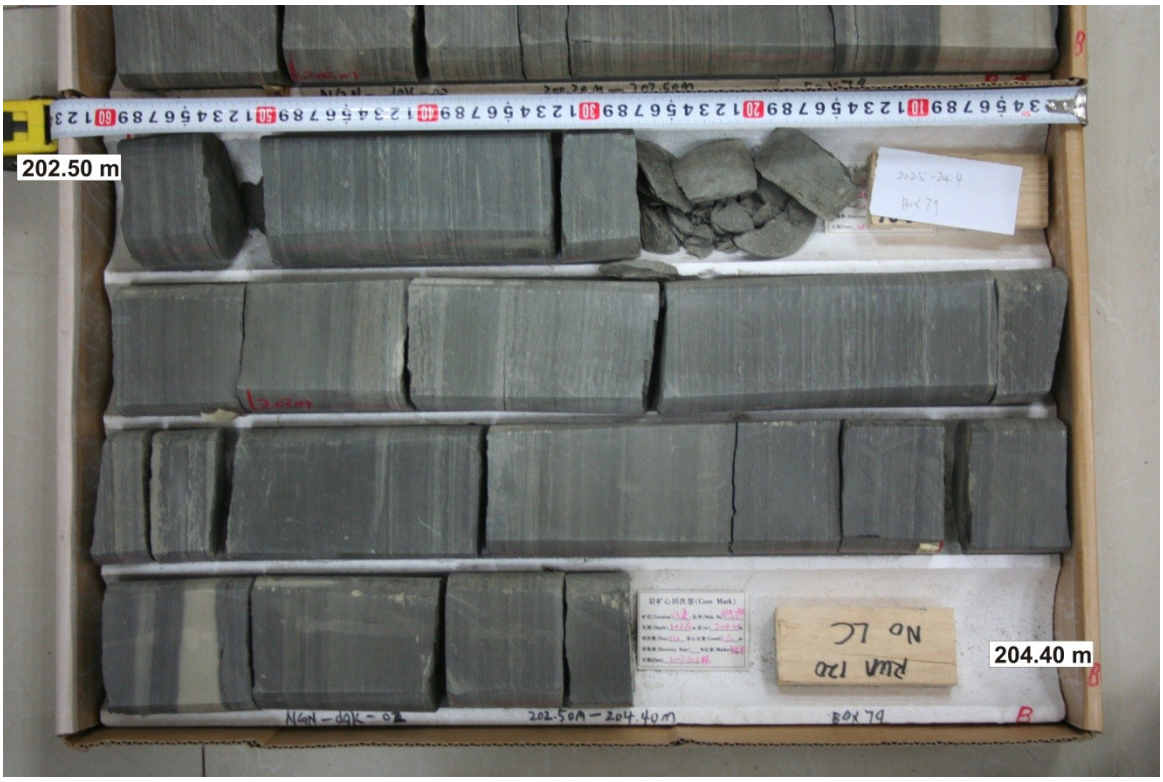
202.50 m
204.40 m
NGN-09K-02
202.50M-204.40M
BOX 79


204.40 m
56
RUN 121
205.73-205.88m
Sample 03
206.58 m
NGN-09K-02
204.40M-206.58M
BOX 80


206.58 m
208.75 m


208.75 m
55
RUN 123
LC 0.10m (208.90 - 209.00m)
RUN 124
Pick up 0.10m (208.90 - 209.00m)
LC 0.10m (210.40-210.50m)
210.40 m

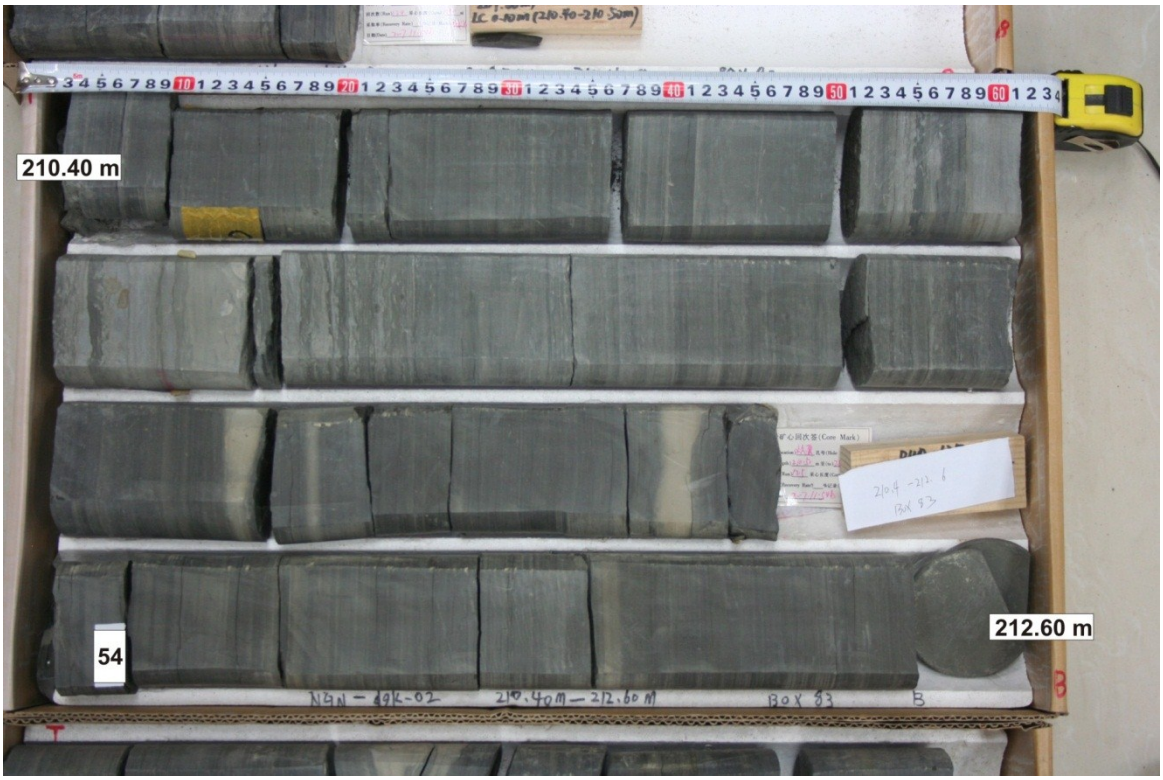
210.40 m
212.60 m
54
NGN - 09K-02 210.40m - 212.60m BOX 83 B

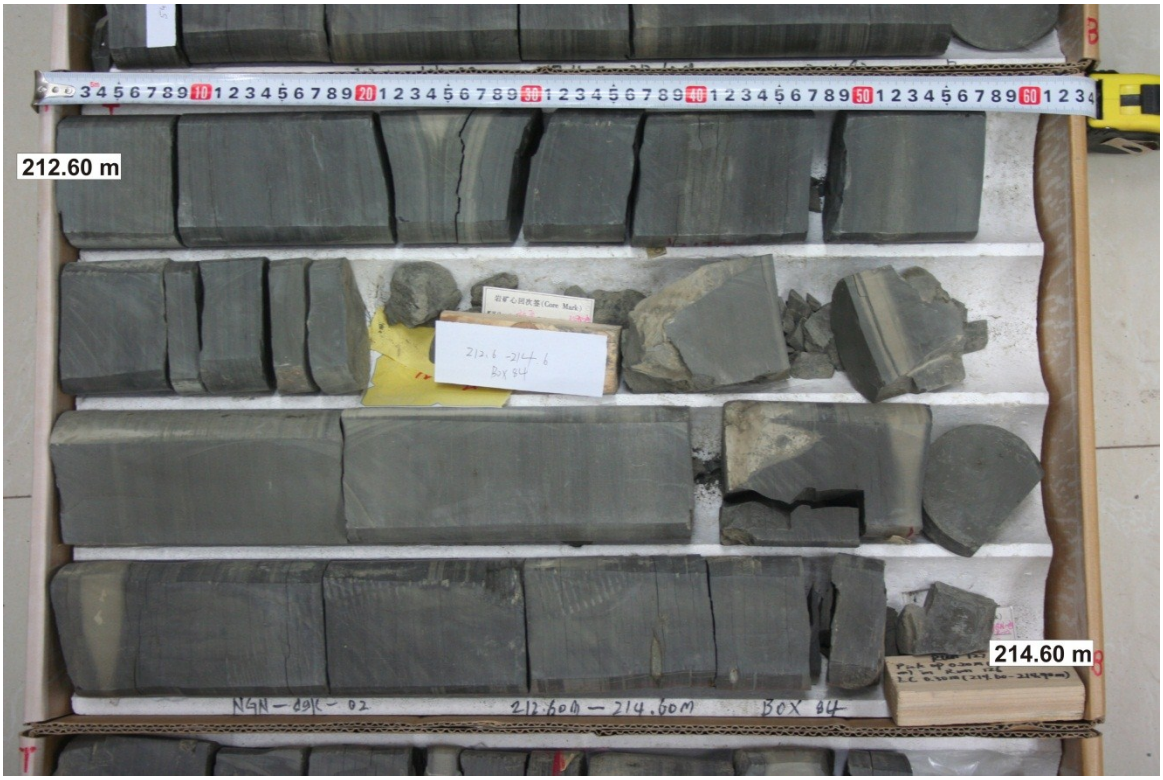
212.60 m
214.60 m
NGN-09K-02 212.60m - 214.60m BOX 84


214.60 m
53
RUN 128
216.60 m

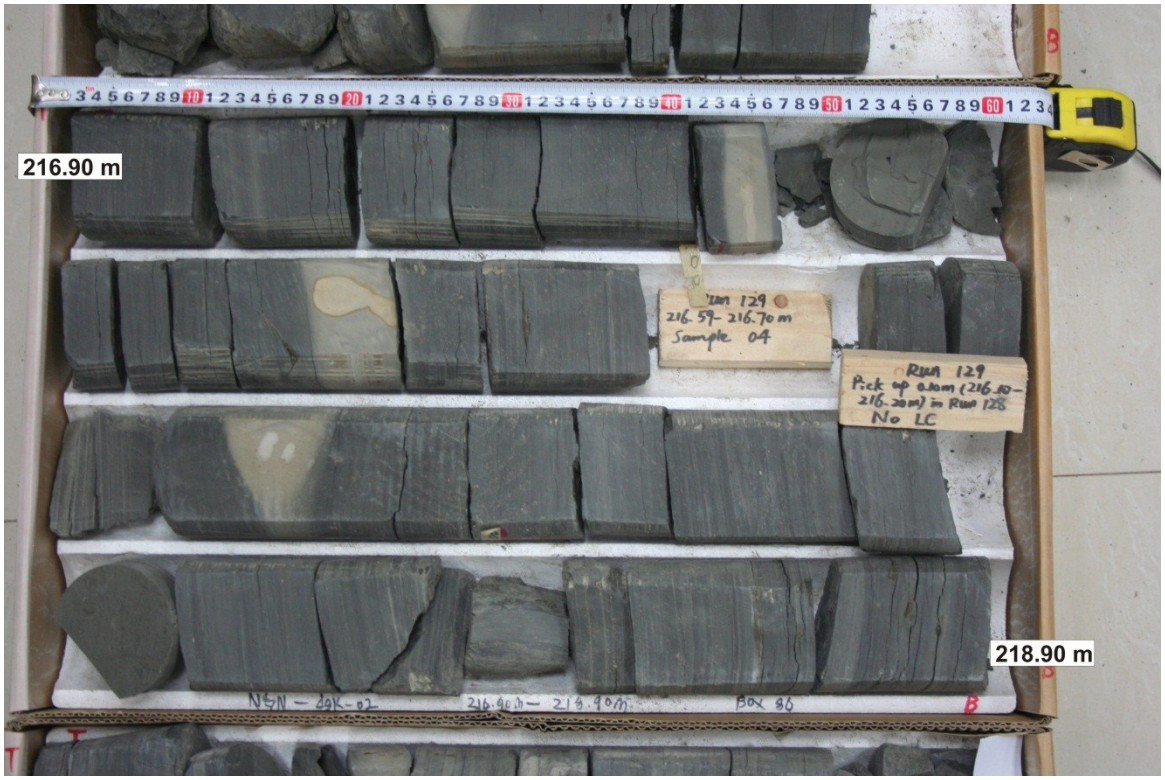
216.90 m
RUN 129
216.57-216.70 m
Sample 04
RUN 129
Pick up 0.30m (216.80-
216.30m) in RUN 128
No LC
218.90 m


218.90 m
52
220.90 m

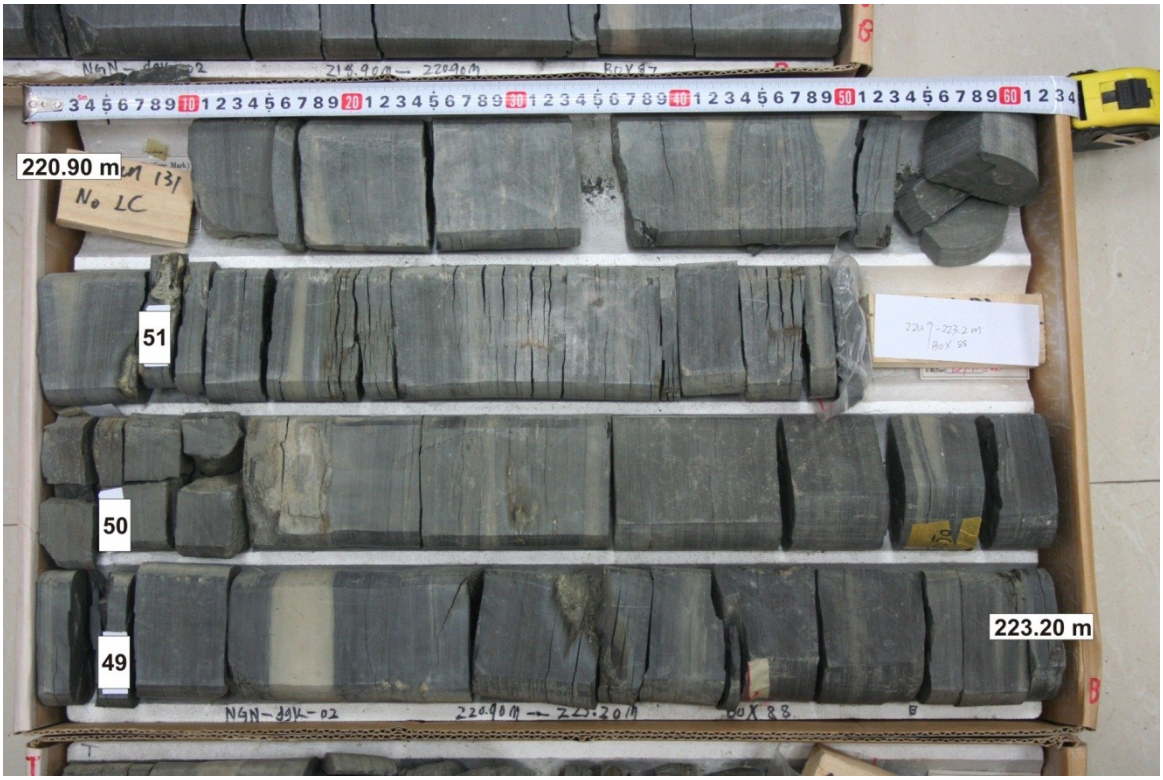
220.90 m
No LC
51
50
49
223.20 m

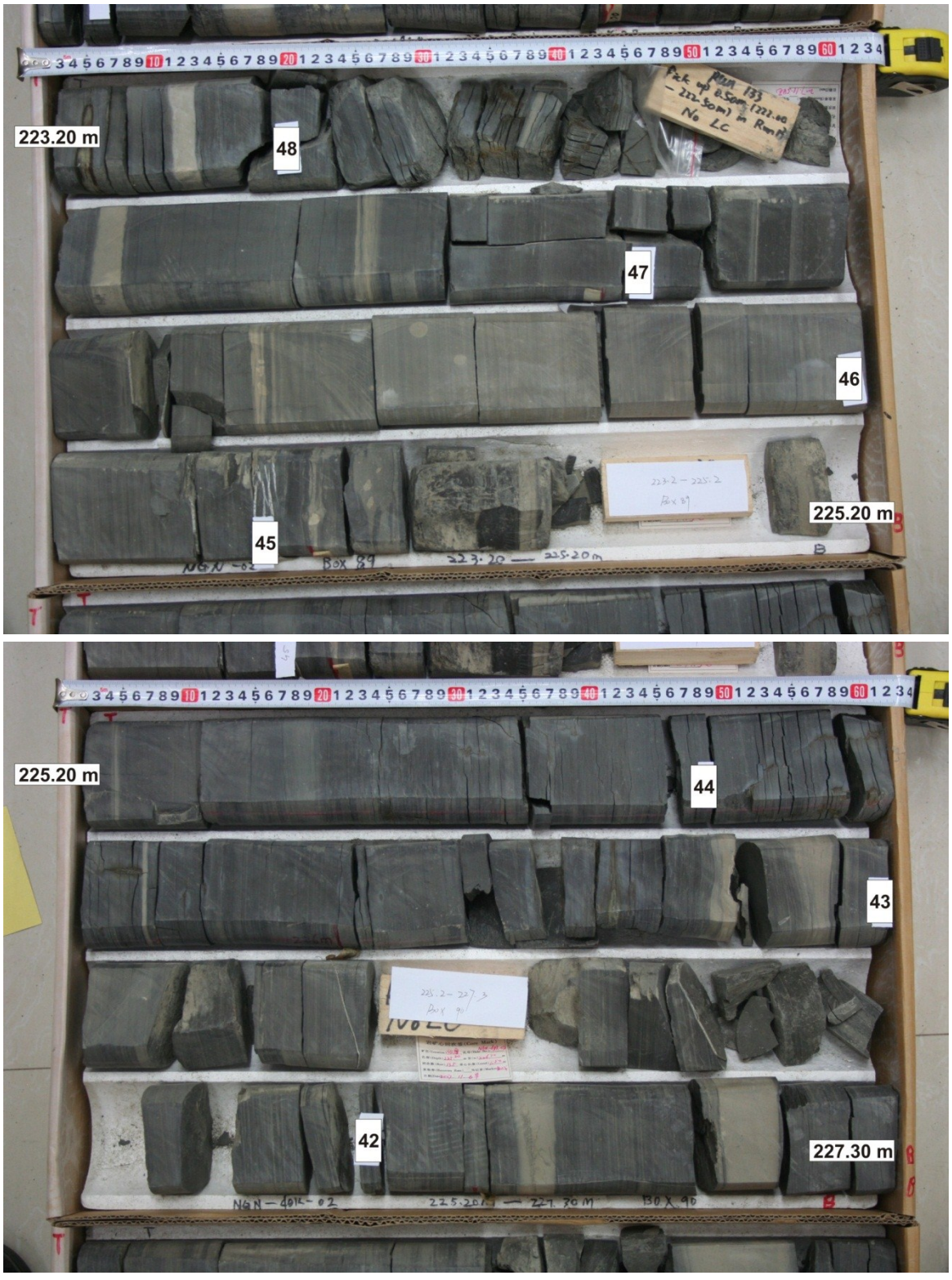
223.20 m
48
47
46
45
225.20 m
225.20 m
44
43
42
227.30 m


227.30 m
41
40
Run136
No LC
39
38
Run137
No LC
229.15 m
229.15 m
37
36
35
34
231.33 m
33

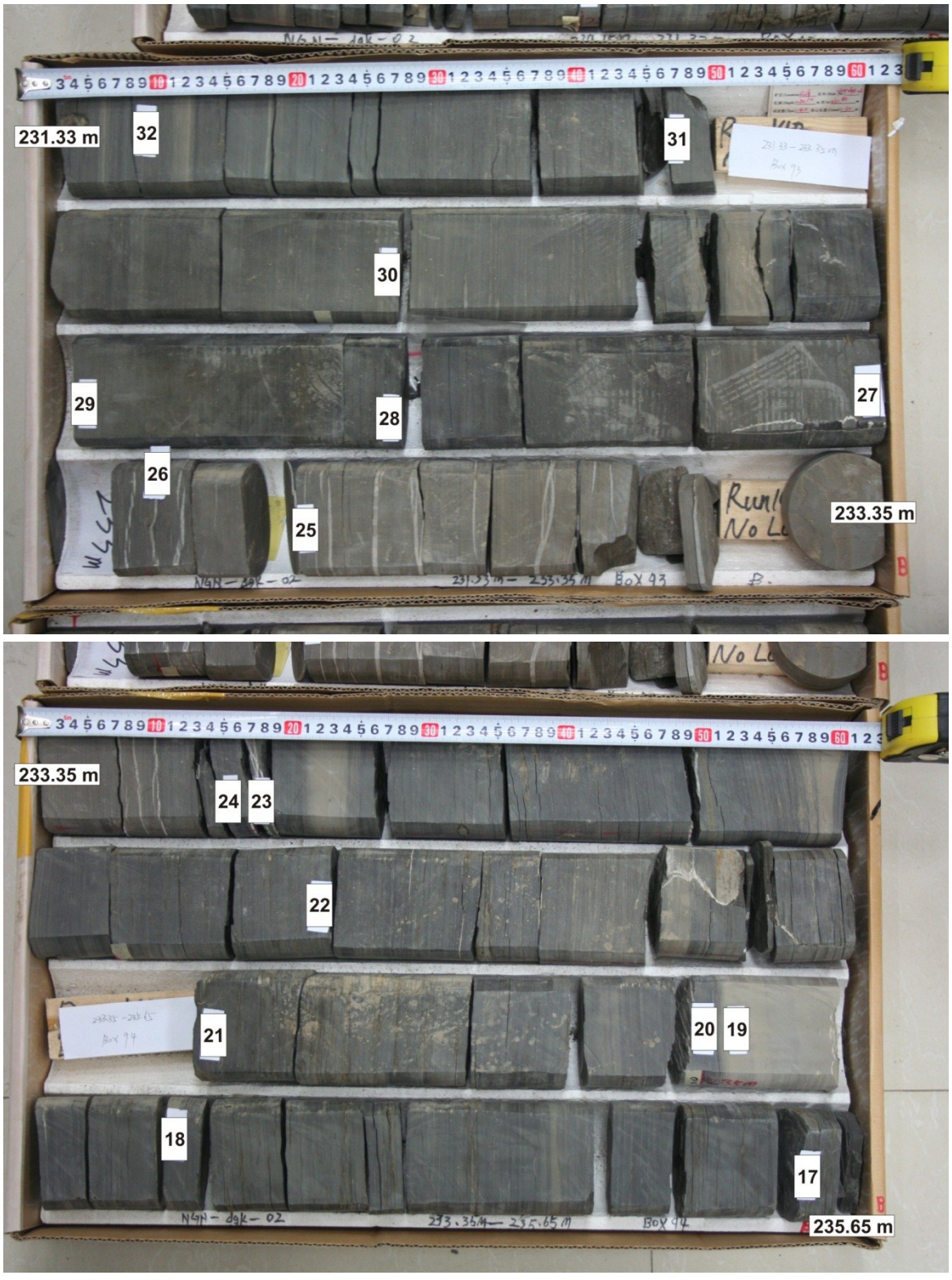
231.33 m
32
31
30
29
28
27
26
25
233.35 m
233.35 m
24
23
22
21
20
19
18
17
235.65 m

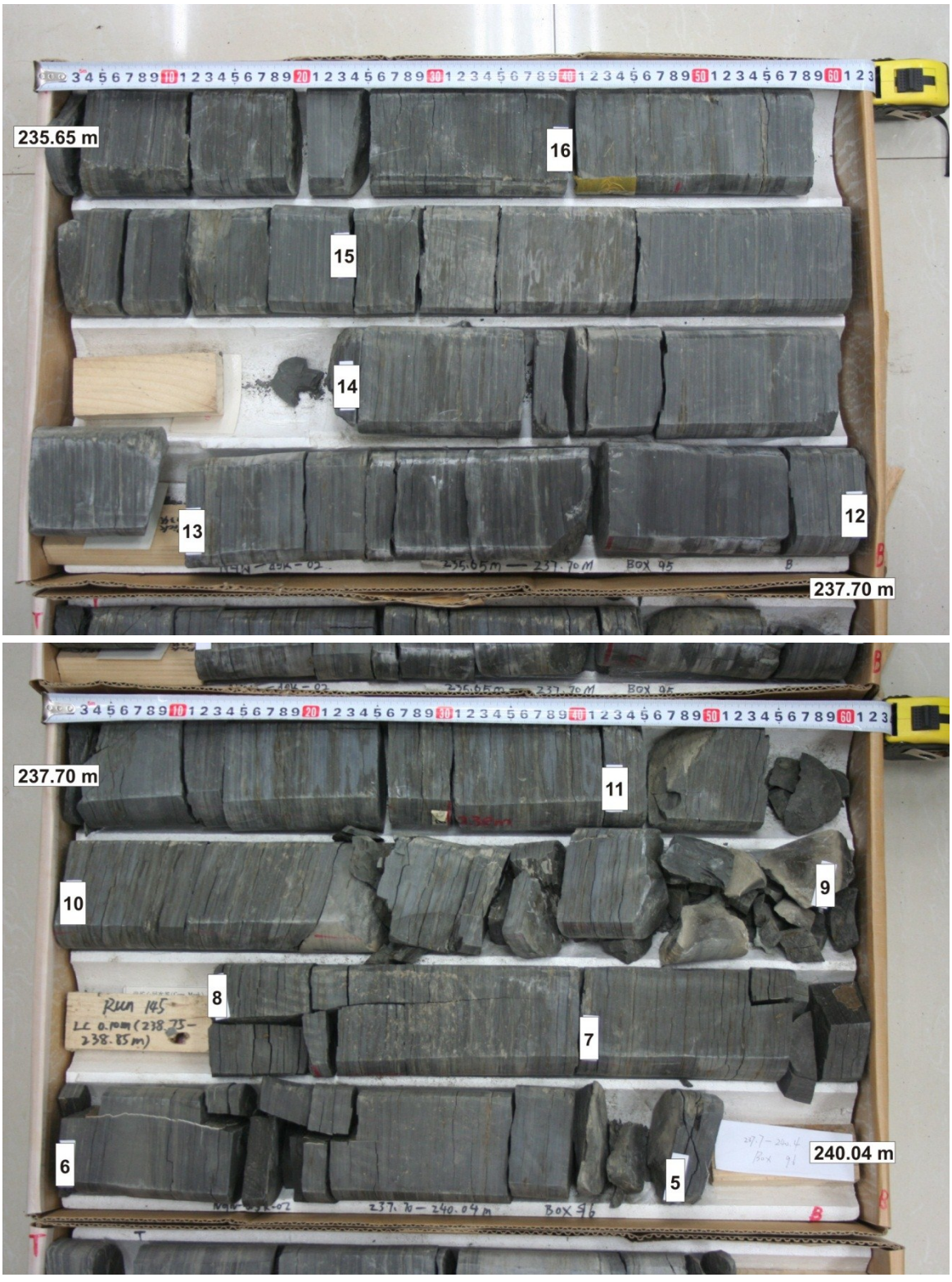
235.65 m
16
15
14
13
12
237.70 m
237.70 m
11
10
9
8
Run 145
LC 0.1m (238.75-
238.85m)
7
6
5
240.04 m

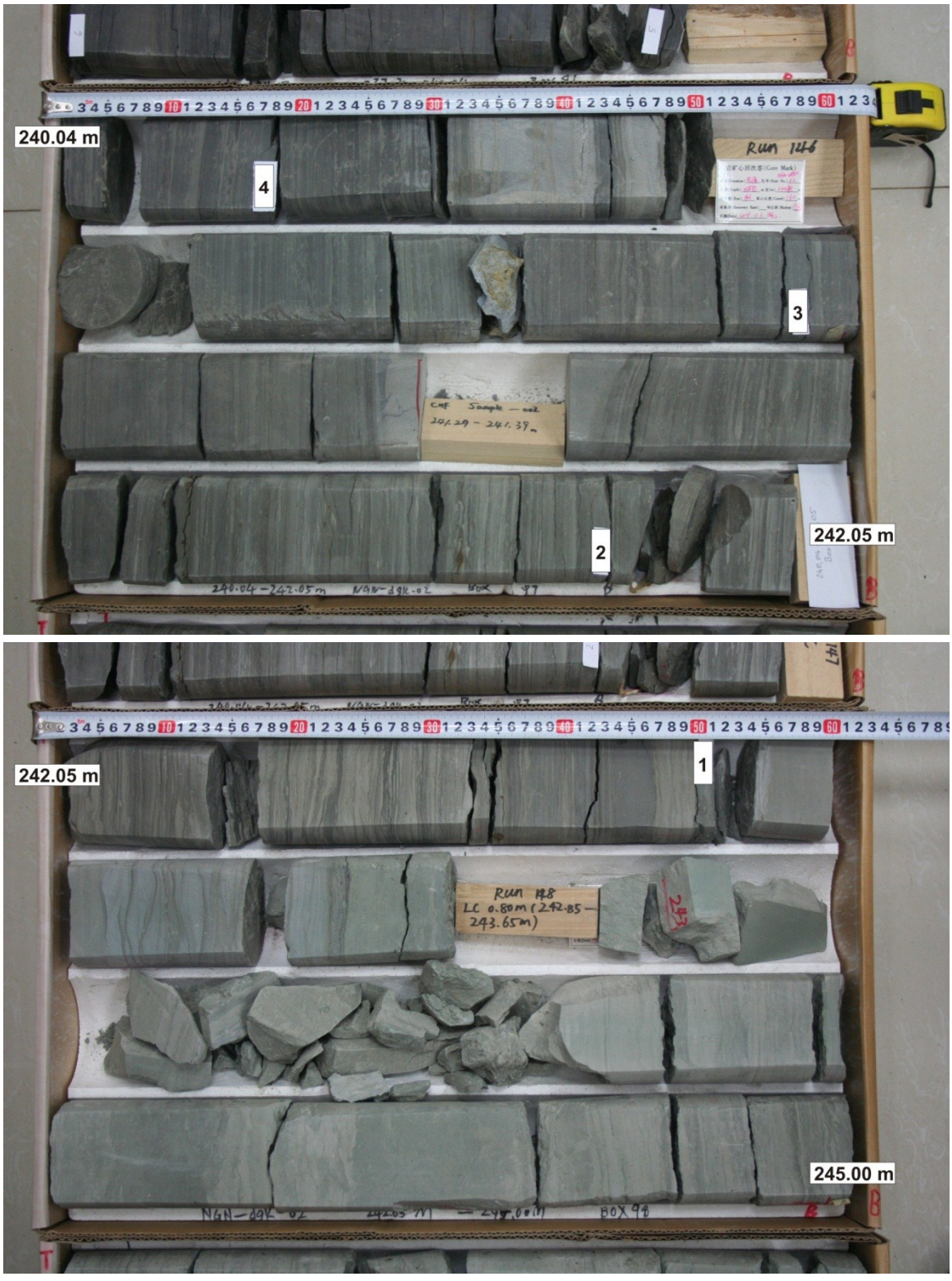
240.04 m
Run 126
4
3
2
242.05 m
242.05 m
Run 127
LC 0.80m (242.85 – 243.65m)
1
245.00 m

7.2 Leco data

Appendix 2: Leco data (TC=total carbon, TOC=total organic carbon, S=sulphur, TIC=total inorganic carbon, Calc.equiv=calcite equivalent).

Sample	Depth [m]	TC [%]	TOC [%]	S [%]	TIC [%]	TOC/S	Calc.equiv. [%]
70	156.23	1.62	0.84	0.94	0.78	0.89	6.50
69	159.22	6.11	6.10	0.84	0.01	7.22	0.05
68	163.48	5.40	3.97	1.14	1.43	3.48	11.88
67	166.96	2.39	1.77	0.82	0.61	2.16	5.11
66	170.71	2.92	2.26	1.37	0.66	1.64	5.49
65	174.39	2.82	1.62	1.23	1.19	1.32	9.95
64	178.28	5.70	5.22	1.55	0.48	3.37	4.02
63	178.30	10.75	2.77	0.40	7.98	6.93	66.50
62	182.32	6.06	4.79	0.86	1.27	5.59	10.57
61	186.00	4.40	2.69	1.10	1.71	2.44	14.27
60	189.62	5.46	5.13	1.07	0.33	4.77	2.75
59	193.73	3.42	2.67	0.69	0.75	3.88	6.25
58	197.66	4.66	3.68	0.98	0.98	3.74	8.19
57	201.67	10.22	8.04	0.98	2.18	8.21	18.13
56	205.55	4.34	3.78	0.98	0.56	3.86	4.64
55	209.00	5.69	5.31	1.02	0.38	5.23	3.15
54	212.04	7.48	7.42	1.01	0.06	7.36	0.54
53	216.15	4.63	4.20	0.64	0.43	6.56	3.55
52	219.70	3.34	2.29	1.29	1.05	1.77	8.79
51	221.43	2.57	1.70	2.50	0.88	0.68	7.31
50	222.05	8.61	8.12	5.29	0.49	1.53	4.07
49	222.64	5.18	4.57	2.67	0.61	1.71	5.06
48	223.39	9.86	9.05	1.30	0.81	6.94	6.72
47	224.25	7.88	4.69	1.06	3.19	4.42	26.58
46	224.60	8.88	6.03	1.19	2.86	5.05	23.79
45	224.75	7.97	3.14	1.28	4.83	2.46	40.26
44	225.66	2.89	2.17	1.35	0.71	1.61	5.95
43	226.41	7.65	7.41	1.26	0.24	5.87	1.98
42	226.90	8.19	7.26	1.33	0.94	5.47	7.83
41	227.63	3.53	2.56	1.28	0.97	2.00	8.08
40	228.21	3.36	1.95	1.58	1.41	1.23	11.73
39	228.23	4.87	4.01	1.73	0.86	2.32	7.17
38	228.55	3.64	2.61	0.99	1.03	2.63	8.61
37	229.66	4.29	3.96	1.93	0.34	2.05	2.80
36	230.31	3.14	1.96	0.96	1.18	2.05	9.86
35	230.35	7.82	0.71	0.39	7.11	1.82	59.21
34	230.47	3.26	2.75	1.84	0.50	1.49	4.20
33	231.00	3.03	3.03	1.65	0.00	1.83	0.01
32	231.41	6.15	5.59	1.51	0.56	3.71	4.69

Sample	Depth [m]	TC [%]	TOC [%]	S [%]	TIC [%]	TOC/S	Calc.equiv. [%]
31	231.79	11.92	11.21	2.29	0.71	4.89	5.92
30	232.19	11.22	10.67	4.28	0.55	2.49	4.57
29	232.15	23.98	23.82	2.19	0.16	10.86	1.36
28	232.40	13.76	13.90	1.81	-0.14	7.67	-1.20
27	232.74	13.11	12.65	2.67	0.47	4.74	3.88
26	232.81	11.69	10.93	2.16	0.76	5.05	6.33
25	232.94	13.31	8.19	1.27	5.12	6.43	42.63
24	233.39	4.94	4.30	1.88	0.64	2.28	5.35
23	233.42	7.23	3.54	1.64	3.69	2.16	30.74
22	234.17	6.62	7.27	1.74	-0.65	4.17	-5.43
21	234.65	8.31	8.80	2.69	-0.50	3.27	-4.13
20	235.00	5.70	5.74	1.45	-0.04	3.95	-0.30
19	235.02	10.73	1.24	0.35	9.49	3.54	79.10
18	235.15	5.63	6.00	1.77	-0.37	3.38	-3.08
17	235.60	5.52	5.90	2.20	-0.38	2.68	-3.18
16	235.90	2.90	3.01	2.72	-0.12	1.11	-0.99
15	236.47	3.74	4.15	2.08	-0.41	1.99	-3.40
14	236.71	5.39	5.61	2.42	-0.22	2.32	-1.85
13	237.21	4.27	4.38	1.55	-0.11	2.82	-0.95
12	237.69	4.10	4.48	1.68	-0.38	2.66	-3.15
11	238.11	4.09	4.36	2.28	-0.27	1.91	-2.27
10	238.32	2.88	3.09	2.66	-0.21	1.16	-1.77
9	238.90	9.82	0.91	0.77	8.91	1.18	74.27
8	239.43	3.94	4.19	2.37	-0.25	1.77	-2.07
7	239.60	4.47	4.75	2.66	-0.28	1.78	-2.36
6	239.80	6.83	6.90	2.83	-0.07	2.44	-0.56
5	240.23	4.21	4.36	2.62	-0.14	1.66	-1.19
4	240.20	5.92	5.42	2.59	0.49	2.10	4.09
3	241.22	1.48	1.52	2.19	-0.05	0.70	-0.38
2	241.85	1.08	1.02	2.19	0.06	0.47	0.49
1	242.55	0.78	0.74	2.21	0.04	0.33	0.34

7.3 Rock Eval data

Appendix 3: Rock Eval data (S_1+S_2=hydrocarbon generation potential, PI=production index, HI=hydrogen index).

Sample	Depth [m]	S_1 [mg HC/g]	S_2 [mg HC/g]	T_{max} [°C]	S_1+S_2 [mg HC/g]	PI	HI [mg HC/g TOC]
70	156.23	0.13	1.29	438	1.42	0.09	154.4
69	159.22	0.43	36.72	438	37.15	0.01	601.6
68	163.48	0.39	30.27	441	30.66	0.01	761.7
67	166.96	0.08	9.14	440	9.22	0.01	515.3
66	170.71	0.25	13.85	440	14.10	0.02	613.1
65	174.39	0.29	7.94	442	8.23	0.04	489.6
64	178.28	0.65	34.72	434	35.37	0.02	665.3
63	178.30	2.77	18.37	430	21.14	0.13	663.6
62	182.32	0.63	34.82	435	35.45	0.02	727.3
61	186.00	0.37	16.05	440	16.42	0.02	596.4
60	189.62	0.42	34.28	439	34.69	0.01	668.2
59	193.73	0.21	13.49	437	13.70	0.02	505.4
58	197.66	0.41	25.28	435	25.69	0.02	687.1
57	201.67	1.25	65.32	436	66.57	0.02	812.2
56	205.55	0.21	25.14	442	25.36	0.01	664.5
55	209.00	0.48	39.57	442	40.05	0.01	745.4
54	212.04	0.52	58.17	443	58.68	0.01	784.3
53	216.15	0.45	26.53	440	26.98	0.02	631.7
52	219.70	0.45	12.29	437	12.74	0.04	537.5
51	221.43	0.18	5.72	438	5.89	0.03	336.7
50	222.05	1.60	62.65	438	64.25	0.02	771.8
49	222.64	0.80	27.15	436	27.94	0.03	594.1
48	223.39	1.34	69.68	442	71.01	0.02	769.7
47	224.25	1.16	33.72	436	34.87	0.03	718.8
46	224.60	1.77	46.63	439	48.40	0.04	773.6
45	224.75	0.48	23.67	439	24.15	0.02	754.0
44	225.66	0.29	11.61	440	11.90	0.02	534.1
43	226.41	1.49	57.29	438	58.78	0.03	772.6
42	226.90	1.34	53.99	439	55.33	0.02	744.1
41	227.63	0.36	15.32	443	15.68	0.02	598.7
40	228.21	0.54	10.70	436	11.23	0.05	548.7
39	228.23	0.90	29.12	440	30.02	0.03	726.3
38	228.55	0.64	17.22	439	17.86	0.04	659.4
37	229.66	1.08	23.78	436	24.86	0.04	600.7
36	230.31	0.34	9.44	440	9.78	0.03	481.4
35	230.35	0.17	2.00	436	2.17	0.08	279.9
34	230.47	0.49	16.05	435	16.54	0.03	582.7
33	231.00	0.45	19.28	442	19.73	0.02	635.9
32	231.41	1.15	40.69	438	41.84	0.03	728.1

Sample	Depth [m]	S_1 [mg HC/g]	S_2 [mg HC/g]	T_{max} [°C]	S_1+S_2 [mg HC/g]	PI	HI [mg HC/g TOC]
31	231.79	3.48	79.63	433	83.11	0.04	710.6
30	232.19	3.60	68.25	431	71.84	0.05	639.4
29	232.15	5.68	173.97	439	179.65	0.03	730.5
28	232.40	2.53	105.90	443	108.43	0.02	761.7
27	232.74	3.64	93.81	436	97.45	0.04	741.7
26	232.81	2.89	68.16	437	71.04	0.04	623.7
25	232.94	3.23	66.29	437	69.51	0.05	809.4
24	233.39	0.84	27.39	438	28.23	0.03	637.3
23	233.42	0.65	23.28	439	23.93	0.03	657.5
22	234.17	1.08	49.64	441	50.72	0.02	682.6
21	234.65	2.08	52.67	432	54.75	0.04	598.3
20	235.00	1.48	36.25	432	37.72	0.04	631.6
19	235.02	0.50	6.20	434	6.69	0.07	498.4
18	235.15	1.29	38.14	430	39.42	0.03	636.1
17	235.60	1.53	36.47	435	37.99	0.04	617.8
16	235.90	0.61	15.14	438	15.76	0.04	502.4
15	236.47	0.79	24.05	438	24.84	0.03	580.1
14	236.71	1.25	34.48	436	35.73	0.03	614.5
13	237.21	0.91	27.72	437	28.62	0.03	632.5
12	237.69	0.88	24.79	438	25.67	0.03	553.4
11	238.11	1.31	23.40	432	24.71	0.05	536.1
10	238.32	0.91	12.04	431	12.95	0.07	389.2
9	238.90	0.45	2.88	437	3.33	0.14	316.8
8	239.43	0.89	20.80	431	21.68	0.04	496.8
7	239.60	1.10	24.08	432	25.18	0.04	507.0
6	239.80	2.35	44.45	432	46.80	0.05	644.0
5	240.23	0.96	24.36	433	25.31	0.04	559.1
4	240.20	0.73	40.50	440	41.23	0.02	746.7
3	241.22	0.16	6.03	439	6.18	0.03	395.1
2	241.85	0.11	1.99	438	2.10	0.05	194.4
1	242.55	0.11	0.14	434	0.26	0.44	19.5

7.4 Microscopy

Appendix 4: Relative amounts of different macerals and mineral matrix per sample (500 points counted per sample).

Sample	Depth [m]	Vitrinite [%]	Inertinite [%]	Lamalginite [%]	Telalginite [%]	Sporinite [%]	Fishbone [%]	Pyrite [%]	Exsudadinite [%]	Matrix [%]
45	224.75	0.00	0.20	34.60	0.00	0.00	3.00	2.80	0.20	59.20
36	230.31	0.00	0.00	15.80	13.60	0.00	0.00	6.60	0.00	64.00
35	230.35	0.00	0.00	5.20	0.00	0.00	0.00	3.40	0.00	91.40
30	232.19	0.20	0.00	30.40	4.00	0.00	5.20	7.60	2.60	50.00
29	232.15	0.40	0.20	59.20	2.40	0.00	1.00	2.60	0.00	34.20
27	232.74	0.60	0.40	39.00	4.00	0.20	6.00	4.20	2.80	42.80
25	232.94	0.40	0.20	37.60	21.40	0.00	2.20	4.20	0.00	34.00
17	235.60	0.00	0.00	30.00	6.00	0.00	2.00	4.60	0.20	57.20
12	237.69	0.20	0.00	18.00	7.40	0.00	0.40	22.00	0.00	52.00
4	240.20	0.60	0.00	30.40	0.00	0.00	5.60	4.20	0.20	59.00

Appendix 5: Relative amounts of different macerals per sample, mineral matrix free (500 points counted per sample).

Sample	Depth [m]	Vitrinite [%]	Inertinite [%]	Lamalginite [%]	Telalginite [%]	Sporinite [%]	Fishbone [%]	Pyrite [%]	Exsudadinite [%]	Matrix [%]
45	224.75	0.00	0.57	99.43	0.00	0.00	0.00	0.00	0.00	0.00
36	230.31	0.00	0.00	53.74	46.26	0.00	0.00	0.00	0.00	0.00
35	230.35	0.00	0.00	100.00	0.00	0.00	0.00	0.00	0.00	0.00
30	232.19	0.58	0.00	87.86	11.56	0.00	0.00	0.00	0.00	0.00
29	232.15	0.64	0.32	95.18	3.86	0.00	0.00	0.00	0.00	0.00
27	232.74	1.36	0.90	88.24	9.05	0.45	0.00	0.00	0.00	0.00
25	232.94	0.67	0.34	63.09	35.91	0.00	0.00	0.00	0.00	0.00
17	235.60	0.00	0.00	83.33	16.67	0.00	0.00	0.00	0.00	0.00
12	237.69	0.78	0.00	70.31	28.91	0.00	0.00	0.00	0.00	0.00
4	240.20	1.94	0.00	98.06	0.00	0.00	0.00	0.00	0.00	0.00

Appendix 6: Microphotographs of the polished sections. Macerals are labelled (inert=inertinite, vit=vitrinite, lamalg=lamalginite, telalg=telalginite, exsud=exsudadinite – pyr=pyrite, fish=fishbone). Microphotographs on the left side were taken using reflected white light, on the right side using fluorescent light.

Sample 4:

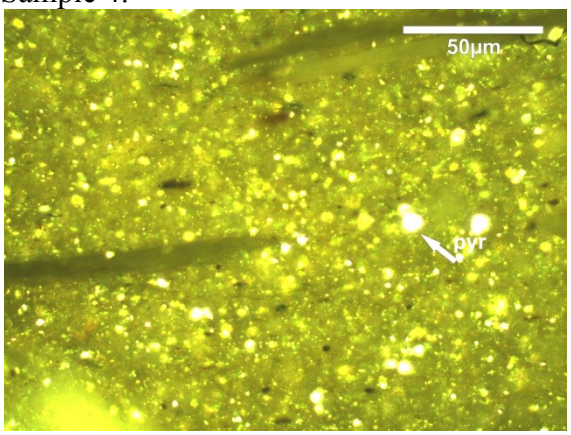

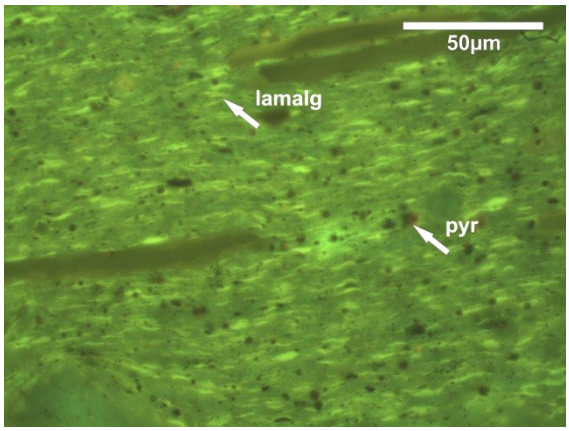

Sample 12:

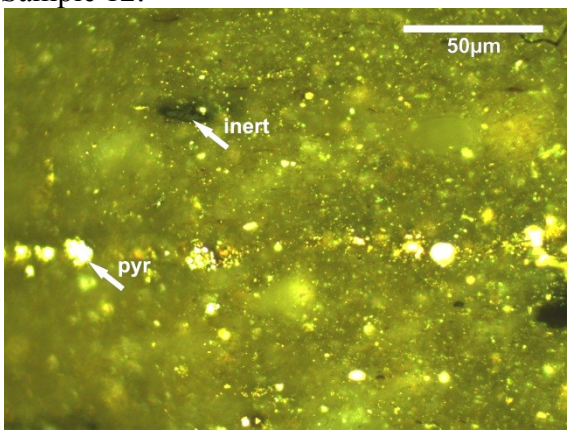

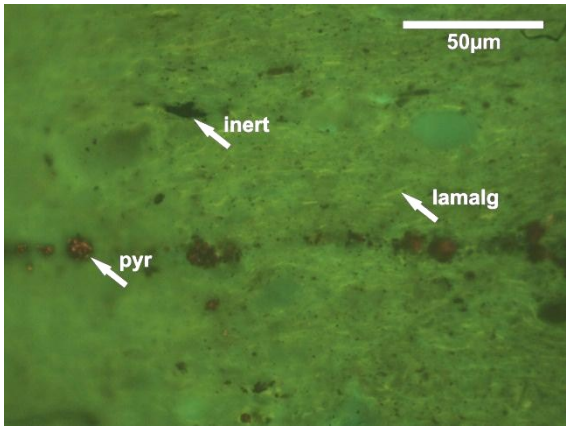

Sample 17 (continues at following page):

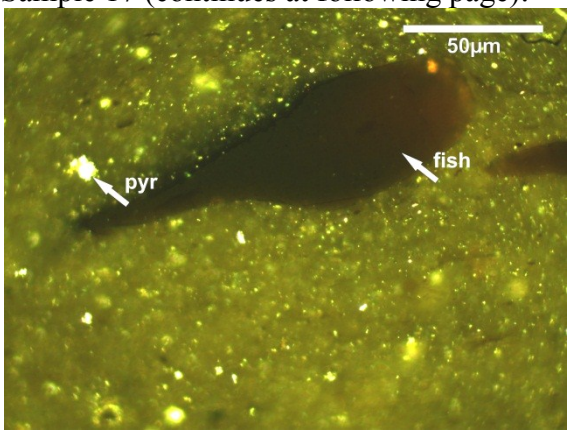

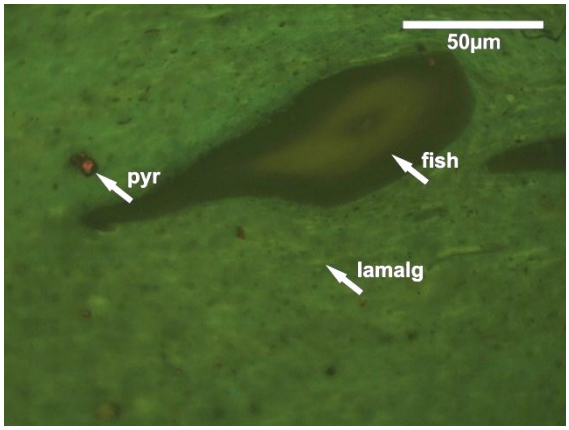

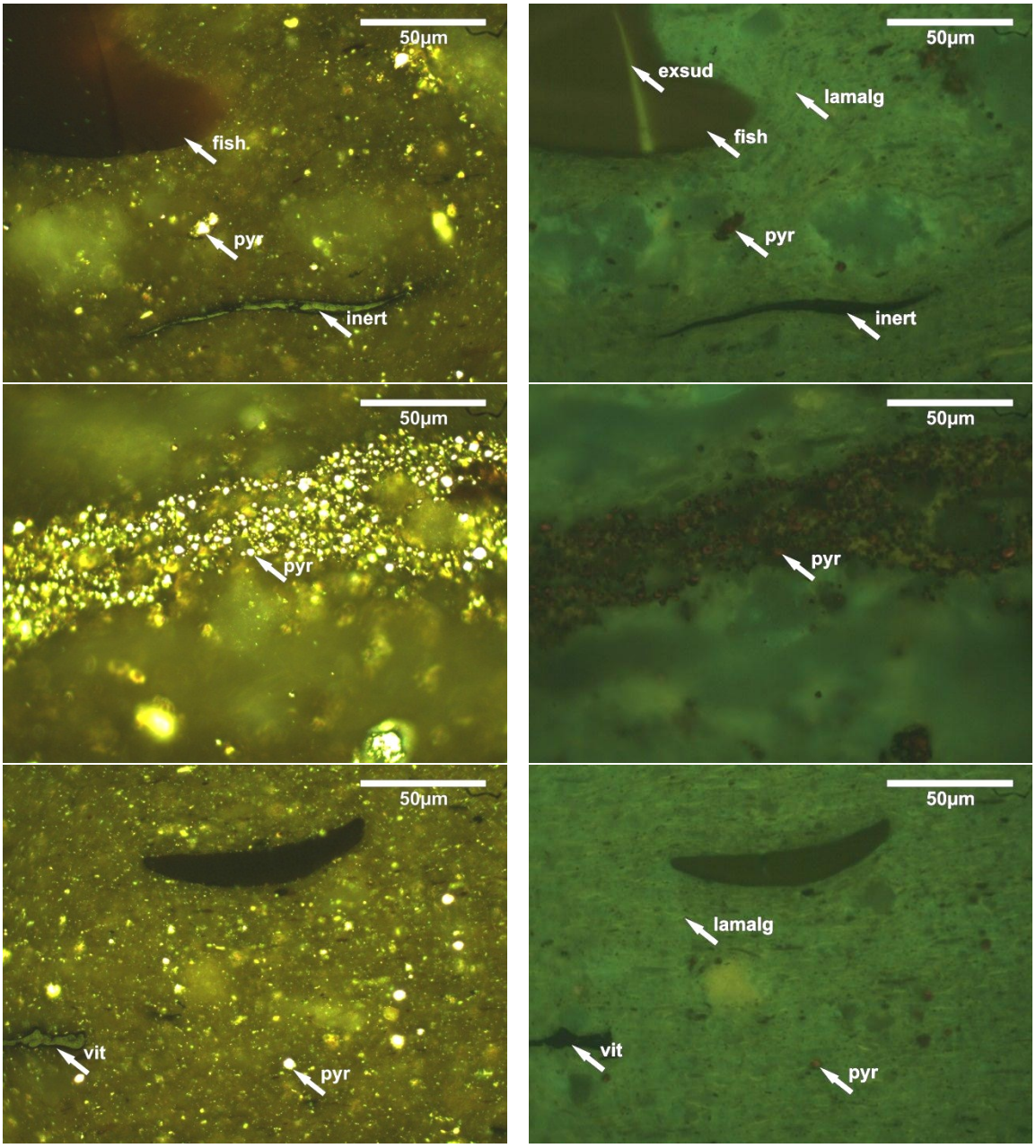
50µm
fish.
pyr
inert
50µm
exsud
lamalg
fish
pyr
inert
50µm
pyr
50µm
pyr
50µm
vit
pyr
50µm
lamalg
vit
pyr

Sample 25:

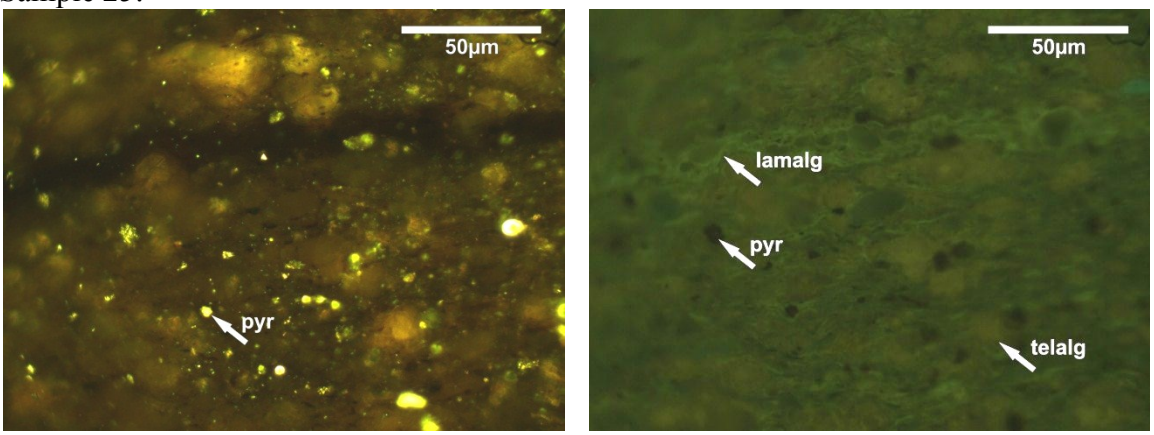
50µm
pyr
50µm
lamalg
pyr
telalg

Sample 27:

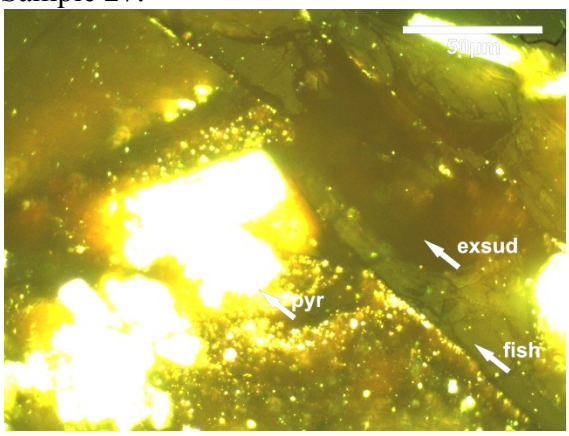

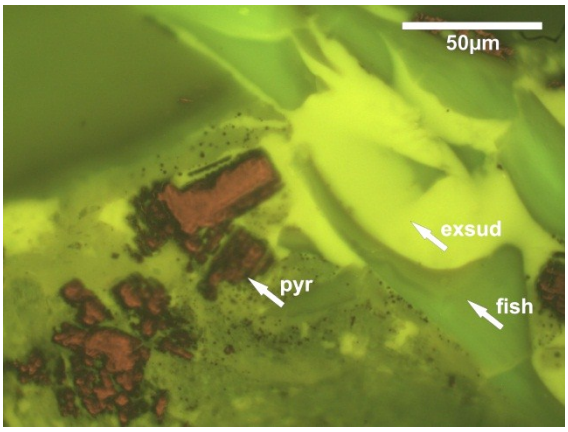

Sample 29:

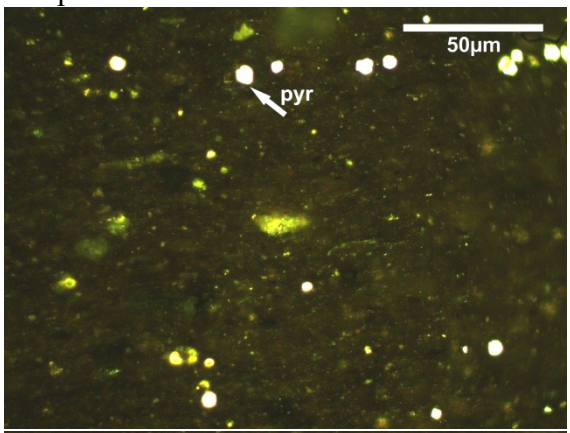

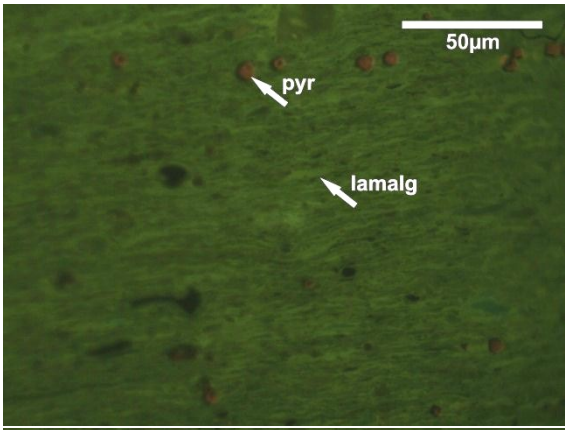

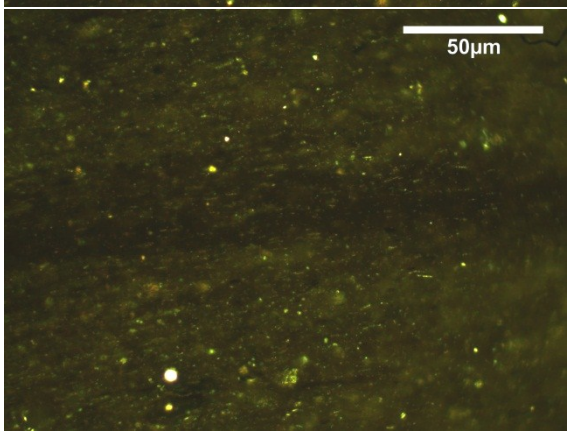

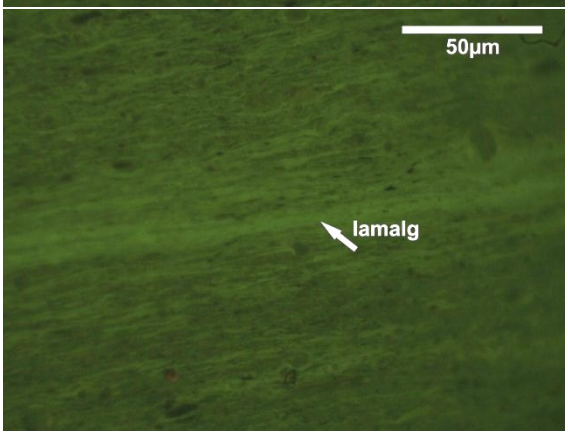

Sample 30:

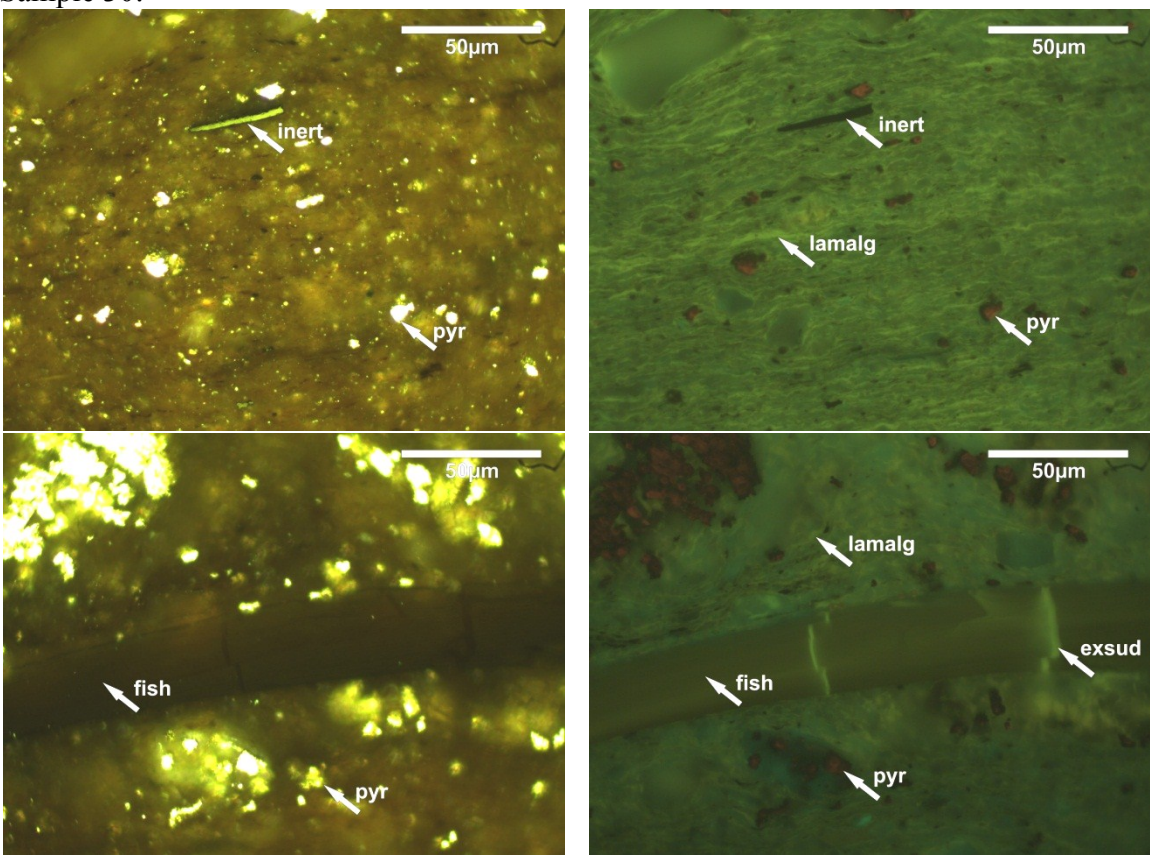

Sample 36:

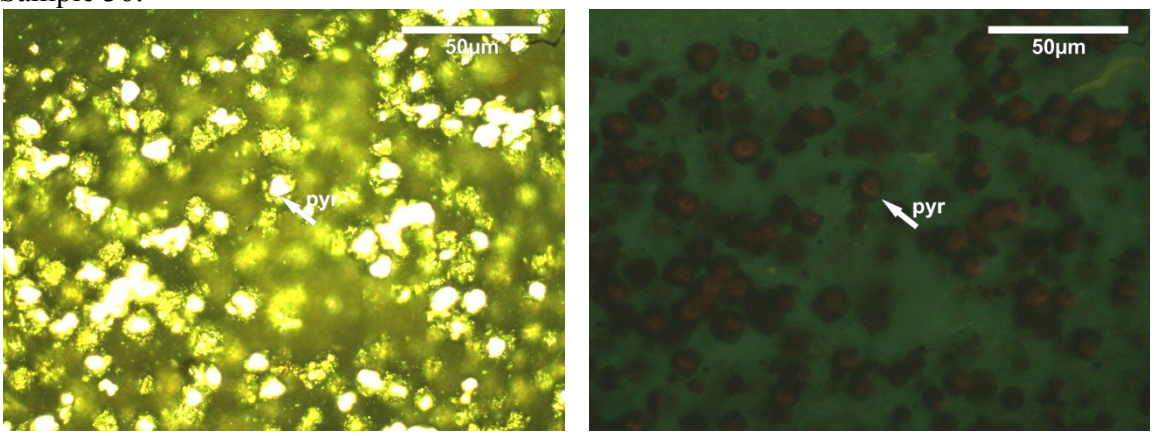

Sample 45:

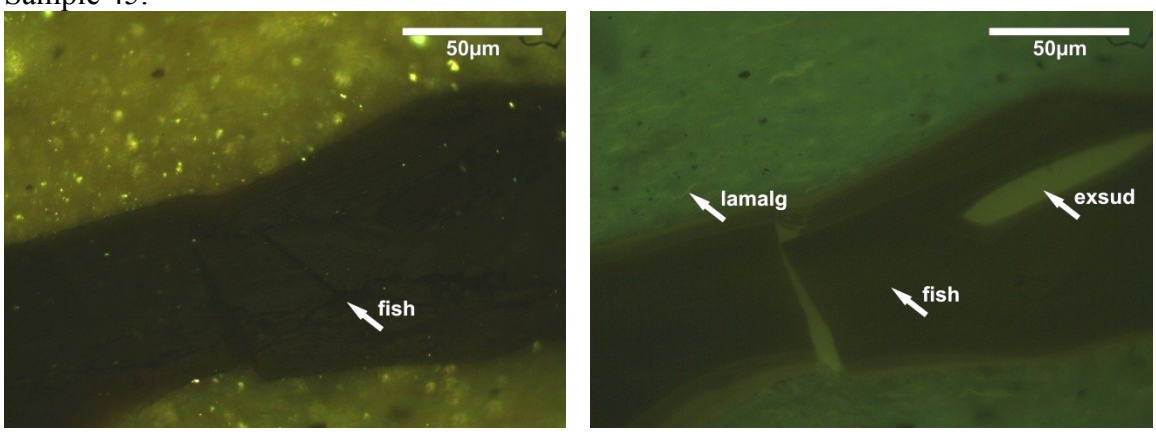

7.5 Biomarker analysis

Appendix 7: Concentrations and concentration ratios of compounds and compound groups in the hydrocarbon fractions (CPI=carbon preference index, Pri/Phy=pristane/phytane).

Sample	Depth [m]	Sum *n*-Alkanes [mg/g TOC]	*n*-C_{15-19}/ *n*-Alkanes	*n*-C_{21-25}/ *n*-Alkanes	*n*-C_{27-31}/ *n*-Alkanes	CPI	Pri/Phy	Steranes [µg/g TOC]	C_{27} Steranes/ Steranes
69	159.22	791	0.21	0.32	0.31	1.5	0.76	117	0.24
65	174.39	1201	0.20	0.30	0.31	1.3	0.60	465	0.26
62	182.30	1046	0.28	0.29	0.26	1.6	0.99	360	0.34
58	197.66	862	0.13	0.37	0.31	1.5	0.84	251	0.27
56	205.60	1818	0.15	0.26	0.40	1.2	0.92	261	0.26
54	212.00	1073	0.15	0.28	0.37	1.2	0.70	177	0.26
50	222.05	963	0.09	0.45	0.27	1.2	0.44	424	0.26
45	224.75	1458	0.11	0.35	0.35	1.2	0.43	853	0.29
41	227.63	1552	0.10	0.38	0.32	1.1	0.45	902	0.18
36	230.31	1334	0.11	0.46	0.24	1.0	0.36	987	0.24
35	230.35	1059	0.10	0.45	0.27	1.2	0.41	854	0.34
30	232.19	541	0.13	0.38	0.32	1.6	0.36	868	0.44
29	232.15	656	0.18	0.38	0.28	1.5	0.43	601	0.46
27	232.74	1094	0.16	0.34	0.33	1.4	0.45	1248	0.44
25	232.94	474	0.13	0.29	0.41	1.6	0.33	1009	0.42
22	234.17	1069	0.07	0.26	0.51	1.4	0.42	852	0.41
17	235.60	1619	0.06	0.23	0.53	1.5	0.54	1370	0.44
12	237.69	1328	0.08	0.26	0.49	1.4	0.55	894	0.44
8	239.43	1720	0.07	0.30	0.43	1.4	0.42	1782	0.50
4	240.20	947	0.13	0.28	0.42	1.4	0.40	859	0.45
3	241.22	2166	0.05	0.17	0.52	1.1	0.27	902	0.36
2	241.85	1514	0.05	0.21	0.47	1.0	0.62	822	0.40
1	242.55	236	0.09	0.26	0.46	1.8	0.74	119	0.29
Sample	**Depth [m]**	**Sum *n*-Alkanes [µg/g Oil]**	***n*-C_{15-19}/ *n*-Alkanes**	***n*-C_{21-25}/ *n*-Alkanes**	***n*-C_{27-31}/ *n*-Alkanes**	**CPI**	**Pri/Phy**	**Steranes [µg/g Oil]**	**C_{27} Steranes/ Steranes**
Oil 1	276.90	3935	0.03	0.36	0.41	1.3		3346	0.38

Sample	Depth [m]	C_{28} Steranes/ Steranes	C_{29} Steranes/ Steranes	Methyl-steranes [µg/g TOC]	S/[S+R] αβ-C_{31} Hopanes	Hopanes [µg/g TOC]	C_{31}-Methyl-hopane [µg/g TOC]
69	159.22	0.30	0.46	295	0.39	421	49
65	174.39	0.31	0.43	1172	0.42	554	21
62	182.30	0.27	0.39	1408	0.42	772	56
58	197.66	0.25	0.49	498	0.43	449	44
56	205.60	0.27	0.48	284	0.45	370	47
54	212.00	0.30	0.44	230	0.43	250	21
50	222.05	0.30	0.44	429	0.40	277	21
45	224.75	0.32	0.40	999	0.41	742	45
41	227.63	0.30	0.51	761	0.39	487	34
36	230.31	0.24	0.51	515	0.41	403	20
35	230.35	0.27	0.39	750	0.41	563	22
30	232.19	0.24	0.32	1627	0.42	721	14
29	232.15	0.23	0.31	854	0.40	557	20
27	232.74	0.24	0.32	1050	0.41	661	62
25	232.94	0.24	0.34	850	0.43	559	33
22	234.17	0.23	0.36	1045	0.39	530	23
17	235.60	0.24	0.33	1858	0.40	1239	74
12	237.69	0.22	0.34	1275	0.41	723	45
8	239.43	0.20	0.30	1948	0.41	920	42
4	240.20	0.22	0.34	587	0.41	529	61
3	241.22	0.24	0.40	771	0.45	509	86
2	241.85	0.21	0.39	423	0.39	344	56
1	242.55	0.26	0.44	112	0.40	63	7
Sample	**Depth [m]**	**C_{28} Steranes/ Steranes**	**C_{29} Steranes/ Steranes**	**Methyl-steranes [µg/g Oil]**	**S/(S+R) αβ-C_{31} Hopanes**	**Hopanes [µg/g Oil]**	**C_{31}-Methyl-hopane [µg/g Oil]**
Oil 1	276.90	0.24	0.38	3585	0.54	3771	226

Sample	Depth [m]	Gammacerane Index	β-Carotane [µg/g TOC]	Diterpenoids [Arom.] [µg/g TOC]	Triterpenoids [Arom.] [µg/g TOC]	Steroids/ Hopanoids	MTTCs [µg/g TOC]	MTTC ratio	C_{14}-Aryl-Isoprenoid [µg/g TOC]
69	159.22	0.07	12.2	4.1	6.3	1.0	2.7	0.74	0.6
65	174.39	0.23	34.0	6.6	15.3	2.9	4.7	0.68	0.9
62	182.30	0.16	34.7	7.2	20.3	2.3	8.9	0.83	1.2
58	197.66	0.16	26.7	7.3	8.4	1.7	2.2	0.75	1.7
56	205.60	0.24	40.2	6.5	15.2	1.5	5.8	0.70	1.5
54	212.00	0.27	21.4	6.0	10.4	1.6	7.5	0.73	2.0
50	222.05	0.43	47.2	7.5	21.7	3.0	4.9	0.57	2.5
45	224.75	0.27	68.8	4.6	16.7	2.5	3.7	0.62	1.7
41	227.63	0.28	59.6	3.6	14.6	3.4	4.3	0.65	1.9
36	230.31	0.23	37.6	5.7	15.2	3.7	6.2	0.62	1.8
35	230.35	0.28	21.0	6.1	12.8	2.9	7.8	0.59	1.7
30	232.19	0.28	30.0	13.2	39.9	3.6	23.0	0.66	2.8
29	232.15	0.23	37.2	9.0	25.6	2.7	7.5	0.61	3.0
27	232.74	0.36	66.2	11.5	24.5	3.5	14.4	0.57	2.6
25	232.94	0.34	43.6	6.6	16.6	3.4	9.6	0.55	1.9
22	234.17	0.37	56.8	6.4	27.2	3.6	8.2	0.57	2.3
17	235.60	0.22	48.5	7.2	33.8	2.7	8.5	0.62	1.1
12	237.69	0.23	44.3	6.7	14.4	3.0	7.8	0.56	1.6
8	239.43	0.35	94.9	8.7	23.8	4.3	7.1	0.51	1.8
4	240.20	0.21	23.3	3.3	9.6	2.8	5.9	0.53	1.3
3	241.22	0.29	33.4	3.3	11.2	3.3	4.3	0.50	1.6
2	241.85	0.21	45.7	5.6	10.3	3.6	4.6	0.65	1.2
1	242.55	0.19	1.7	4.8	5.6	3.7	2.3	0.74	0.8

Sample	Depth [m]	Gammacerane Index	β-Carotane [µg/g Oil]	Diterpenoids (Arom.) [µg/g Oil]	Triterpenoids (Arom.) [µg/g Oil]	Steroids/ Hopanoids	MTTCs [µg/g Oil]	MTTC ratio	C_{14}-Aryl-Isoprenoid [µg/g Oil]
Oil 1	276.90	0.31	522.4	107.2	240.1	1.91	0.00		0.00

Appendix 8: Data of molecular composition of hydrocarbons (EOM=extractable organic matter, Sat.HC=saturated hydrocarbons, Aro.HC=aromatic hydrocarbons, NSO=heterocompounds, Asphalt.=asphaltenes).

Sample	Depth [m]	EOM [mg/g TOC]	Sat. HC [%]	Aro. HC [%]	NSO [%]	Asphalt. [%]
69	159.22	18.9	39	7	52	2
65	174.39	38.7	41	9	48	3
62	182.30	32.8	35	9	52	4
58	197.66	28.8	32	9	56	3
56	205.60	21.5	39	8	46	7
54	212.00	15.5	39	11	42	8
50	222.05	45.1	33	9	56	2
45	224.75	43.8	35	8	54	3
41	227.63	61.0	30	7	61	3
36	230.31	69.5	27	7	61	4
35	230.35	47.2	33	9	53	6
30	232.19	57.2	28	10	61	2
29	232.15	43.0	29	11	57	3
27	232.74	52.9	33	10	55	2
25	232.94	52.0	22	6	68	3
22	234.17	42.7	34	9	52	6
17	235.60	49.4	41	8	47	4
12	237.69	45.6	43	8	46	3
8	239.43	59.4	39	9	46	7
4	240.20	37.1	40	7	47	6
3	241.22	38.1	34	6	53	7
2	241.85	34.7	30	7	52	11
1	242.55	24.3	23	17	45	15

7.6 Carbon isotopy

Appendix 9: Carbon isotopy data of selected compounds in saturated hydrocarbon fractions of 11 samples from the Qingshankou Formation.

Sample	*n*-C_{16}	*n*-C_{17}	Pristane	*n*-C_{18}	Phytane	*n*-C_{19}	*n*-C_{20}	*n*-C_{21}	*n*-C_{22}	*n*-C_{23}	*n*-C_{24}	*n*-C_{25}	*n*-C_{26}	*n*-C_{27}
58	-31.2	-31.5	-31.8	-31.2	-31.9	-32.6	-33.2	-33.2	-33.3	-33.4	-33.0	-33.1	-32.9	-33.0
50	-30.8	-31.3	-32.1	-31.5	-31.8	-32.2	-32.7	-32.8	-33.0	-33.5	-32.8	-33.1	-32.7	-32.9
45	-31.9	-32.0	-32.7	-32.3	-32.7	-33.3	-33.0	-33.7	-33.8	-34.0	-33.5	-33.9	-33.4	-34.0
36	-32.4	-32.5	-33.1	-32.7	-33.5	-33.2	-33.7	-34.1	-33.9	-33.7	-34.0	-33.7	-34.1	-33.7
30	-32.9	-33.4	-34.0	-33.5	-34.0	-33.3	-33.1	-33.8	-34.4	-35.0	-34.7	-34.4	-34.1	-34.9
29	-33.2	-33.0	-33.8	-33.2	-33.7	-33.9	-33.5	-34.0	-34.2	-34.1	-34.0	-34.3	-33.8	-34.5
27	-32.7	-33.0	-33.6	-33.2	-33.4	-33.0	-33.6	-33.8	-34.1	-34.3	-33.5	-34.2	-34.1	-34.4
22	-32.1	-32.3	-32.8	-32.3	-33.2	-32.9	-33.1	-33.5	-33.6	-34.2	-34.3	-34.2	-34.5	-34.3
12	-30.9	-31.0	-31.5	-31.2	-31.7	-31.7	-31.6	-32.2	-32.1	-33.1	-33.6	-33.7	-34.0	-34.0
4	-30.4	-30.8	-31.0	-31.0	-31.2	-31.8	-31.3	-32.5	-31.5	-32.3	-32.1	-32.6	-32.2	-32.5
2	-30.1	-30.5	-30.8	-30.8	-31.2	-31.7	-30.6	-31.4	-30.7	-31.3	-31.0	-31.2	-31.5	-31.8

Sample	5a, 20R-C_{27} Sterane	5a, 20R-C_{29} Sterane	4a-C_{28} Methylsterane	4a-C_{30} Methylsterane	4a-C_{30} Methylsterane
58	-31.2	-31.5	-31.9	-31.6	-31.8
50	-30.6	-31.0	-32.3	-31.8	-31.9
45	-31.5	-31.9	-32.6	-32.8	-33.4
36	-32.1	-32.2	-33.1	-32.6	-32.9
30	-32.2	-32.9	-33.3	-34.0	-34.2
29	-32.2	-32.7	-33.4	-34.7	-34.6
27	-33.2	-32.8	-34.4	-34.2	-34.4
22	-32.3	-32.2	-33.2	-33.7	-33.9
12	-31.4	-31.3	-32.6	-32.9	-33.6
4	-31.0	-30.5	-33.0	-33.5	-33.9
2	-31.1	-31.5	-32.0	-32.4	-32.0

Sample	17a, 21b-C_{29} Hopane	17a, 21b-C_{30} Hopane	7a, 21b, 22R-C_{3} Hopane	3a-C_{31} Methylhopane	Gammacerane
58	-34.2	-34.8	-34.7	-48.6	-28.7
50	-35.2	-35.4	-35.9	-47.9	-29.2
45	-35.8	-36.1	-36.4	-47.8	-30.1
36	-35.5	-35.8	-35.9	-45.7	-28.8
30	-36.3	-36.0	-36.5	-47.0	-28.3
29	-36.2	-36.9	-36.9	-48.6	-29.7
27	-36.8	-37.1	-37.6	-46.4	-28.9
22	-36.2	-35.7	-36.4	-47.7	-29.7
12	-35.0	-35.3	-36.1	-43.0	-29.3
4	-34.9	-35.7	-36.3	-49.5	-28.2
2	-35.5	-35.8	-36.1	-44.8	-29.0